Adhesion mechanism between laser sputtered materials, Copper and Aluminum on Silicon substrate

vorgelegt von:

M.Sc. Mohammad Hossein Azhdast

geb. in Teheran, Iran

von der Fakultät IV - Elektrotechnik und Informatik
der Technischen Universität Berlin
zur Erlangung des akademischen Grades

Doktor der Ingenieurwissenschaften

- Dr.-Ing. -

genehmigte Dissertation

Promotionsausschuss:

Vorsitzender:	Prof. Bernd Szyszka
1. Gutachter:	Prof. Klaus Dieter Lang
2. Gutachter:	Prof. Hans Joachim Eichler
3. Gutachter:	Prof. Thomas Schneider

Tag der wissenschaftlichen Aussprache: 29. Juni 2018

Berlin 2018

In childhood we strove to go to school,

Our turn to teach, joyous as a rule

The end of the story is sad and cruel

From dust we came, and gone with winds cool

-Khayyam-

Abstract

The present study aims to the novel technique by laser deposition of Aluminum and Copper nano particles on silicon wafer substrate. Thin μm films have been deposited from one-side coated glass to Silicon wafers by sputtering nano particles using laser radiation. The Distance between donor film and substrate was up to several 100 μm, and it has been optimized as 300 μm.

As soon as the laser energy threshold is reached, particles are expelled from the donor and consequently transferred to the accepting substrate. By deposition of nano particles, the thin film could be made. Copper or Aluminum film formation is described involving four stages, namely nucleation, growth, coalescence, and thickening. In order to make the film thicker, electroless nickel and afterward gold is plated on the particles for further adhesion measurements.

A step-by-step optimization guide for deposition parameters was first developed and presented. Different Nd lasers by considering the various pulse duration (picosecond and nanosecond) and also different wavelengths (Infrared and Green) have been used for implementing nano particles on Si-Wafer substrate. Further, the effect of various parameters on adhesion test and the mechanism for depositing a layer was taken into consideration.

Regarding chemical features and different reflectivity (R), Copper and Aluminum react similarly in Infrared laser for processing material and showing different behaviors in various wavelengths. The different absorption of Al and Cu in a specific wavelength indicates distinguished roughness of thin film on the silicon wafer which has been considered in multiple test conditions. The effect of Al and Cu absorption is determined by Energy-dispersive X-ray spectroscopy (EDX) and Focused Ion Beam (FIB) analysis. The identification of laser energy threshold, pulses per laser shot, in addition to pulse overlapping is essential if the best deposition results are going to be deposited by laser direct writing (LDW) method. This technique is considered as the most critical direct-write alternative for lithographic processes to generate patterns with high-resolution which is a completely masked-less process and no additional vacuum chamber is required.

The deposition of nanoparticles was demonstrated by preparing Under Bump Metallization (UBM) although this technique might be utilized for some other

applications such as bonding and interconnections technology for micro-electronics, micro-mechanical, and micro-optical devices.

Kurzfassung

Die vorliegende Studie beschreibt eine neuartige Technik zur Laserabscheidung von Al und Cu Nanopartikeln auf Silizium-Wafern. Dünne Schichten auf einem Trägerglas bzw. Spenderfolie werden durch Laserbestrahlung (Laser Direct Writing, LDW) auf Siliziumwafer übertragen. Der Abstand zwischen Spenderfolie und Substrat beträgt einige 100 µm, wobei ein Abstand von 300 µm zur Herstellung glatter und gut begrenzter Streifen mit Breiten um 100 µm optimal ist.

Sobald die Laserenergieschwelle erreicht ist, werden die Partikel aus der Spenderfolie emittiert und auf das Si-Substrat übertragen. Die Herstellung von Kupfer oder Aluminiumschichten ist durch 4 Stufen charakterisiert, nämlich Keimbildung, Wachstum, Koaleszenz und Verdickung. Um eine stärkere Schichtdicke bis 500 nm zu erzeugen, werden für Adhäsionsmessungen chemisch Nickel- und anschließend Gold-Partikel plattiert.

Zu Beginn wurde eine Schritt-für-Schritt-Optimierungsanleitung für Abscheidungsparameter entwickelt und anschließend präsentiert. Verschiedene Nd:YAG-Laser mit Pulsdauern von einigen Pikosekunden und Nanosekunden und mit unterschiedlichen Wellenlängen (Infrarot und Grün) wurden zur Abscheidung von Nanopartikeln auf Si-Wafern verwendet. Ferner wurde die Wirkung verschiedener Parameter auf die Adhäsionskraft einer Schicht untersucht.

Die chemischen Eigenschaften und Reflektivitäten von abgeschiedenem Kupfer und Aluminium sind bei Einsatz von verschiedenen Infrarot-Lasern vergleichbar, zeigen jedoch verschiedene Verhaltensweisen bei grünen Wellenlängen. Die unterschiedliche Absorption von Aluminium und Kupfer bei spezifischen Wellenlängen ergibt unterschiedliche Rauigkeiten der Schichten auf dem Siliziumwafer.

Die Wirkung unterschiedlicher optischer Absorption von Al- und Cu-Spendern wird durch Energiedispersive Röntgenspektroskopie (EDX) und Focused Ion Beam (FIB) Analysen untersucht. Die Pulsüberlappung ist von wesentlicher Bedeutung, um gute Abscheidungsergebnisse zu erzielen.

Die LDW-Technik gilt als die bedeutende Direkt-Schreib-Alternative für lithographische Prozesse, um Muster mit hoher Auflösung zu erzeugen. Des Weiteren ist keine zusätzliche Vakuumkammer erforderlich.

Acknowledgements

My most profound gratitude goes to my supervisor, Professor Klaus Dieter Lang for his kindness, patience, support, and faith in my postgraduate studies at the Technical University of Berlin. His guidance helped me in all the time of research and writing of this thesis. I could not have imagined having a better advisor and mentor for my Ph.D. study.

Besides my advisor, I would like to thank Professor Hans Joachim Eichler for his insightful comments, supervision, supports, and encouragement during my Ph.D.

I would also like to give special thanks to Dr. Veronika Glaw and Dr. Oliver Lux, who have always been supportive and caring for all my educational development for my doctoral study period.

I wish to express my special thanks to the experts who were involved in the validation survey for this research and all my colleagues at the Technical University of Berlin. Without their passionate participation and input, the validation survey could not have been successfully conducted.

Finally, I must express my very profound gratitude to my parents for providing me with unfailing support and continuous encouragement throughout my years of study and through the process of researching and writing this thesis. This accomplishment would not have been possible without them. Thank you.

Patents

1. ‘’Arrangement for applying conductive nanoparticles on a substrate’’, United State Patent Application Publication, Mohammad Hossein Azhdast, publication number: US20160346842 A1, SmartPac GMBH Technology Services, Nauen (DE), Pub. Date: Dec.1, 2016

2. ‘’Arrangement and method for the reproducible application of small amounts of liquid’’, Mohammad Hossein Azhdast, Siavash Hosseinpour Tabrizi, USA patent and trademark office, publication number: US20160228967 A1, SmartPac GMBH Technology Services, Nauen (DE), Pub. Date: Aug.11, 2016

Publications

1. ‘’Heating effect in laser direct writing of Al and Cu particles on Si-Wafer substrate‘’, 20th Photonics North Conference, 5-7 June 2018, Montreal, Canada.

2. ‘’Roughness measurements of Al and Cu particles in Laser-Induced forward transferring process‘’, IEEE Laser Science in photonic application conference (CLEO-2018), 13-18 May 2018, San Jose, CA, USA

3. ‘’Laser-induced forward transfer of aluminum particles in different gaseous environment’’, OSA High-brightness Sources and Light-driven Interactions Congress, 26-28 March 2018, Strasbourg, France

4. ‘’Optimization parameters for Laser-induced forward transfer of Al and Cu on Si-Wafer substrate’’, International conference on Photonics (Photoptics 2018), Optics and Laser technology, 25-27 January 2018, Madeira, Portugal

5. ‘’Deposition of Al and Cu nanoparticles on silicon wafer using picosecond Nd:YAG laser: An experiment-based parameter optimization guide’’, IEEE Laser Science in photonic application conference (CLEO-2017), 14-19 May 2017, San Jose, USA

6. ‘’Comparison of nano particle implantation with picosecond lasers by concerning different wavelengths from Aluminum and Copper on silicon wafer substrate’’, IEEE Laser Science in photonic application conference (CLEO-2017), 14-19 May 2017, San Jose, USA

7. ‘’Adhesion mechanism between laser sputtered Aluminum nano particles on Si- Wafer by Nd:YAG laser’’, IEEE Laser Science to Photonic Applications Conference (CLEO:2016), June 2016, San Jose, USA

8. ‘’Nano particle production by laser ablation and metal sputtering on Si-Wafer substrate’’, Advanced Solid State lasers Conference (ASSL), October 2015, Berlin, Germany

9. ‘’Laser melting of metal powders using Nd:YAG and Compact diode laser for micro particle deposition’’, Advanced Solid State lasers Conference (ASSL), October 2015, Berlin, Germany

10. ‘’Picosecond laser and its application in Solar cells’’, Iran and Germany joint conference in Renewable Energy (IGCRE-2014), Shahid Beheshti University, September 2014, Tehran, Iran

Contents

List of Figures

Abbreviations

Nd:YAG	Neodymium-doped yttrium aluminum garnet
LIFT	Laser-induced forward transfer
EDX	Energy Dispersive X-Ray
PPT	Pattern-Transfer Techniques
MCP	Micro contact printing
PL	Photolithography
LDW	Laser direct-writing
MEMS	Micro electromechanical systems
RF	Radio frequency
DC	Direct current
PCB	Printed circuit board
LDWM	Laser direct-write modification
LDWS	Laser Direct-Write Subtraction
HAZ	Heat affected zone
SFF	Solid free-form fabrication
SLS	Selective laser sintering
LDWA	Laser direct write addition
DRL	Dynamic release layer
MAPLE	Matrix-assisted pulsed laser evaporation
LCVD	Laser chemical vapor deposition
CW	Continuous-wave
TFTL-CD	Thin-film-transistor liquid-crystal display
AOM	Acoustic-optical modulator

DMD	Digital micro-mirror devices
LDT	Laser display technology
LED	Light emitting diode
IPA	Isopropyl alcohol
ENIG	Electroless nickel immersion gold
FIB	Focused ion beam
UV	Ultra violet
LIBWE	Laser-induced backside wet etching
CIGS	Copper indium gallium selenide solar cell

List of symbols

R	Reflectivity index
Δ	distance between laser pulse
Eth	threshold energy
k	thermal diffusivity of material
T	laser pulse duration
α	optical penetration depth
ℓ	heat diffusion length
σP	surface tension
Pc	permeability coefficient
Dc	diffusion coefficient
Sc	solubility coefficient
M^2	beam propagation factor
λ	laser wavelength
Ra	average roughness
Rz	roughness depth
Rsk	roughness skewness
ε	distance between donor and wafer
ns	nano second
ps	picosecond
σ_0	target conductance
ε_0	permittivity of free space
β	laser velocity in vacuum
v	laser velocity

I_0	laser intensity
ω	incident laser angle
∇T	thermal conductivity
ΔH	enthalpy
c_p	heat coefficient
ρ	density
ΔV	heat influence in small volume
τ	laser irradiation time
G	electron-phonon coupling factor
T_e	electron temperature
T_l	lattice temperature
T_F	Fermi temperature
ε_F	Fermi energy
k_B	Boltzmann constant
γ	electronic heat capacity constant
m_e	electron mass
n_e	number density

1. Introduction

The goal of this thesis is to perform a novel study of Laser deposition, structuring, and adhesion mechanism on the deposited particles as one of the generative manufacturing processes with laser radiation. Lasers can deposit controlled amounts of energy in any desired locations. Among the many features of the laser radiation, such as the long coherence length, low divergence, the mono chromaticity and “drop energy in place” idealized lasers for material processing. Lasers can create micro patterns by adding material. In this case, the controlled energy of lasers is implemented to transfer material accurately and precisely from a source to a distinct location on a substrate.

The Nd:YAG laser is the most commonly used types of the solid-state laser at present. Neodymium-doped Yttrium Aluminum Garnet (Nd:YAG) possesses a combination of unique properties for laser operation. The YAG has excellent optical quality and also high thermal conductivity. Furthermore, the cubic structure of YAG favors a narrow fluorescent line width, which results in a high gain and low threshold for laser operation [1]. In Nd:YAG, trivalent neodymium substitutes for trivalent yttrium, so charge compensation is not required.

Laser-induced forward transfer (LIFT) is a laser-based additive of direct-write techniques in which laser pulses are implemented to elicit material from a donor film and deposit it in a receptor substrate. This method can print droplets of solutions and also micro/nano particles with a high resolution. Furthermore, it can work in the air (at atmospheric pressure and room temperature), being a non-contact technique which avoids contamination problems, and the possibility to integrate it with laser micro-machining. LIFT techniques provide some opportunities for models, forms, and devices which cannot handle traditional photolithography tools and they are perfectly suitable for digital micro-fabrication applications. Laser-induced forward transfer procedures are ideal for many fast prototyping applications which completed the design, fabrication, and testing of a given structure quickly because they are non-lithographic digital micro-fabrication processes. LIFT has high speed in writing for roll-to-roll applications. This technique, which is going to explain in more details in the present study, is

used to produce thin films from one-side coated glass to a silicon wafer substrate with micro/nano particles by using laser radiation.
The present research aims to study an adhesion mechanism of the thin film made of aluminum and copper deposited particles. Film formation is commonly explained by a model, including micro/nano transferred particles and thickening stage. The adhesion tape test was implemented to see whether the selected substrates can adhere to sputtered particles or not. The influence of different operating modes of lasers and different pulse durations (Nano & Pico second) are examined, as well as the average power and beam quality of solid-state lasers.

1.1. State of the art

The studies of the implementation of micro/nano particles as seeds in the substrates have been assigned to the representation of the technique to transfer the materials without any changes to their specific properties. It means that the particular method should not have any chemical reaction till the material properties will be steady during the process. The further remark was how the deposition rate can be accelerated. Chemical Vapor Deposition (CVD) and Laser Chemical Vapor Deposition (LCVD) are the deposition methods which are often used in the semiconductor industry to produce thin films.
In LCVD technique the deposition rate was approximately 10μm/s (In the LIFT method the process can be increased up to 30 m/s). The next important consideration for producing thin film was not to utilize and the process should be performed even in room atmosphere. The other important point was to transfer micro/nano lines for pads in bonding applications. This dimension of deposition the particles were similar as patterns that could be generated by lithographic technique. Photolithography is a process which uses light to transfer material from a photomask to the substrate.
This procedure is used in the micro-electronics industry and micro-electromechanical systems. The study has illustrated that micro wires in the range of 10 μm can be fabricated by using electron beam lithography. This method had its disadvantages. The process should be done in completely flat

substrates to make effective patterns. Photolithography needs very clean conditions without any contaminations. The mask was too expensive and it could be used just for one application and the process was not flexible. The procedure includes multiple chemical steps which make environmental pollution.

Laser Direct Writing (LDW) allows deposition in non-flat substrates despite photolithography technique. Furthermore, wide range of materials can be deposited including metals, polymers, dielectrics and composites. It is able to transfer complex patterns from donor to acceptor substrates. Wide range of fluids with different viscosity could be carried out in LDW. In addition, multilayer structures will be achieved by different materials in various types of ribbons.

The penetration depth of the particles has an essential role in the attachments of the transferred metals from the substrate. The permeation of transferred particle in the substrate varies from some nanometers to 1-2 μm in adsorption and absorption phase respectively.

For having a smooth thin film with LDW procedure, some essential parameters such as optimized laser pulse energy, laser pulse overlapping, donor thickness, laser pulse duration, should be considered which all have been explained and measured in Chapter 5. Adhesion is one of the most important indexes to check the quality of the thin films which has been evaluated by doing tape test and shear test during the process.

Thin films have the potential to be the pioneer mechanism for devices with dimension from micro-to-millimetre range requiring large forces over large displacements. Multilayer thin films are implemented as metallic contacts, which rely on Micro Electro Mechanical Systems (MEMS). The vastest applications of thin films are MEMS and medical devices. The MEMS are applied widely as intelligent integrated electrical systems such as electrical contacts and relays, hybrid circuits (high frequency), optical detectors, mirrors and radio frequency (RF) switches. LDW technique has an advanced microfabrication processes to pattern thin layers of conducting and insulating materials on silicon or polymer substrates. The high rate and low cost technique in laser direct writing made

this method very effective in small production and rapid prototype fabrication of high precision printed circuit boards (PCB).

1.2. Material processing on Si-Wafer

Surface engineering is described as the improvement or modification of a surface by using thin coatings. The range of applications is different, extending from various tasks to some applied reasons such as developing electrical features and bio-compatibility. According to [8-10], the sustainability of the surfaces and the physical properties would be increased by using the heating process.

The higher surface coverage is attained by precipitating smaller particles directly into the silicon, through a higher homogeneity and better adhesion [11]. One of the methods of making thin films is sputter deposition. In this procedure, the particles will be ejected from the material owing to the bombardment of the solid target by energetic atoms. Sputtering takes place when the transfer of an atom is directed at a target with the energy which is necessary to establish bonds with other atoms. Linear sputtering occurs when recoiling target atoms can surpass the surface barrier. A deposition of sputtered particles is attained after atoms and their subsequent transport. The yield rate relies mainly on the ion energy in addition to involving the atomic masses [2]. Sputtering does not occur below a particular energy threshold [3-5].

Pattern-Transfer Techniques (PTT) is considered as the most economical selection regarding those large-scale manufacturing situations, in which the parallel creation of identical patterns is fundamental. In this case, the selected model is produced into the substrate in one step at the same time. PTT is mostly limited to constant and uniform substrates [14, 15]. Micro Contact Prints (MCP) and Photolithography methods (PL) are regarded as the most widely-used PTT. Further, the photolithography has more advantages in comparison to the modern technological progress, which paved the way for micro structure production. However, some disadvantages should be taken into consideration for both MCP and PL. For instance, the creation of a mold or a mask should be done in advance, which is expensive and time-consuming.

Fig.1.1 shows the schematic picture of the LIFT process in the studies. As it can be seen in the picture, a piece of a glass (25 mm diameter and 1 mm thickness), which was coated with copper or aluminum (500 nm thickness; tolerance: ± 10%) were implemented in this method. The particles are going to be transferred from the covered side of the glass to the upper side of the substrate. An inert gas (argon) can be utilized in the process to prevent oxidization of the sputtered particles in the substrate. Electroless metal deposition [7] is regarded as a surface-finishing technology whereby one or more metallic atom layer films are plated into a material surface. After nickel plating onto copper and aluminum, the results indicated that plating appears precisely on the line of copper or aluminum seeds on the Si-wafer. This transfer is defined as the movement of atoms from a donor surface into the substrate by using a laser source.

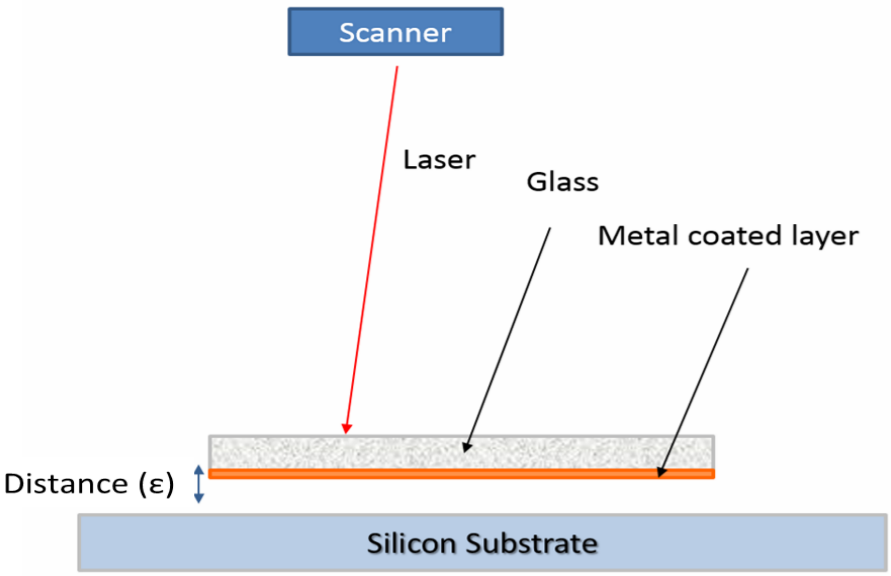

Fig.1.1 Schematic picture of metal deposition on Si-wafer substrate

Various repetition rates produce a different average output power by picosecond laser which will be explained in chapter 5. In this regard, both the pulse energy and intensity of each sputtering line are calculated.

The process of laser deposition has made a lot of improvement in the production of sensors, micro batteries, interconnects, antennae and solar cells.

The integration of various LDW techniques is implemented to fabricate the embedded electronic devices and circuits. For instance, the devices implanted

in the pockets associated with laser micro-machining are cabled to establish working circuits by laser deposition of the metal interconnects. Furthermore, there is a possibility for using the LDW technique to transfer the entire instruments which are capable of performing the same task of pick and place machines implemented in assembling a circuit board. It is worth mentioning that, this broad range of capacities cannot be recommended for other processing technique having the same setup for the rapid prototyping of electronic circuits. In spite of the availability of these capabilities, LDW techniques involve a limited use to repair, modify and customize the integrated circuit applications. LDW is the output of the requirements in feature size, layer thickness, cross-contamination and material properties for these devices. Nearly ablation threshold fluence was noticed for all pulse durations and multiple-pulse irradiation [16, 19].

LIFT is capable of writing all kinds of patterns for a wide range of surfaces both in contactless and non-lithographic conditions [17, 18]. The donor substrate, like glass or unique synthetic materials, is usually regarded as a laser-transparent substrate, which is covered on the side with a specific material. Laser pulses pass through the transparent side of the donor substrate and the coated film on its other side [20]. Particles are expelled from the donor when a particular laser energy threshold is obtained, and accordingly, they are transferred to the acceptor substrate. The laser fluence is mainly responsible for specifying the size of the particle sizes. Indeed, no transfer of material is going to take place under a certain fluence threshold [21]. Increasing the laser fluence causes the asymmetrical sphere forms which are usually characterized by different volumes and frayed edges [22-23].

Copper and gold are interestingly suitable to conduct electricity due to the low resistivity, good conduction and high resistance to corrosion. However, the connection between the noble metals such as Au or Ag and the oxidized layer on the substrate is weak. In some cases, adherence of the film to the substrate is improved by the creation of the oxide layer with the intermediate layer.

Material science, chemistry, electrical and mechanical science, physics, and manufacturing process are all combined in the process of fabrication and

machining thin films for MEMS applications [24- 28]. Some applications such as electrical contact relays need high conduction, reliability, and low resistance. The multilayer thin films are implemented in technologies such as Electro Mechanical Systems. The diffusion layer in metals functions as a diffusion barrier and an adhesive layer [29, 30]. Laser direct write is a novel and reliable technique for thin film deposition, and it is going to be used in industry for large-scale production.

1.3. Scope and structure of the work

There are some different methods of thin film production such as Photolithographic deposition and etching technique which is the most common method for circuit board manufacturing. This technology is a complex and multi-step process which has many disadvantages, for instance, expensive mask requirement and also an etching process which has environmental pollution because of corrosive chemical usages. The other alternative non-lithographic method is a Laser Chemical Vapor Deposition (LCVD) which has a slow deposition rate, and the process should be performed in a vacuum chamber. The Laser-Induced Forward Transfer (LIFT) was a good alternative and advantageous solution as a laser direct write technique in comparison with Photolithography and LCVD. No mask neither vacuum chamber is needed for this process. Vast types of materials, even glass or plastic substrates can be used despite the LCVD process. The transferring process is so fast based on the laser scanning speed, and it can be done in room atmosphere as well. Also, using a direct transferring method to implant conductive micro/nano particles on the silicon wafer substrates has some more advantages such as; high resolution and high flexibility to control particle size.

LIFT process could be a new alternative for deposition technique and also for Under Bump Metallization (UBM) applications. The adherence of the deposited particles on the substrate is so important in the LIFT technique. For that, some different thin films are printed as lines, and tape tests are done on the samples based on its classification standard chart. The general goal of this study was to transfer the Aluminum and Copper particles on the Silicon Wafers and check

how well they have adhered to the substrate. The penetration rate and depth have an essential role which must be considered to have a smooth film. For UBM application, the deposited Copper and Aluminum particles are Electroless plated with nickel and gold to be prepared for the shearing test.

The 80μm SAC305 alloy (Sn 96.5%, Ag 3%, Cu 0.5%) is bumped on the lines with different laser parameters. The shear test is done on the solder balls to check the film quality and the printed lines and also adhesion between solder balls and the printed lines.

Based on the standard shear test, all the bumps were removed with effective shear force, and the trial was passed successfully. Some features such as excellent controllability, agility, and efficiency are used by lasers to remove small amounts of metal from a surface. Different laser factors in this study include laser energy (between 0 and 300 μJ), translation distance (∆, the distance transferred between each laser pulse, 1-20 μm), number of passes through the same position (1-10 passes).

The very first study of this research goes to design a plan for the nano particles transferring system which has been registered as a patent in Europa and USA (US20160346842). Fig.1.2 illustrates the schematic plan of the project. An inert gaseous medium guides nano particles that are ablated from the metal parts or metal powders which are located on the sides of the chamber. The laser focus on the material and the particles will be implemented through the substrate. Then, a laser scanning system ablates the metal parts located at the end of the final chamber. The ablated particles are combined with the liquids, and they are transferred as a drop with a cluster of nano particles. Fig.1.3 shows the particle size produced by laser radiation from the explained setup in Fig.1.2. The nano particles are ablated from the copper in distilled water in nano range. In these tests, some metals such as aluminum, copper, brass, and stainless steel have been used in liquids such as distilled water, ethanol, and glycerin. Nano particles can be synthesized via laser ablation [73].

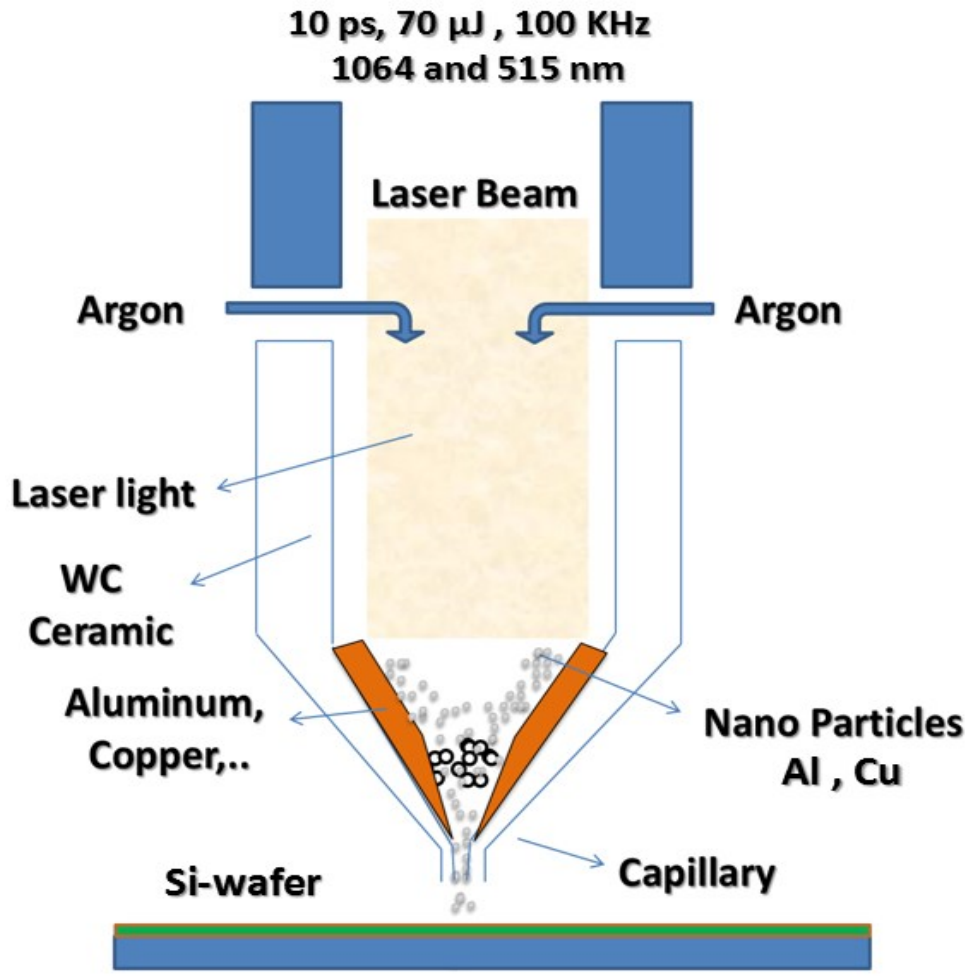

Fig.1.2 Nano Particle Production by Laser radiation

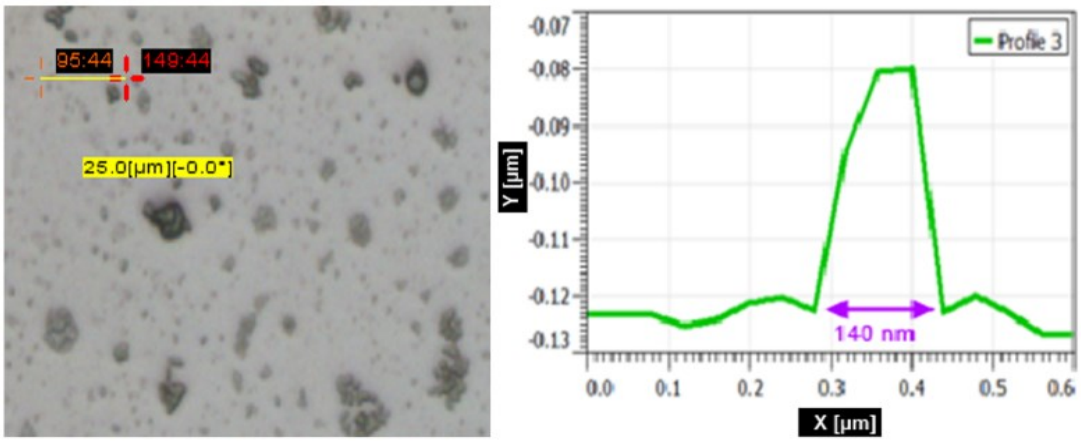

Fig.1.3 Copper ablated in Distilled water- Particle measurement by AFM

Laser Direct Writing techniques, as used in this study, are well suited for prototyping as well as for fast fabrication of small unit numbers. The laser beam

is absorbed through the coated glass to ablate the particles for the next implementation process. The ablation threshold of metal particles correlates with the average dissociation energy of a coated glass and its ability to reflect or absorb ultra-short laser pulse radiation. The parameters are optimized to produce a smooth distribution of micro aluminum particles for layer structure. In this study, the short description of different Laser Direct Writing (LDW) process has been explained. It is essential to inform about the history of this work and technical set up which has been used for the tests and measurements. Different types of suitable adhesion tests are explained to specify or modify the film and coating properties. The short description of electroless nickel plating on aluminum and copper particles is illustrated. Printed particles on silicon wafer substrate are shown by electron microscopy and Focused Ion Beam (FIB). The comparative effect of two lasers with different pulse duration on the samples is shown. The pulse energy, laser shots and also shots overlapping to have a smooth thin layer on the silicon wafer is optimized. Roughness parameters are explained and measured based on different laser parameters on aluminum and copper. Finally, a conclusion of the present work and an outlook of the future technical challenges in adhesion tests and results are given.

2. Laser Direct Write - Theory and deposition technique

The present study aimed to represent a laser transfer process for the direct-write of thin film into different types of substrates. The most common method for thin film production in circuit boards application is to place a conductive layer on a nonconductive layer using a photo-lithographic deposition and etching technique.

There are a lot of deficiencies in this complex and multi-step procedure which have been explained in chapter 1. Mainly, limitations were to minimize the line widths and spacing possible due to the wet chemical processes [31]. Therefore, the flexible and high accurate method was considered for developing a newer, cheaper and safer alternative technology. Printed electronics based on soluble materials such as organic and micro materials have gathered a lot of attention due to various modern devices.

The laser-induced forward transfer (LIFT) is the most important and known process in Laser direct writing technology. The LIFT process consists of three steps. First, a single laser pulse is focused onto the donor material through the transparent donor substrate to ablate the material. Second, the ablated material from the acceptor substrate is transferred to the receiver substrate. Finally, the transferred material gets deposited and adheres onto the acceptor substrate. The results indicated that the process of laser-induced forward transfer processes is implemented to establish the patterns of metallic thin films for some micrometers in width and submicron thicknesses under the right test conditions. A wide spectrum of different results has been reported for variations in wavelength, pulse length, pulse energy, beam profile, and the temporal shape of the pulse, all of which can have significant effects on the process [74-76]. These tests are reported in chapter 5.

2.1. Overview and origin of the LIFT process

The first report regarding the laser-induced forward transfer was a patent which was registered in 1967 by Brisbane et al. Levene et al. performed the earliest

LIFT report of material across in room atmosphere in 1970 [66,67]. Although the primary purpose of the study was to develop a laser-based deposition or marking process, their work also emphasized highlighting the simplicity and high writing speed of the technique. Further, a simple model was also proposed based on melting and vaporizing the transferred material as a result of the laser pulse energy. The method used by the authors was not applied to other types of materials in late 1990. However, the laser-induced forward transfer process, through the metals, was regenerated in 2005. Bohandy et al. (1986) summarized copper metal pattern disposition by using laser forward to transfer inside a vacuum chamber [55]. Two years later, in 1988, the same group developed their process which could be performed in room atmosphere conditions without needing a vacuum chamber.

Bohandy's group invented the laser-induced forward transfer to represent the process and suggested a more detailed but similar model which was designed by Levene to explain the process [141].

In 1991, Gold was utilized to be transferred by Baseman et al. and afterward aluminum was used for deposition by Schultze et al. Kantor et al. achieved success to transfer titanium in 1992 and tungsten in 1994. LIFT was used to print nickel by Sano et al. in 2002. It is worth mentioning that the lasers had a pulse duration of nanoseconds (except microsecond laser which was used to transfer tungsten). Tolbert et al. studied the use of multilayered films and displayed one of the first applications of an absorbing layer in the LIFT process. Based on this method, a thin layer, which is usually a metal, is sputtered on the transparent glass and the material is then transferred [142].

In spite of detailed works about LIFT process on metals, donor films of oxides like AL_2O_3 (Greer et al. 1988), In_2O_3 (Zergioti et al. 1998 and 2002), V_2O_5 (Chakraborty et al. 2007) were additionally utilized for transferring through this procedure. The prior research group that showed the practicality of the LIFT for depositing complex material was from Naval Research Laboratory (NRL) in Washington D.C [143].

Distinctive inorganic compounds have deposited efficiently with this system, for instance: $BaTiO_3$ or NiCr (Chrisey et al. 2000) to manufacture circuit

components for microelectronics or TiO_2 (Kim et al. 2004, 2006) for solar cell applications. Moreover, inorganic/organic materials, like epoxy resin with carbon and silver or carbon/polyepichlorohydrin have additionally been used for the production of polymer thick film resistors and chemical sensors by Moli et al. 2001 and Alberto Pique et al. 2003 respectively.

Nowadays, the LIFT technique has been implemented to transfer different kinds of materials. LIFT is regarded as an interesting technique to fabricate conductive patterns in microelectronics with its wonderful characteristics such as compatibility with a various class of substrates including glass, polymer, ceramics, and silicon.

2.2. Light absorption in material

The material properties utilized within LIFT process, consider absorption coefficient and reflectivity. The medium absorption is characterized by the proportion of absorbed radiant power to the incident radiant power. Reflectance, transmittance, and absorption are specified as ratios of radiant power values, and they are dimensionless. These quantities are used to depict the optical facts in materials. The optical properties of materials rely on the thickness of the sample, surface conditions, and angle of incidence, temperature and polarization impacts. These factors can be classified into optical and thermo-physical properties.

2.2.1 Absorption Coefficient (α):

The absorption coefficient is a function of wavelength (λ). Relinquishing the non-linear impact, the absorption index, α [1/m] of material could be measured by using the formula below.

$$\alpha = \frac{4\pi k}{\lambda} \tag{2.1}$$

k is the extinction factor.

The inverse of α provides information regarding the optical penetration depth of the material. The absorption coefficient of copper expands by long wavelength

because of variation in refractive index and extinction coefficient of the material. Likewise, by ignoring the non-linear and also quantum effect, then the transmission factor (T_f) of a material decline exponentially with the thickness and the equation can be written in the simple term as,

$$T_f = \exp(-\alpha t) \tag{2.2}$$

Where α is absorption coefficient, and t is the thickness of the material.

The absorption coefficient can also change by paying attention to the target temperature. The equation [131, 138] for absorption coefficient as a function of temperature at a determined wavelength is explained for Aluminum in Eq.2.3.

$$\alpha(T) = \sqrt{\frac{4\pi\sigma_0}{\varepsilon_0 \lambda c[1+\beta(T-T_0)]}} \tag{2.3}$$

Where T[K] illustrates temperature at a given position and time, σ_0 [$\Omega^{-1}m^{-1}$] target conductance, ε_0 [Fm^{-1}] permittivity of free space, λ[m] laser wavelength, C[ms^{-1}] laser propagation velocity in a vacuum, $\beta[k^{-1}]$ target temperature coefficient of resistance, T_0[K] initial temperature.

2.2.2 Reflectivity (R)

The Reflectivity of a material is a function of wavelength and temperature. For a determined wavelength, R can be calculated by Eq.2.4.

$$R = \frac{(1-n)^2 + k^2}{(1+n)^2 + k^2} \tag{2.4}$$

Where n and k are refractive index and extinction coefficient of material respectively. Reflectivity is also related to the temperature. It decreases with raising the temperature, and the distinction is visible for longer wavelength.

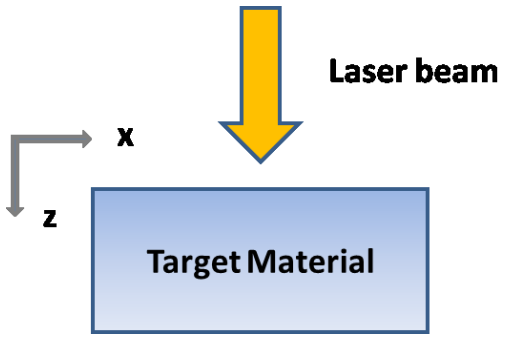

Fig.2.1 normal incidence on a material

The complex refractive index will be explained by Eq.2.5 as

$$n_c = n + ik \tag{2.5}$$

As explained before, n is the refractive index and k is extinction coefficient.

Accepting that the pulsed laser beam has normal impact to the target surface, the electric field intensity inside the material can be defined by Eq. 2.6.

$$E(z,t) = E_0\, exp\left[i\omega(\frac{z}{v} - t)\right] \tag{2.6}$$

where $E(z,t)$ is the electric field intensity in the target, E_0 is the electric field intensity at z = 0, ω is the incident laser angle frequency, v is laser propagation velocity in the target which is specified by Eq.2.7.

$$v = \frac{c}{n_c} \tag{2.7}$$

C is the laser proliferation speed in vacuum. Replacing Eq.(2.5) and Eq.(2.7) in Eq.(2.6) we get the addendum equation:

$$E(z,t) = E_0 \exp(-i\omega t) \exp\left(-i\omega \frac{zn}{c}\right) \exp\left(-\omega \frac{zk}{c}\right) \tag{2.8}$$

In the target material, the laser intensity is equivalent to square of $E(z,t)$ i.e, $I(z,t) = |E(z,t)|^2$, thusly bringing those squares from claiming Eq.2.8 provides for,

$$EE^* = |E_0|^2 \exp(-2\omega \frac{zk}{c}) \tag{2.9}$$

The attenuation of laser intensity in the material is determined by Lambert-Beer law.

$$I(z,t) = (1-R) I_0 \exp(-\alpha z) \tag{2.10}$$

Where I_0 (W/m^2) is the incident laser intensity at a given time, t (s), z (m) is the thickness of the material, R, reflectivity and (m^{-1}) is absorption coefficient which depends on the material, wavelength, and laser intensity. $I(z,t)$ is the intensity at specific times, t and depth, z.

Comparing Eq. 2.9 and 2.10, it could be concluded:

$$\alpha = \frac{2\omega k}{c} = \frac{4\pi \nu k}{c} = \frac{4\pi k}{\lambda} \tag{2.11}$$

Based on Lambert-Beer law, it can be written

$$I(z,t) = (1-R) I_0 \exp(-\frac{4\pi k z}{\lambda})$$

2.3. Heat transfer in LIFT

Laser-induced forward transfer of metal will be commanded to pursue thermal processes; in this manner, laser ablation is substantial to comprehend the physical mechanism of LIFT. The thermal ablation process provides a specific explanation of transfer mechanism throughout LIFT. Based on laser pulse duration, the transfer mechanism during LIFT can be classified into some notable subdivisions, such as photo-thermal, photo-chemical and photo-mechanical [132].

2.3.1 Heat conduction equation

In heat transfer, conduction is described as the transfer of power by diffusion and collisions of particles due to heat gradient. Thermal transit in a material can be essentially explained by Fourier's Law of heat conduction [133]. It means that "the heat transfer via material is proportional to the negative temperature gradient". Assuming that heat flows regularly to the surface area, Eq.2.12 defines the heat conduction equation mathematically in differential form.

$$\frac{dQ}{dt} = -k\nabla T \tag{2.12}$$

Where ∇T [W/m.K] coefficient is thermal conductivity, Q [W/m^2] is the total heat flux, dQ/dt is the flow rate of heat and ∇ is the gradient operator.

Laser irradiation transfers energy in the material resulting in heat and therefore a localized change in temperature. The quantity of energy transferred inside the material can be explained as Enthalpy, H. The temperature change, Δ, due to small variation in enthalpy, ΔH, among a mass of material, m [kg], is given by Eq.2.13.

$$\Delta H = mc_p\Delta T \tag{2.13}$$

The quantity c_p [J/kg.K] is the particular heat at the steady pressure. This can be illustrated concerning volume by introducing the density, ρ [kg/m^3] of the material and represented by Eq. 2.14 below.

$$\Delta H_v = \rho c_p\Delta T \tag{2.14}$$

The negative sign in Eq. 2.12 is illustrative of heat flows from the hot end to the

cold end to the thermal slope. Accordingly, heat transfer among the small volume element, ΔV, have to either flow to the other direction or alternate the enthalpy of the element. This heat transference can be mathematically represented with the help of divergence factor. Since heat is a relative quantity, it is sufficient to take the dot product which is described by Eq. 2.15.

$$\nabla.\frac{dQ}{dt} = -\frac{dH_v}{dt} \tag{2.15}$$

The laser source, S(z, t) is used as an additional source of energy which is distributed in the z-direction, and it causes enthalpy variation. Therefore, Eq.2.15 modifies to Eq.2.16.

$$S(z,t) - \nabla.\frac{dQ}{dt} = \frac{dH_v}{dt} \tag{2.16}$$

Using Eq.2.12 and expanding left side of Eq. 2.15 we get Eq.2.17

$$-\nabla.\frac{dQ}{dt} = \nabla.(k.\nabla T) = k.\nabla^2\mathrm{T} + \nabla\mathrm{k}\,.\nabla\mathrm{T} \tag{2.17}$$

Using Eq.2.14, 2.15 and 2.16 in Cartesian coordinates, the heat diffusion equation in three dimensions can be specified by Eq.2.18.

$$\frac{dT}{dt} = \frac{k}{\rho c_p}\left[\frac{\partial^2 T}{\partial x^2} + \frac{\partial^2 T}{\partial y^2} + \frac{\partial^2 T}{\partial z^2}\right] + \frac{1}{\rho c_p}\left[\frac{\partial k}{\partial x}.\frac{\partial T}{\partial x} + \frac{\partial k}{\partial y}.\frac{\partial T}{\partial y} + \frac{\partial k}{\partial z}.\frac{\partial T}{\partial z}\right] + \frac{S(z,t)}{\rho c_p} \tag{2.18}$$

Assuming that the intensity of the laser beam at a time (t[s]) is $I_0(0, t)$ [W/m^2], the exponential decline of the intensity into the surface can be written as,

$$I(z,t) = (1-R)I_0(0,t)\exp(-\alpha z) \tag{2.19}$$

So the source term can be represented by Eq.2.20.

$$S(z,t) = \alpha * I(z,t) \tag{2.20}$$

The analytical and scalar models of heating a material by using a laser beam as a heat origin require solving Eq.2.18, by considering the source term which was described by Eq.2.20. Assuming that the laser beam is perpendicular to the objective material, the one dimensional of heat formula depicts temperature by paying attention to time and depth which is represented by Eq.2.21.

$$\Delta T(z,t) = 2(1-R)\alpha I_0 \frac{\tau}{\pi k\rho C}\, ierfc\, \frac{z}{2\sqrt{\frac{k\tau}{\rho C}}} \tag{2.21}$$

Where *ierfc* is called the integral complementary error characteristic and τ is the laser irradiation time. From Eq.2.21, it can be considered that, if the thickness of

the material (z) is bigger or equal to the thermal penetration depth and simultaneously the laser energy is high enough to melt the material, then the ascent in temperature is appropriate to $\sqrt{\tau}$. This is an executive parameter for a variety of various materials such as metals, semiconductors, and dielectrics for a laser pulse length less than or equal to 10 picoseconds [134].

2.3.2 Laser-induced temperature change

If the laser pulse duration is longer than the electron-phonon thermal relaxation time, it is assumed that the electrons and the lattice are at the same temperature since the absorbed laser energy transformed immediately into heat. The laser heating process can be explained using one-step heating process, neglecting to the convective and radiative losses and the microscopic photon-electron and electron-phonon interactions. The laser pulse length is in the order of nanoseconds to few tens of picosecond. It can be represented mathematically by using Eq.2.18, and the final term is given by Eq.2.22 below.

$$C(T).\frac{\partial T}{\partial t} = \nabla.(k.\nabla T) + S(z,t) \tag{2.22}$$

When the laser-pulse length is equal or less than the electron-phonon thermal relaxation time, the electron and phonon regulation processes are separated. The electrons and the lattice are not in thermal balance and ought to be divided into two different sub-systems. A two-step heating method developed by Anisimov et al [135] that used a model for heating mechanism and it can be categorized as,

(i) Absorption of laser (photon) energy with the aid of electrons

(ii) Heating of lattice via electron-phonon coupling

Mathematically, this model is illustrated by Eq. 2.23 and Eq.2.24 respectively [137].

$$C_e\,(T_e).\frac{\partial T_e}{\partial t} = \nabla.(k.\nabla T_e) - G(T_e - T_l) + A \tag{2.23}$$

$$C_e C_l(T_l).\frac{\partial T_1}{\partial t} = G(T_e - T_l) \tag{2.24}$$

Where G is electron-phonon coupling factor, T_e is electron temperature and T_l is

lattice temperature. The above equation is a popular as parabolic two-temperature model.

In the case of metallic material, the heat flux is conveyed in general by the electrons; therefore it is reasonable to omit energy transport by phonons. If $T_e < T_F$ (Fermi temperature, normally in the range of 104 K) where $T_F = \frac{\varepsilon_F}{k_B}$, (ε_F is Fermi energy and k_B is the Boltzmann constant), thus the electronic heat capacity is proportional to electron temperature

$$C_e(T_e) = \gamma T_e \tag{2.25}$$

γ[J/m^3K^2] is the electronic heat capacity. The value of G can be derived using free electron theory, and it is determined by Eq.2.26.

$$G = \frac{\pi^2 m_e n_e v^2}{6\tau(T_e)T_e} \tag{2.26}$$

Where τ (T_e) is electron mean free time between collisions at temperature T_e [K], m_e [kg], electron mass, n_e [m^{-3}] , number density, v [ms^{-1}] , sound velocity.

2.3.3 Heat diffusion equation in 3-dimensions

(a): From Eq.2.16 and Eq.2.17 we comprehend

$$S(z,t) + \nabla.(k.\nabla T) = \frac{dHv}{dt} \tag{2.27}$$

Substituting Eq.2.14 in Eq.2.27, we can realize

$$S(z,t) + \nabla.(k.\nabla T) = \rho C_p \frac{dT}{dt} \tag{2.28}$$

By reordering the terms, we perceive Eq.2.29

$$\frac{dT}{dt} = \frac{k}{\rho C_p}\nabla^2 T + \frac{1}{\rho C_p}(\nabla k.\nabla T) + \frac{S(z,t)}{\rho C_p} \tag{2.29}$$

(b): The incorporated integral error function will be given by,

$$ierfc(z) = \int_z^\infty erfc(\xi)d\xi \tag{2.30}$$

Where,

$$erfc(z) = 1 - \mathrm{erf}(z) = 1 - \frac{2}{\pi}\int_0^z e^{-t^2}\,dt \tag{2.31}$$

In case of lasers with nanosecond pulse durations, it is a proper approximation to use a one-step heating procedure. The electron-phonon thermal relaxation

time is so short in comparison with the laser pulse length and it obtains enough time to make local thermal balance with the lattice.

It is assumed that the laser energy is converted into heat immediately. Eq.2.32 can represent the heat transfer by using a nanosecond to lots of picosecond pulse lengths.

$$\rho C \frac{\partial T}{\partial t} = \nabla.(k.\nabla T) + Q(x,y,t) \quad (2.32)$$

where Q(x,y,t) [W/m^3] is the laser energy density exerted to the target material. It is a factor of laser intensity and Lambert-Beer law which proved by Eq.2.33 below.

$$Q(x,y,t) = I(x,t) * (1-R) * \alpha * \exp(-\alpha * y) \quad (2.33)$$

Here I(x,t) [W/m^2] is the laser intensity factor. A Gaussian laser pulse in a temporal and spatial area is utilized, and therefore it can be modeled in mathematical form as explained in [133] and represented by Eq.2.34 below.

$$I(x,t) = I_0 * \exp\left(-\frac{x^2}{r^2}\right) * \exp\left(-\frac{3.5(t-\tau)^2}{\tau^2}\right) \quad (2.34)$$

The incident laser intensity I_0 [W/m^2] can be declared by Eq.2.35.

$$I_0 = \frac{E}{\tau * A} \quad (2.35)$$

The optical properties of the materials (R and α) are a characteristic factor of wavelength and also temperature. Also the thermo-physical properties, for instance; thermal conductivity, heat capacity, and material density can react differently at high temperatures.

2.3.4 Surface heating

There is another method to formulate laser heating. In this procedure, the heat is made on the surface. The laser intensity is performed as the boundary situation in the irradiated target area and Eq.2.32 modified as Eq.2.36 below.

$$\rho C \frac{\partial T}{\partial t} = \nabla.(k.\nabla T) \quad (2.36)$$

And the boundary condition at the irradiated surface is expressed by

$$n.(k\nabla T) = (1-R) * I(x,t) \quad (2.37)$$

It is acknowledged that, the peak surface temperature associated with some parameters as laser fluence, donor thickness, and pulse width. It can be concluded that when a nanosecond laser pulse is utilized, the transferring process is a thermal procedure and the pulse energy converted into heat immediately. Raising the laser energy density causes linear amplification in the peak temperature of the material which shows in melting and boiling [139, 140]. Furthermore, a thicker donor layer (1-5 μm) requires more energy to melt compared to thin donor layer (100-500 nm). While using ultrashort laser pulses, it is pointed out that, physical processes such as photochemical action play an important role with the thermal proceeding. Thicker layer in donor permits more heat rising and the temperature across is comparable to a very thin layer. The application of theory is described in chapter 5.

2.4. Description of deposition technique

The source called ''the target, donor, or ribbon'' in the literature, is regarded as a laser-transparent substrate, coated with the copper and aluminum materials. Laser pulses are distributed through the transparent substrate and absorbed by the thin coated layer. The material is ablated from the donor and ejected toward the receiving substrate. The laser beam enables the transferring of the material from a source to the receiving substrate to establish a complex pattern in three dimensions. Neither particular vacuum nor clean room equipment is required for this process, and it can be performed under standard laboratory conditions, which is contrary to other film deposition and patterning techniques. Despite the different thin film production techniques, these approaches are based on the principle of preserving the transferred material properties rather than a chemical reaction or other material modification to make the deposition.

The combination of a high power laser with direct write techniques can generate features without any physical contact between the desired material and the substrates. This will lead few methods to share the capabilities of laser direct write by modifying materials with many different length scales from micrometer to millimeter. The desired pattern of LDW can be built in both two and three dimensions on differently shaped surfaces. Laser direct writing can be regarded

as a rapid prototyping tool, and it could be applied immediately without building any masks. The main features of LDW systems include three subsystems: (1) laser source, (2) beam transmission system and (3) substrate/target mounting system. The laser source is the most critical part of any LDW process. Typical experiments and applications are implemented from ultrafast pulsed lasers to continuous wave (CW) systems using solid-state, gas, fiber, semiconductor, etc. It should be regarded to choose a suitable source, for the main interactions of lasers with the desired material. Knowledge of the laser pulse duration, wavelength, beam divergence, and other optical and temporal features is required to determine the energy absorption and the material reaction.

Laser direct-write is regarded as a comprehensive term which includes laser-based modification, subtraction and addition processes which can generate material patters directly on substrates without using lithography or masks. The effect of the laser interaction on the substrate, or any other surfaces, can lead to the modification of the material such as melting, sintering, and ablating material. The use of laser removal for micro-machining is related to subtractive LDW to generate the desired pattern by either moving substrate or the laser beam. The LDW technique, as a “functional materials printer,” plays an effective role regarding additive mode. Therefore, the processes of laser-forward transfer are implemented for metal deposition, oxides, polymers and composites under surrounding conditions into any surface. Finally, according to experimental requirements or industrial applications, the substrate is mounted and can be manipulated in many directions to accomplish the desired result. There is a vast range of LDW processes. In this regard, they are divided into three main categories such as laser direct write subtraction (LDWS) which removes by ablation; laser direct-write modification (LDWM) which modify the material to generate a proper effect; and laser direct-write addition (LDWA), which add the material from the laser [32-37].

2.5. Laser Direct-Write Subtraction (LDWS)

LDWS is the most prevalent type of laser direct-write, and it involves the processes which would have some results, including photochemical, photo-

thermal and photo-physical ablation on a target surface, and finally, it has directly led to the desired features. Common processes include laser scribing, cutting, drilling, or etching to generate structures or holes in materials under controlled atmospheres. This technique is used in different industrial applications such as high throughput fabrications, inkjet, and fuel injection fabrication and high-resolution manufacturing and the texturing of implantable biomaterials. Chemically assisted techniques such as laser drilling ceramics and Laser-Induced Backside Wet Etching (LIBWE) of glass are more recently developed in LDWS. In fact, laser cleaning can be regarded as a controlled LDWS process. The thermal interactions can lead to material removal, regarding primarily material features and the laser pulse duration. These actions directly influenced the quality of the features. For example, a heat affected zone (HAZ) aims to happen in the surrounded areas of removing materials. The formation of a HAZ, which is generated by thermal and multiphoton absorption process, can be reduced by ultrafast lasers and faster scribing speed [38, 39].

2.6. Laser Direct-Write Modification (LDWM)

In LDWM, the incident laser energy is usually not appropriate for producing ablative effects; however, it is suitable for a permanent change in the material features. Typically, these processes, which provide a structural or chemical change in the material, depend on thermal modifications.

The rewritable compact disc is a typical example of these processes which is a diode laser that generates a phase transition between crystalline and amorphous material in it [40]. In many LDWM applications, a specific optical response is required for the desired material beyond simple thermal effects. Optically induced defects or changes in mechanical properties can cause several non-ablative material modifications. Alternatively, many deficiencies in the photo-etch-able glass, ceramics or other optical materials through single and multiphoton mechanisms can be generated by LDW. These mechanisms can implement new applications in optical storage, photonic devices, and microfluidics [41-43].

2.7. Laser Direct-Write Addition (LDWA)

LDWA is probably the most recent technology of the laser direct-write techniques. In this method, many laser-induced processes are implemented to add the material to a substrate. Many techniques are extracted from the laser-induced forward transfer (LIFT); a sacrificial substrate of solid metal is placed in the vicinity of the second substrate to obtain the removed material. The desired material absorbed the incident laser and caused local evaporation. This vapor moved toward the receiving substrate as an individual three-dimensional pixel or voxel of solid material. This general technique is more useful than other additive direct-write processes, because these laser approaches do not need to make connections between the depositing material and a nozzle, and can transfer many materials. Alternatively, LDW techniques can depend on the laser parameters to move particles or clusters into precise positions, or on chemical changes in liquids and gases to generate patterns.

The laser-induced forward transfer (LIFT) was first used to depose copper metal patterns inside a vacuum chamber. Laser pulses emphasized the back surface of a source substrate involving a thin copper film, generating a voxel of transferring material on the facing substrate. Based on the proposed model for LIFT, the laser pulse heats the film interface at the source substrate. The heat will be distributed through the film, in which the material is superheated at the interface beyond its boiling point and the pressure resulted from vapor-induced pressure ejects the material to the acceptor substrate. The LIFT technique is widespread, which is utilized in a variety of solid film materials, especially Cu, Ag, Al, W and Cr. Similarly, multilayered structures can also be deposited. Traditional LIFT is an appropriate process for transferring simple materials which are evaporated or melted. However, regarding complex materials, it is necessary to preserve the properties of the material which the modifications are required for the process.

Fig.2.2 illustrates a schematic plan for the fundamental elements which are necessary for the laser forward-transfer mechanism. In all sections, the substrates are shown in yellow.

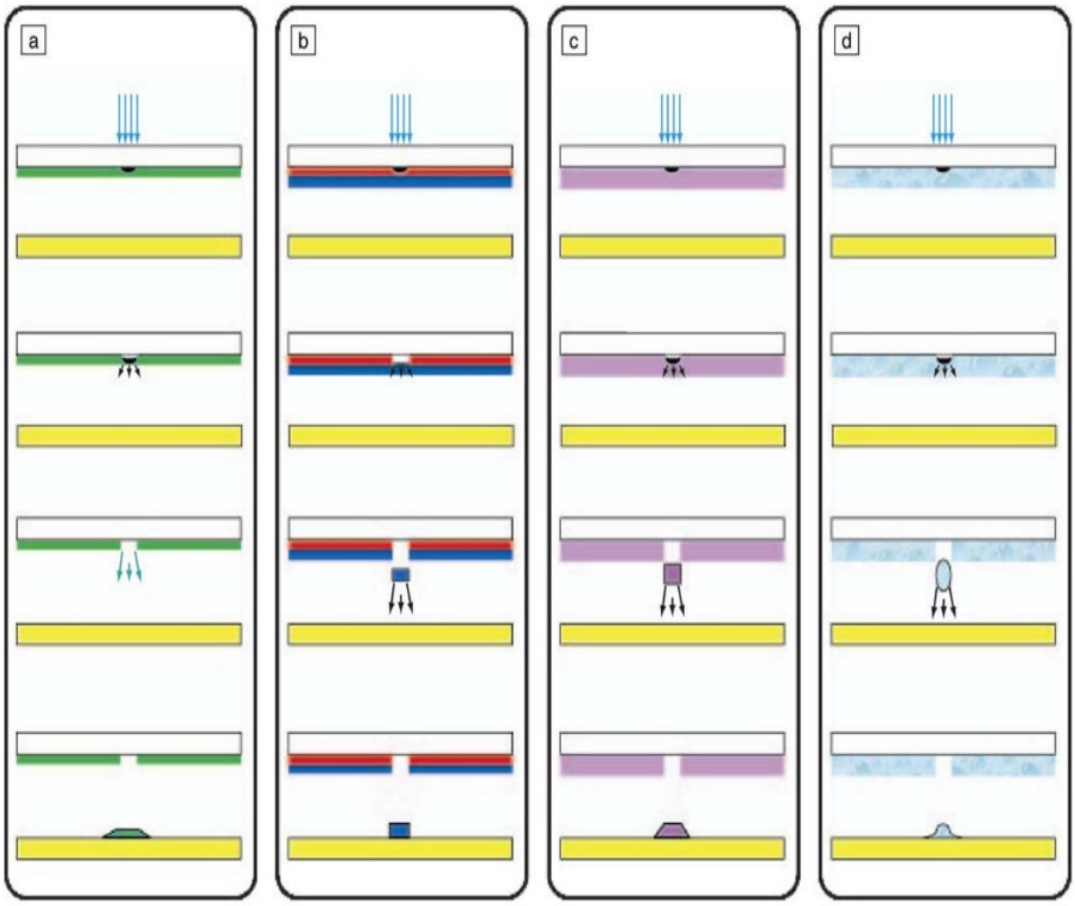

Fig.2.2 Schematic illustration of laser direct-write addition (LDWA); (a) Traditional LIFT (b), LIFT with dynamic release layer (DRL), (c) Matrix-assisted pulsed laser evaporation (MAPLE) and (d) LDW of rheological systems [15]

Having a closer look at Fig.2.2, the first column (a) belongs to the traditional Laser-Induced forward transfer. The laser vaporizes the entire thin film in the region of laser focus. Traditional LIFT technology is adequate for transferring functional materials that can be evaporated or melted, however, for complex materials, the modification to the process should be considered. In Figures 2.2(b)-2.2(d), all three of these modifications signify an essential difference from usual LIFT technology, as simple materials which are transferred without vaporization, as ought to affect on their physical, mechanical, or chemical properties after condensation on the receiving substrate. In the second column (b), the dynamic layer is vaporized and propels the film forward. During LDW+, the vapor layer generates sufficient force to shear a voxel of material from the second layer and towards the receiving substrate. The main superiority of this

method is that the deposited materials have not been evaporated or melted, and do not obtain considerable power from the laser or a significant rise in temperature during transfer. Another version concerning the LIFT method is to transfer different materials in powder shape mixed with an organic or polymer binder. These combos are utilized as a smooth coating on the donor substrate. During the MAPLE-DW (Matrix-assisted pulsed laser evaporation direct-write) in the third column, the binder absorbs the laser energy, and it is vaporized. This leaves the material unharmed utilizing the laser energy and permits for transferring to the acceptor substrate. In Fig.2.2d, the material is dissolved in a liquid to form the ink, which is propagated on the donor substrate. This related method is according to get rid of solid-phase binder materials toward multiphase and multicomponent liquid systems. The shape of the deposited particles can vary in the different methods [15].

During LDW, an interaction takes place between the laser pulse and the absorbing layer, called the dynamic release layer (DRL). It leads to the vaporization which takes place in LIFT similarly. Transferring different materials in powder form integrated with an organic or polymer binder is regarded as another modification of the LIFT process.

It is evident that some laser parameters including fluence, pulse duration, pulse shape, and wavelength play an essential role in the LDW process. Also, some coated parameters such as the composition, thickness, viscosity, the content of solids, and the particle size of solids can remarkably influence in the ability to transfer a particular fluid, voxel or nano particles. Furthermore, some other parameters should be taken into consideration such as the distance between the donor and receiving substrates, the material of the substrate, the temperature of the substrate, and the chemistry of the surface and the morphology of the substrate. LDW is utilized for depositing materials for fabricating micro power sources and also to transfer complex materials including ultra-capacitors, batteries, and solar cells [44, 45].

According to the new presented techniques, direct deposition is possible for the materials such as metallic nano-inks from a donor substrate to the receiving substrate while keeping the size and form of the area similar as the laser

transfer pulse demonstrated it. The lines used in this technique have the same scale as lithographic techniques established them. The application of lithographic techniques which necessitates the vacuum deposition of a thin film and its subsequent etching to attain the desired pattern is not practical. Like a laser chemical vapor deposition (LCVD), some direct-write processes can generate such thin film patterns; however, they are limited by their rate of slow deposition, narrow selection of materials, and complexity such as the need for vacuum operation [46, 47]. The new technique of laser direct-write, entitled as "laser decal transfer" which is regarded as an appropriate technique for the production of the thin film by considering its additive capacity under atmospheric conditions. The placement of highly precise transfer, adaptability with different electronic materials and the resolutions of arranging in few micrometers are some of the advantages. The patterns of the thin film are laser cured in-situ after the laser is printed to obtain the favorable properties such as adhesion, chemical resistance, and electrical conductivity.

2.8. Physical layer considerations

The deposition of the laser energy into a solid is usually observed in the quantum-mechanical forms of particle transitions. After irradiation with short laser pulses, re-solidification of molten material has occurred in two stages of amorphization and re-crystallization [48]. The amount of energy left in the material (the temperature) and the next cooling velocity has caused the differences. The process relies on the number of pulses implemented to the same spot and the laser fluence. The ambient environment is the primary factor in the build process and forms the microstructures [49]. Different parts of amorphization and crystallization were distinguished by some early experiments on laser-induced modification of silicon surface. Fig.2.3 illustrates the ultra-fast laser pulses and their threshold fluence.

The ablation threshold is determined by the thermal properties of the materials like; heat capacity, thermal conductivity, etc. Ablation will occur when the incident power density is high enough to set up a thermal gradient in the material that is sufficiently high to ensure minimal melting and complete

subsequent vaporization of the molten phase. Surface defects and contamination can drastically reduce the ablation threshold.

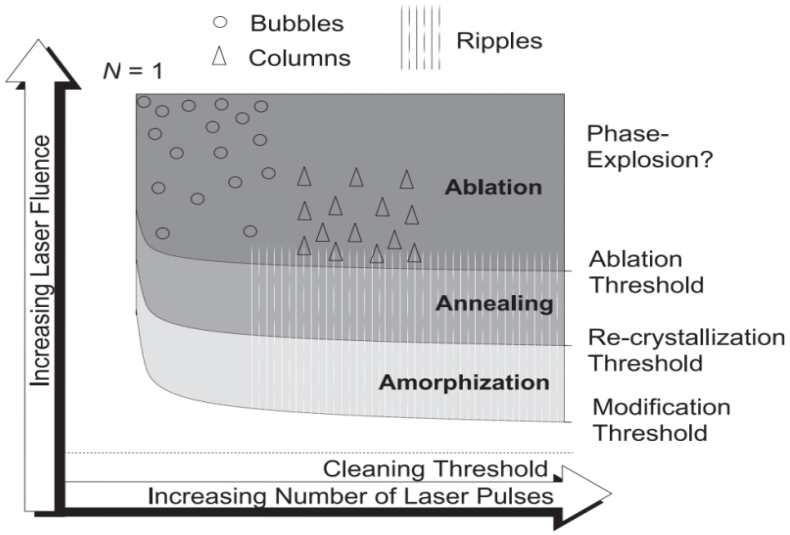

Fig.2.3 Physical processes during the modification of silicon [50]

Fig.2.4 summarizes the morphological features (bubbles, ripples, micro columns) after irradiation of the silicon surface with linear polarization of femtosecond laser pulses of typically 100 fs duration.

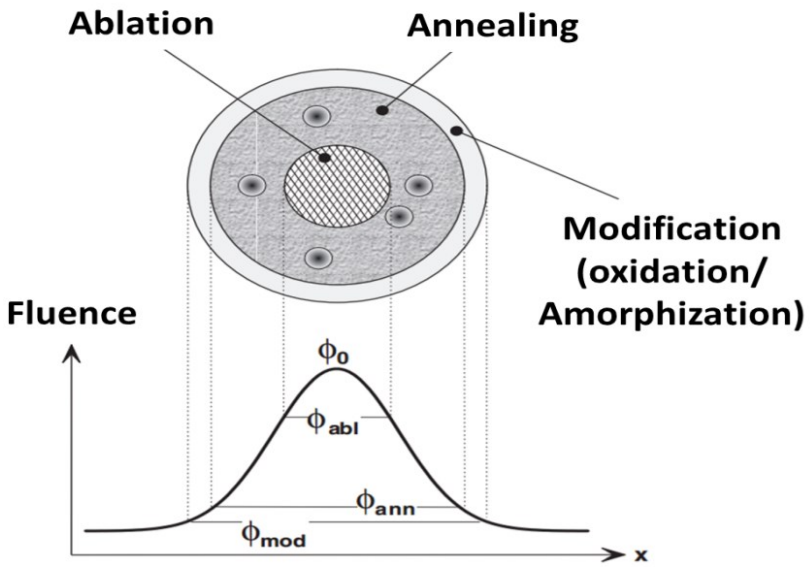

Fig.2.4 Scheme of the different morphological phenomena [50]

A specific method of these surface patterns production was provided by lasers because they are capable of modifying physical and chemical properties over multiple length scales.

Traditional lithographic patterning cannot efficiently perform fast and precise micro-sized grooves on non-planar surfaces. Recent developments in photolithography helped to accomplish grooves on many polymeric substrates to be applied in microelectronics processing [51]. While photolithography helps to study topology on a single size precisely, other techniques, such as lasers direct writing, can easily facilitate to implant surfaces and produce features on multiple scales [52]. LDW can prepare a fast and easy method to change metal surfaces and improve the growth and adhesion of cells [53, 54]. It paves the way for the direct writing of materials, including metallic nano-inks or material particles from a donor to a receiving substrate that the size and shape of the area are fixed, and it can create continuous and homogenous metallic lines. When the transferring process is done, the lines are thermally preserved by a CW laser which can be used for electrical conduction. This modern laser direct-write technique is usually appropriate for the application of digital micro-fabrication, which is implemented for developing, customizing, modifying and repairing microelectronic circuits.

Laser chemical vapor deposition and laser direct-write are mentioned as some examples of direct-write techniques. Altogether, these non-lithographic methods can pave the way for depositing separate 3-dimensional pixels of any material in the pre-defined locations to establish a given pattern by extracting little waste materials. LIFT has some distinct advantages over its chemical counterpart LCVD (Laser Chemical Vapor Deposition). First, since no chemical reaction is involved, the purity of the microelectronic material is retained. Second, LIFT can be performed under ambient atmospheric conditions; no expensive vacuum deposition apparatus and complicated gas handling systems are required [61]. Third, LIFT is a much faster technique than LCVD [62]. Fourth, the LIFT technique is location sensitive. One of the main disadvantages of LIFT is that it can cause the transferred material to be the vaporized or melted. Due to phase transformations, oxidation, decomposition, the formation of undesired phases and poor uniformity play a negative role in depositing the quality through LIFT.

Fig.2.5 shows four different stages in permeation process: adsorption, absorption, diffusion, and desorption. The particles are indicated in blue and the

solid membrane in orange. The studies about adhesion utilize different methods of thought.

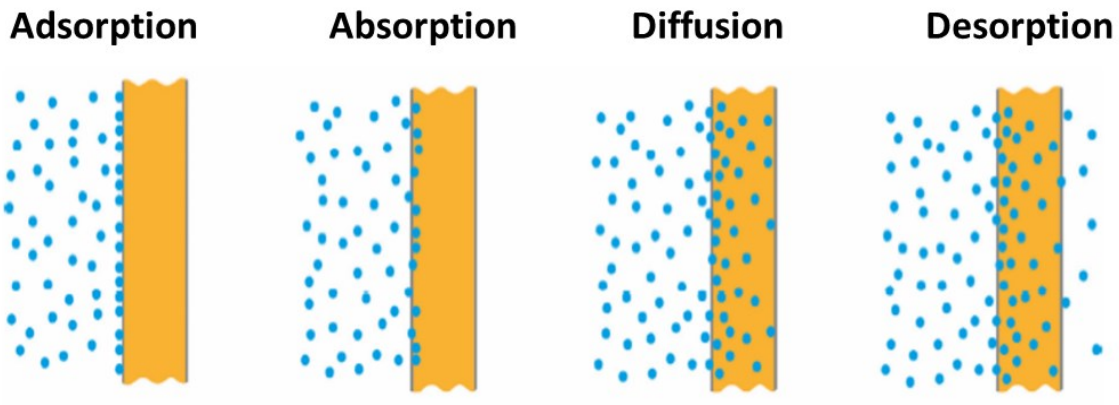

Fig.2.5 Illustration of the permeation process in laser direct writing of particles in the four different stages [124]

This assortment of the methodology is accentuated toward the fact that numerous hypothetical models of adhesion have been proposed thoroughly. One of the most critical factors that impact the bonds will be the structure of the joint. All adhesive bonds include molecules in good contact and also physical adsorption which should be considered. A critical requirement for the successful utilization of adhesion technique is that the particular parts are suitability planned for bonding. Structure treatment will be the second factor that impacts the adherence. It is essential to carry out specific pre-treatment to guarantee an excellent adhesion. The bonding of an adhesive to an object or a surface is the entirety of various mechanical, physical and chemical forces that impact each other.

2.9. Evolution of the LIFT

Traditional LIFT processes depend on melting, the laser pulse energy and the vaporization of the material being transferred. Different versions of the LIFT process were developed to decrease the additional heating of the tolerating material transfer [56]. The second variety of LIFT hinges more on the interaction between the laser pulse and fluids in the donor substrate, rather than relying on solids. The fluid might be a simple liquid or a more complex system in which the

solids are in a solvent, such as ink [57]. Regarding ink, the transferred material is moved by the propelled fluid which is achieved to the receiving substrate accordingly. The illustration of a new approach to LIFT, inks or pastes are regarded as the main feature of the laser transfer systems. This representation is done by reducing the coating layer in the donor substrate as the laser pulse demonstrates it. Regarding that, the different variety and the vast number of variables influencing the process of laser transfer, a simple plan explains the behavior of LIFT with fluids as shown in Fig.2.6. This straightforward jetting transfer represents what is observed in most conditions.

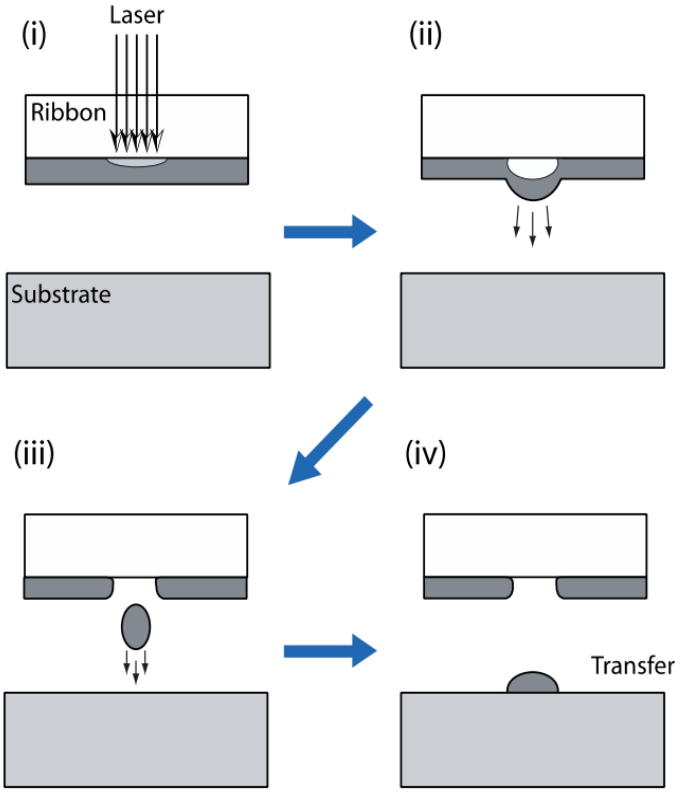

Fig.2.6 Schematic representation of the LIFT steps [55]

As it can be seen in Fig.2.6, the schematic diagram of the steps in LIFT about liquid films is illustrated. In section (i), the laser pulse is absorbed in the ribbon interface. In part (ii), the absorption of the laser pulse heats the solvent and forms a bubble. (iii) Shows a droplet or voxel of fluid is ejected away from the donor substrate towards the receiving substrate. In (iv), the removed material is collected on the receiving substrate. Spherical droplets are generated from the

donor substrate when the threshold for fluence transfer is attained. If there is an increase in fluence, the irregular droplets are established. It is worth noting that such features are impossible to achieve with inkjet, where the nozzle determines the voxel size, in which the deposition of the viscosity and chemical reactivity of the fluids can take place. In general, the dimensions of the jetted droplets are different by adapting the density or fluence of the laser pulse energy. When there is an optimum threshold level of the fluence transfer, well defined spherical droplets are established as they move away from the donor substrate.

2.10. Industrial application of LIFT

Practical application of laser-induced forward transfer is still in early stages; however vast technologies have been demonstrated for different utilization. A rapid method is required in writing to utilize LIFT processes in large-scale industrial uses like roll-to-roll (R2R) deposition. Further, an unchanging voxel size should take place during transfers with accurate placement into the receiving substrate. For this purpose, DI Projekt AG designed the Lasersonic technique to represent the record of high write speeds with LIFT, in Aurentum GMBH. The industrial-grade Lasersonic system implements a 300W CW fiber laser beam (λ: 1064 nm) which is regulated by an acoustic-optical modulator, and it is focused by using f-theta lens system at the surface and then at the absorption layer. The interaction among droplets should take place at this high speed of transferring and high resolution of the pixel. Hennig et al. emphasized different strategies used to alleviate these effects [58], and both groups who focused their attention on this work in Barcelona [59] and Princeton [60] studied the spatial and temporal dynamics of the interactions among bubbles established in a specific condition.

2.11. The future of LIFT

Using spatial light modulators, by commercial digital micro mirror devices (DMDs) can adjust the dynamic of the size and shape of the laser pulse, and as

a result, they can enable to print reconfigurable voxels. In fact, it can be noted that these voxels can be printed dynamically using spatial adjustment of the laser pulse in LDT, and a micro mirror-based spatial light modulator. It means that the size and the shape of voxels or particles can be different from the previous ones; therefore, a full design is generated by faster pattern production and overall optimization of the deposition sequence. In this regard, a disruptive technology combined LDT with DMDs in digital fabrication which is implemented to change a serial process into a parallel deposition technique.

Certain kinds of patterns are produced by integrating LIFT processes with spatially modulated laser pulses, and these models can be produced in some other direct-write techniques. Grid printing in solar cell application is one of the examples. As it has been noticed in inkjet or traditional LIFT, the overlapping lines will be inflated and lose the resolution in a grid to print excessive material in the intersections. It is possible to write the whole grid pattern with LDT and a DMD shaped laser beam with one single laser pulse.

The laser pulse is arranged to create the grid by the DMD; while it ensures the shape and pattern of the laser pulse by LDT. From an applications viewpoint, these LDT examples are integrated with fast writing, which can be achieved by the Lasersonic process. This procedure represents the future applications for LIFT in printed electronics, device interconnects, circuit repairs, and when they are integrated with a lot of functional inks and pastes. Since the early studies conducted on laser interactions with materials, direct-write techniques have been essential and related techniques were used to modify, add, and subtract materials for a wide range of systems and applications including metal cutting and welding. Direct-write processing indicates on any procedures that can create a pattern on a surface in a consecutive or “spot-by-spot” way. At first, it may be considered that direct-write approaches are slower or less significant than these parallelized approaches. However, the direct-write approach helps material properties with high resolution to be controlled precisely, and it also helps impossible or impractical structures to match with traditional parallel techniques.

In a typical LIFT process, the size of the transfer spot is determined by the laser beam characteristics and the thickness of the donor film, with a Gaussian beam profile usually used. The spot size is proportional to the area of the incident beam above the transfer energy threshold [47]. We can achieve the minimum transfer spot size by reducing the donor film thickness and lowering the incident fluence to the transfer threshold.

Regarding the types of micro fabrication techniques, there are two different approaches to fulfill the requirements. The first one is the so-called pattern-transfer techniques [64]. In this set of procedures, the pattern is produced onto the substrate, and all its elements are transferred at the same time. The most representative technologies in pattern-transfer techniques are photolithography and micro contact printing. The mask or mold is previously produced from the designed pattern in these methods, and it is directly transferred from this element. This technique is suitable for large-scale applications because the parallel production of identical units is allowed here [65].

It should be noted that the creation of a mask is expensive and time-consuming, especially when a rapid transfer between design and production is needed, which usually happens in the first stages of the development of the product. Furthermore, pattern transfer techniques are complicated and restricted (generally to the utilization of rigid flat substrates). A different convenient approach entitled as direct-writing techniques (DW) is suitable for fast prototyping applications and the cases required for high versatility. They are naturally serial, that means the various divisions of the pattern are sequentially conveyed one after another. This technique provides higher flexibility than pattern-transfer techniques [68-72].

After the publications of Bohandy et al., LIFT was accepted as a technique to deposit inorganic materials, especially metals, from solid donor films. LIFT was implemented to successfully transfer gold, aluminum, titanium, tungsten, nickel, and germanium. Lasers with different wavelengths, ranging from ultraviolet to infrared were used to conduct these processes. Fig.2.7 illustrates the principle of the LIFT process. Regarding the mechanisms of the LIFT process of solid donor films, it should be concerned that there are various possible scenarios

based on the incident laser fluence. As it has been explained before, Bohandy et al. (1986) proposed a mechanism followed by fluence which leads to melting and also vaporization of the interface material. When the material at the interface achieves the boiling temperature, a high-pressure vapor pocket is formed and then moves the molten material towards the receptor substrate. This explanation is supported by evidence of molten and re-solidified material on the deposited features, while this mechanism is responsible for feature deposition in most studies conducted on the LIFT of solids. The irradiated material can be vaporized entirely at high enough laser fluence. The molten material reaches its boiling temperature, and thus the material is vaporized. When there is a decrease in the size and an increase in performance of semiconductor devices, the capacity for connecting smaller pads with ultra-thin pitch (< 50 μm) and reducing the interconnect height (< 60 μm) is necessary for many microelectronic, optoelectronic and bioelectronics instruments.

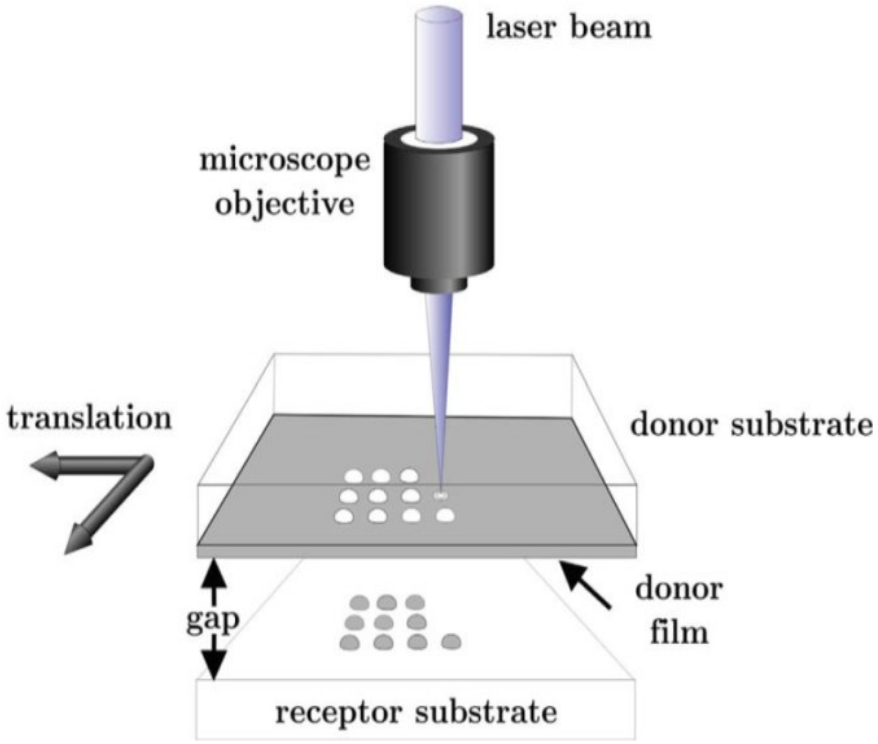

Fig.2.7 Scheme of the principle of operation of the LIFT technique [56]

3. Adhesion mechanism in the LIFT process

Adhesion has played a significant role in thin film technology which usually has 1 μm and 50 nm thickness in some applications. Adherence is very influential in specifying the durability of thin film devices such as in microelectronic circuits. Some factors can play a significant role in the adhesion of thin films such as substrate cleaning, contamination removal, deposition and penetration rate, film thickness, types of substrate, purity of source material, substrate temperature, the pressure during deposition, etc.

The word "adhesion" generally means sticking two materials together in such a way that the term "autohesion" or "homohesion" is applied if the materials are the same and they are regarded as "heterohesion" when dissimilar materials are used. Adhesion is measured based on the maximum required force per unit area when the materials are separated. Alternatively, it is considered as the action of separating the two materials from each other. Adhesion forces formulate the performance of thin films as a result. The film structure is aggregated when the cohesion energy is more than the adhesion energy. In addition, the stability of thin films relies on their adhesion to the substrate as the ease of film removal which is determined through this process. Adhesion plays an important role in surface chemistry and physics on interatomic forces. Excellent adhesion of thin films is essential for the environmental protection such as the guarding of corrosion from substrates [77, 78].

3.1. Adhesion definition

Adhesion means the way that two different materials tend to stick together, and the measurement of adherence is an indicative force which is necessary for separating them. There are two definitions of adhesion:

Definition 1:

If X is the adhesion of material A to material B, some characteristics should be involved:

1) There is the same meaning of X for all practitioners who would attach A to B.

2) X can be calculated by one or more specific methods.

3) Understanding X lets the practitioner anticipate the loading conditions. It paves the way for material A to delaminate from material B.

Two different coatings can cause distinct material morphologies in several levels of stress. The layer having higher stress is more likely to delaminate than other kinds of coating.

Definition 2:

1) The adhesion of A to B is considered as a relative model which represents the tendency of A to stick or attach to B. This is originated from a measurement which is qualitative, semi-quantitative, or entirely quantitative.

2) The exact meaning of the term relies on the measurement technique and the experimental contexts which raise the hierarchy of definitions. Therefore, it is possible to mention that A is considered as excellent adhesion to B concerning the observation that A was never isolated from B under various conditions of loading.

This definition is based on the systematic adhesion of one material to another. In other words, adhesion is obviously measured within the context of the specific measurement technique. The fundamental adhesion of each material is considered as an essential theoretical notion.

Therefore, it is implied that the practical adhesion refers to some complicated functions of fundamental adhesion which is not essential to recognize under most conditions. Further, the results indicated that physicochemical tools could adjust the initial adhesion between two materials and it is considered as an instrument for adapting practical adhesion. The term "delamination" takes place when a coating is isolated from its substrate. Adhesion measurement methods are divided into destructive or nondestructive categories. A majority of the techniques belongs to the destructive category, by which a loading force is implemented to the coating and finally the damage has resulted. Nondestructive methods implement a pulse of energy to the coating/substrate system, which is trying to recognize the mechanisms which are operated only at the interface.

3.2. Adhesion Mechanisms and measurements

Adhesion failure is regarded as the adherence that is observed in such coating failures which leaves the coating intact over the substrate. Controlling the impurity is very important as it can influence adherence to hardness, stress, and structure.

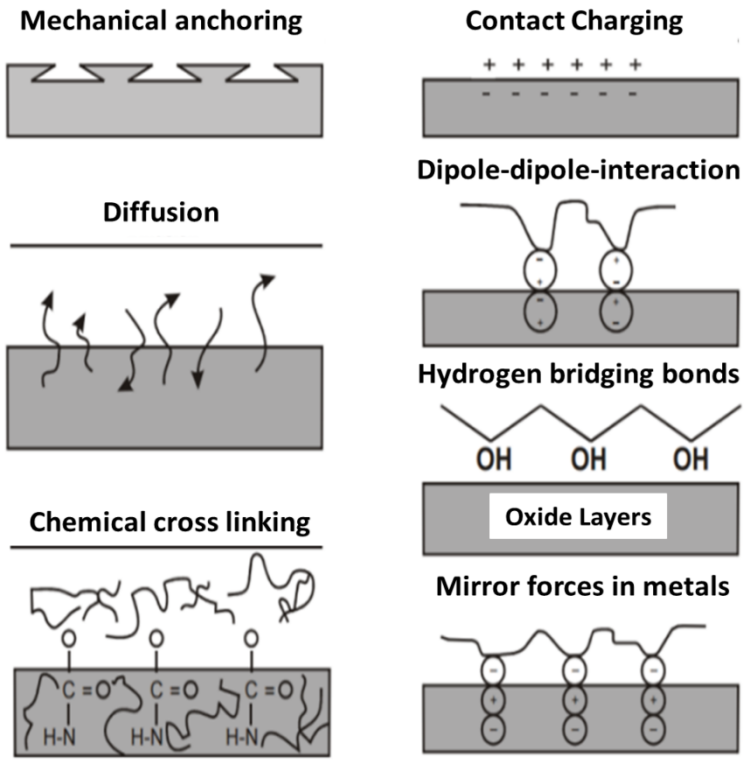

Fig.3.1 Physical and chemical causes for the adhesion of coatings to the substrate source: BASF Hand Book on Basic of Coating Technology 2003

Fig.3.1 shows physical and chemical features for the adhesion of coatings to the substrate. Regarding the most influential factors which are responsible for good or bad adhesion of films on a substrate, we can refer to the formation of chemical or physical bonds across the interface, physical adhesion and the contamination of the interface, the formation of new phases inside a broad interface and film stress. All these factors might be influenced by ion bombardment either by the activation of bonds and preferred sputtering of impurities or by mixing ion beam, which results in broadening interface and establishing phase. To improve the adhesion of metals on polymers, the activation of bond formation plays the most significant role [81-83].

There is a direct correlation between the increase in adhesion and the reduction in tensile stress. Regarding the multilayer structures, the permeation is explained as the penetration of the solid material by the selected permeants.

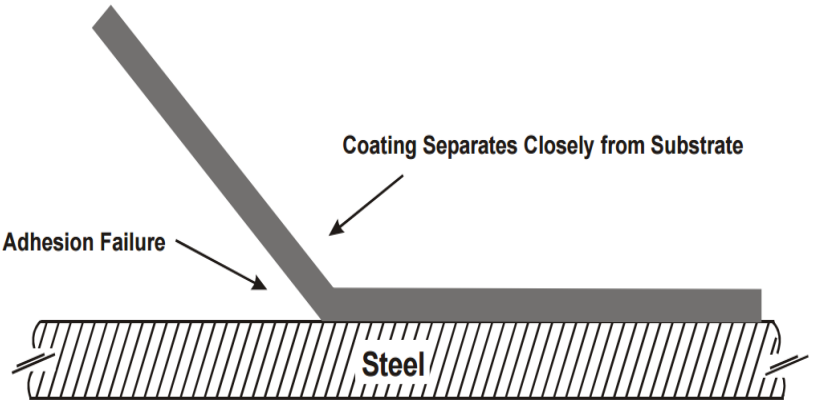

Fig.3.2 Adhesion failure of a coating [80]

In order to describe the permeation process, the general diffusion theory involving four different stages is used. The permeability coefficient can define the entire permeation process at steady state for similar materials as Pc. Pc is specified as the product of the diffusion coefficient (Dc) and the solubility coefficient (Sc). The material-specific coefficient D is used to quantify the diffusion process, and S represents the absorption process.

$$Pc = Dc \times Sc \quad (3.1)$$

The inorganic layers (Silicon Nitride in the tests) with extra high density are combined to establish a robust composite barrier to decrease the permeability of the thin films during the LIFT process.

3.3. Methods of adhesion measurements

Before focusing on the different adhesion techniques, two critical issues should be taken into consideration:

a) The practical adhesion cannot be regarded as a direct measurement of the fundamental adherence.

b) The quantity of experimental adhesion which is calculated by different methods should not be compared directly.

In order to measure the adhesion of thin films, different methods can be implemented such as, qualitative and quantitative, destructive and non-destructive, mechanical and non-mechanical, wholly and partly developed procedure. Two different routines and applicable methods for the measurements will be explained in the LIFT process as; the Scotch tape test and the Peeling test. In addition, Shear test is the 3rd adhesion test which is going to be explained in 3.8, in order to check the quality and the solderability of the deposited particles after Laser direct writing process.

3.4. Scotch tape test – Advantages and disadvantages

The scotch tape test is considered as a somewhat classical technique used to evaluate adhesion. A pressure sensitive tape is first compressed into the film and then it is rapidly eradicated. Therefore, three possibilities are used as follows: (a) the film is completely removed from the substrate (b) film is not removed, and (c) the film is partially removed. It is almost impossible to determine the area involved in any situation in the tape test. The results are mentioned as any performing energy in each target area. Thus, the results obtained from tape test cannot be directly compared to the results made by implementing other techniques, providing adhesion rates based on the force in the area.

If the film is completely eradicated from the substrate to do the measurements, it will be demonstrated as poor adhesion for those interfaces. There are some characteristics for any comprehensive adhesion test. For example, the test should be quantitative, reproducible, not too time-consuming, easily flexible, simple for performing relative adhesion measurement of thin films, non-destructive, independent of the film thickness, no depending on the operator's experience, implemented to all integration of film materials and substrates, valid over a wide range of sample sizes, appropriate for products and processes, and finally independent of the case for performing the test. The adhesion between the adhesive and the film should be higher than that of the film and the substrate. Also, the adhesive should not change the properties of the film-substrate interface.

The scotch tape test is too qualitative. The small differences in adhesion are not observable, and the result interpretation is entirely subjective. This test is easy to perform and requires inexpensive equipment. The force analysis of this test is somewhat complicated. Furthermore, some factors such as; the peel angle, test strip width, peeling rate, the viscoelasticity of film features are regarded to be considered.

In addition, peel values described in force/length cannot be directly compared to the shear values, recorded regarding force/area. Regarding the scratch test, some advantages such as swiftness, reproducibility, and applicability can be mentioned. Further, this test is used quite profitably to study the impact of deposition variables. The scratch test is regarded as a very appropriate technique, although further research is necessary to fully comprehend the specific mechanics of scratch formation and the variables involved in the final results.

3.5. Peel test - Advantages and disadvantages

The peel test is regarded as a method related to unchangeable coatings on rigid substrates as it can satisfy many of the criteria for the ideal adhesion. Two major classes are available for regarding destructive adhesion tests: those related to rather soft-flexible coatings and those associated with the hard-fragile ones. The peeling test is considered as the most well-known test for flexible surfaces. The coating delaminates if the adhesion level is not satisfactory between the layer and substrate.

Figure 3.3(a) represents the common peeling test of 90º, which is regarded as flexible coatings on rigid substrates. In other words, it is recognized as the most common of all the peeling tests. The 180º version of Figure 3.3(a) is shown in (b) section. Further, it is evident that the peel test is utilized at any angle between 0 and 180º. Angles except 90 or 180º is not usually considered due to some practical purposes unless there are geometric limitations imposed by the sample or test apparatus. Nevertheless, different variety of peeling angles can set the grounds for the effect of mode integration on peel strength. The climbing drum test is illustrated in Figure 3.3(c). Regarding the merit of this version,

compared to others, the curvature radius of the peeling film could be mentioned, which is adjusted by the drum radius and makes the numerical analysis easily. Finally, the T-peel test in Figure 3.3(d) is implemented to examine the adhesion level between two flexible films. There are four types of configurations for standard peeling test: (a) 90º peel test, as the most well-known configuration, (b) 180º test which is favored when available space hinders the 90º test, (c) climbing drum or peel roller test, which is preferred for handling the radius of curvature of the peel strip, and (d) T-peel test, used during the adhesion testing of two flexible strips.

The peel test satisfies some of the criteria for the ideal adhesion test in many configurations. The peel force is used to measure the coating adhesion to the substrate semi-quantitatively, which can be implemented for ranking or controlling the adhesion quality. Another advantage of this type of testing refers to the determination of the delamination rate and controlling the locus of failure accurately. Regarding the reason, it is emphasized that a very high concentration of stress is available where the coating just lifts off the substrate. In this regard, the failure region is carefully emphasized for the geometric interface between the coating and substrate, which is considered as the area of interest in any adhesion test.

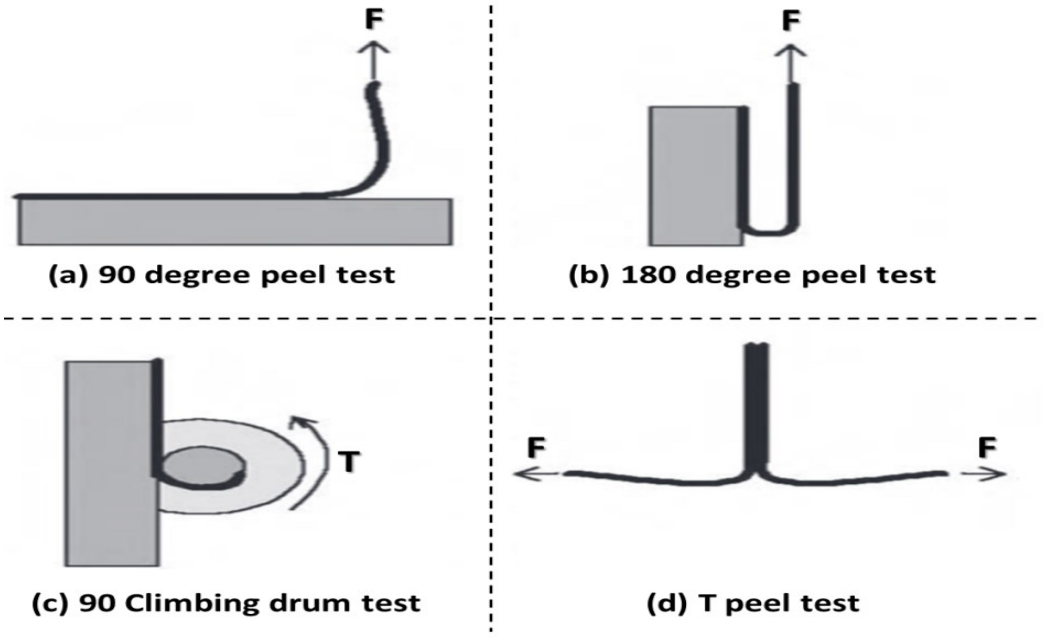

Fig.3.3 Four standard peel test configuration [86]

Some factors can play a significant role in the measured peel test such as adhesive molecular weight, adhesive thickness layer, peel rate and the peel angle of the film. Specifically, the peel force relies on the peel rate with three fundamentally different modes of peeling. At low speed, a flow of the tape adhesive is responsible for handling the peel force, which strongly depends on the rate. Little thick deformation takes place at high speeds, and the peel force is not substantially related to the rate. At intermediate peel rates, the peel force demonstrates cyclic inconsistency driven by alternate strength and distribution of elastic energy. Therefore, a considerable degree of complexity was introduced just by individual properties of the tape irrespective of the coating and substrate features. One of the disadvantages related to peel test is that it causes the coating to rather high strain levels near the peeling bend, which are never observed under common end-use conditions in most coatings. The coating strain can quickly reach 25% or higher at the peel bend, while real layers delaminate under about strain-free circumstances [107]. The peel test is only implemented for robust, flexible coatings, which is another shortcoming of the peel test. Furthermore, another limitation of using a peel test is related to the fact that the position of failure on the peel front can become unsettled.

3.6. Adsorption and Electrostatic theory

This theory primarily considers adhesion as an exclusive property of a phase interface, where polar molecules are oriented. The adsorption model explains the phenomenon of adhesion without penetration by the adhesive to the substrate. The bond is made by the contact between the adhesive and the substrate. The adsorption hypotheses clarify the adhesion theory of concepts, for example, contact edge, wettability and surface tensions. According to the electrostatic method, an adhesive attraction force is explained concerning electrostatic effects at an interface. The theory has been originated from an electrical double layer phenomenon established at the cross-section of the two materials. An electrical double layer is generated at each boundary, and accordingly, the coulombic efficiency might explain the adhesion and separation resistance. The main important issue is that adherence results from the inter

diffusion of the adherent and the adhesive. Adhesion, on the other hand, is a unique interfacial phenomenon, which is relevant to the surface tension of two different materials take place in that area. In particular, it should be differentiated between the adhesion forces and adhesive joint strength [79]. The adhesive joint strength is relevant to the areas covered in engineering mechanics, which is essential for design purposes. Therefore it is regarded as the most important engineering features of an adhesive material.

The nucleation model relies more on observing the kinetics of formation of thin films, which are labeled as non-destructive methods. Indeed, adhesion is regarded as a mechanical characteristic of the film. However, based on atomic approach, the removal of the film includes breaking the links among the detached atoms of the film and the substrate. There is a relation between the adsorption energy of a single atom from the substrate and the total film adhesion. Based on the above justification, the adherence which is characterized by nucleation methods is related to the fundamental definition of adhesion when only the adsorption forces take into consideration. Therefore, the addition of specific adsorption energy of adatoms should be separated from other processes which include the mechanical methods. It is worth mentioning that the nucleation methods rely on measuring nucleation rate, island density, critical condensation and finally the residence time of the depositing atoms involved in the film.

3.7. Surface Preparation

The adhesive should carefully saturate the surface of each substrate for adequate bonding. Further, a chemical bond should be established between the surface of the adhesive and the substrate. In order to meet these conditions, the surface of the substrate should be clean, adequately smooth, and chemically sensitive to the selected adhesive. The quality of a coating directly depends on the nature of the adhesion. In other words, adhesion is defined as the energy needed to set aside the interface between the two materials.

Some theories are available concerning the adhesion mechanism, including adsorption such as Van-der-Waals forces, electrostatics, diffusion, chemical

bonding, mechanical interlocking, etc. In order to create an optimum adhesion, it is fundamentally necessary to guarantee proper wetting by utilizing the coating material, which can create ideal conditions to force the film molecules to approach the substrate. In general, the surface tension of the coating material (σp) should be lower than or at least equal to the surface tension of the substrate if good substrate wetting is regarded as the primary purpose.

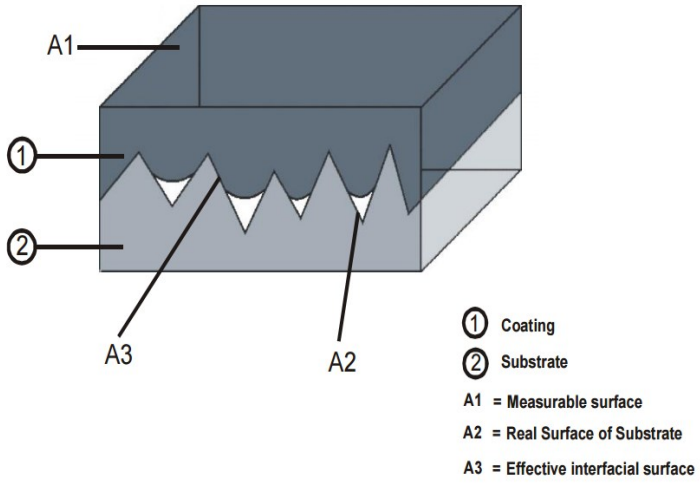

Fig.3.4 Surface effects determining the measurement of adhesion
Source: BASF Hand Book on Basic of Coating Technology 2003

Based on the optimum bonding, the adhesion of a layer is not exclusively characterized by the coating. In order to create an excellent adhesion, cleaning processes or pre-treatments should be done before the coating process. Therefore, appropriate levels of adhesion do not only rely on the coating, but an adaptation of coating materials and the substrate can also play a pivotal role. Concerning the adhesion of coatings, some terms such as adhesive strength, adhesive ability, and bond strength are also so important.

3.8. Shearing test

The purpose of this test is to define the procedure for measuring the shear strength of the interface between the printed lines by LIFT method and solder balls. In the other word, the adhesion test is the minimum shear strength requirements for this interface. This test method applies to all solder balls with

the same soldering parameters. The reliability of solder joints and the minimum force under mechanical shock is a significant concern.

As it can be seen in Fig.3.5, a schematic illustration of a standard shear test is shown. An appropriate shear tool will be located behind the solder ball, and the required force will be measured by pushing the solder ball till it would be removed from the pad. The chisel size must be bigger than the solder diameter of the solder balls which have been used for bumping. (100 μm chisel is used for 80 μm solder balls in the tests).

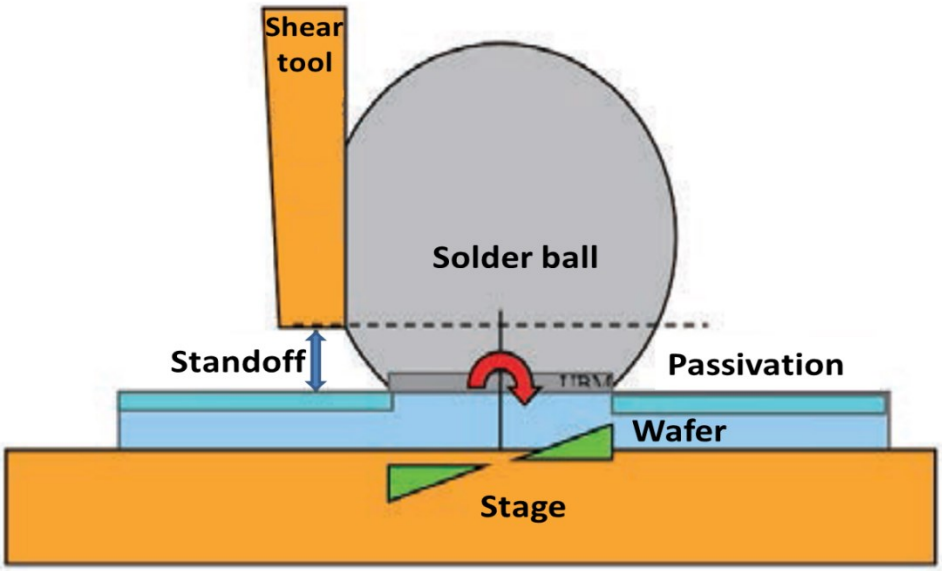

Fig.3.5 Schematic illustration of shear test [112]

The outcomes obtained from these studies ought to be exceptionally useful for the electronics fabrication industry to denote their testing information and determine the acknowledgment criteria for the items with solder ball connections. The ram height and shear speed can play a substantial role in the shear strength of solder balls [113].

The dependability of solder balls under mechanical shock is a noteworthy concern. Brittle breaks on the interfaces between solder joint and substrate bond pads are considered as a rejected mode. It is great to know that Bump Shear Test (BST) requires high power dissemination. Moreover, the shear instrument forces a rotational moment corresponding to push force and shear height, which like this brings notable results in a lifting power at the main edge of the UBM/bump framework.

Figure 3.6 demonstrates the distinctive stages of the shear test. Mode1 illustrates the solder ball break above the surface of the solder mask within the bulk solder material. In mode2, partial solder is sheared (75%), and the rest will be retained on the surface. Mode1 and mode2 are two accepted shear tests. If the sheared solder partial is less than 75%, then the test is rejected (mode3). In Mode4, Solder ball lifts from the pad. Solder/intermetallic do not entirely cover the substrate, and the top surface of the pad plating is uncovered. The next mode is the fifth one. Solder pad lifts with solder ball; lifted pad may include ruptured base material. Mode 6 shows the cratered solder. The break is at the solder/intermetallic interface or intermetallic/base metal interface.

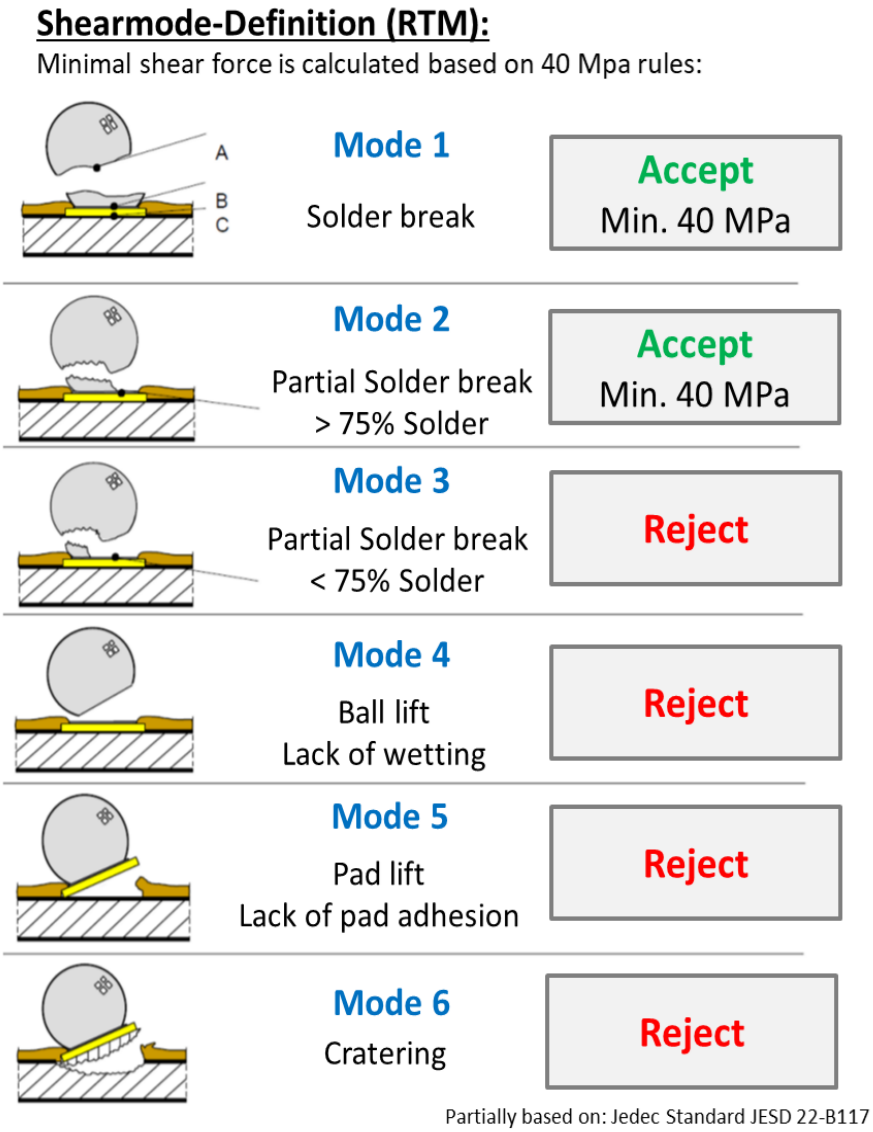

Fig.3.6 Shear mode standard for acceptance and rejection- Jedec Standard

The first shearing pad should be located on the upper left of the chip and the average shear pressure for SAC305 alloy must exceed 40 Mpa. The following equation will calculate the required force:

$$F = \frac{Pad\ Area\left(\mu m^2\right) * 40\ MPa}{10\ 000} \quad (3.2)$$

For having a rectangular pad area as 110μm width and 100μm length, the minimum required force is approximately 44 cN (40 Mpa). The interfacial fracture may extend across the entire pad or be the dominant failure mode in the tool contact region. If multiple rejection modes will be seen within a single solder joint, then the predominant failure mode at the tool contact ought to be recorded as the failure mode for the test.

4. Experimental Setup for LDW and E-less plating

In this chapter, the experimental setup for Laser Direct Writing process will be explained. The chapter is divided into two sections. The specification of the laser with all its different elements is going to be described. Furthermore, the sample preparation procedure before deposition in presented. The second section is focused on the Lab-setup for zincating and activation of aluminum and copper for Electroless nickel plating which will be described.

4.1. Experimental setup for Laser Direct Writing Process

In the present study, two different Infrared and frequency doubled (515 nm wavelength) Nd:YAG ps lasers were implemented for transferring the aluminum and copper particles with pulse energies of a few hundred µJ at Kilohertz repetition rates. When the ps-laser pulse is appropriately focused on the donor side of the glass, it will ablate the material layer of 10-100 nm in a non-thermal process. The remaining material will not be heated; it will not develop micro crack, burr or recast. The Lumera laser which has been used for this dissertation is a 2 W picosecond laser generating ten ps pulses at 1064 nm with different pulse rates as high as 500 kHz and pulse energies of more than 30 µJ at repetition rates ≤ 10 kHz.

In addition a diode-pumped passively mode-locked Nd: Vanadate laser was used for generating high average power picosecond pulses. The laser has eight ps pulse width, and the average power is about 3 W. In order to get higher energies, the chosen pulses are enhanced in a transient amplifier. This amplifier utilizes a similar gain material as an oscillator, a neodymium-doped Vanadate, which is notable for a high increase in cross-section prompting a high amplification. The amplification factor can surpass 500, contingent upon the repetition frequency of the pulse sequence. The energy of a ps pulse is increased from the 60 nJ (~ 3W, 50 MHz) to the most extreme of more than 30 µJ for under 10 kHz. The average output powers are measured based on different repetition rates, and they are summarized in table 4.1. The maximum

output power achieved in 1000 kHz as approximately 12W. The output power has a good stability in room atmosphere at any repetition rates.

Table.4.1 Average output power vs repetition rates

Rep.Rate (kHz)	Power (W) Powermeter	Power (W) Photodiode Output
1	0,36	0,37
2	0,64	0,65
10	2,56	2,70
20	4,46	4,82
25	5,16	5,57
50	6,99	7,34
80	8,03	8,30
100	8,52	8,72
160	9,46	9,57
200	9,87	9,97
250	10,2	10,3
320	10,6	10,7
400	11,0	11,0
500	11,3	11,3
640	11,6	11,6
800	11,9	12,0
1000	11,9	11,9

The optional second harmonic generation (frequency doubling) occurs in nonlinear optical crystals. Frequency doubling is a method for producing a new laser beam with a half wavelength out of a principal beam. The output laser beam is blocked by using a shutter, which can be operated by the laser control software. For safety reasons, there is a Hall - sensor inside the laser head that gives feedback when the shutter is in the "shut" position; the correct position of the shutter is demonstrated. When there is no power to the shutter, the output beam is blocked. The Lumera laser system consists of a laser head and a control unit, which contains a power supply and a closed loop water chiller. The pulses are picked up by an electro-optic modulator (EOM), which is driven by digital delay generators.

Fig.4.1 shows the experimental setup for a Lumera Nd:YAG laser with eight picosecond pulse duration. F-theta lens with 163 mm focal length is used for the process. There is a suction hole in the adjustable table to fix the sample during

the process without any movements. The table is programmed to have a small motion in the Z direction to have a focused beam on the sample.

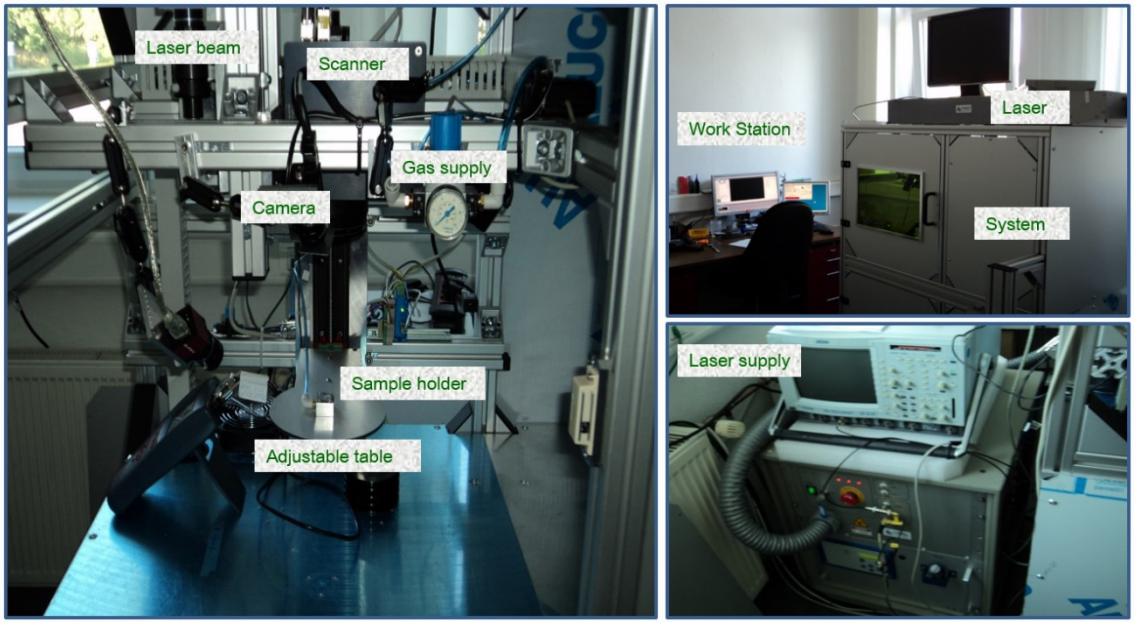

Fig.4.1 Experimental Setup (PS laser)

Fig.4.2 illustrates the beam quality factor diagram which has been made by CCD camera at 100 kHz (The most used repetition rate in the measurements). The laser has M^2 of 1.26 and 1.23 in X and Y axis respectively at the mentioned repetition rate. The divergence angles for X and Y were 2.1 and 2.15 mrad.

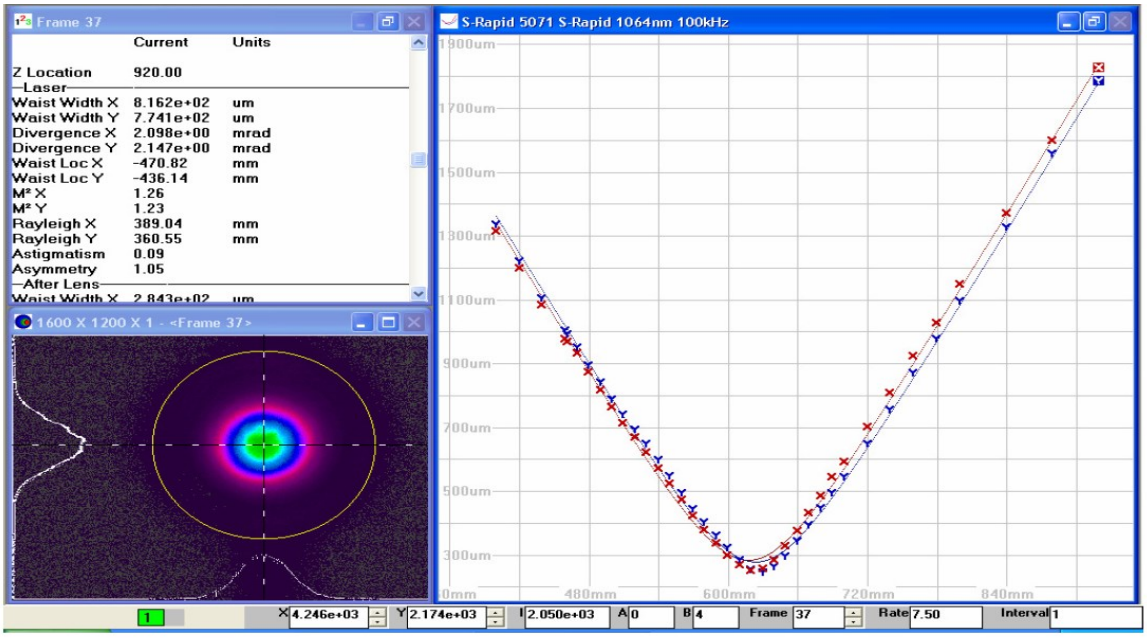

Fig.4.2 Beam quality factor measurements-CCD camera

A glass with a 1-inch diameter (25 mm) and 1 millimeter thick has been used as a donor for the experiments. The copper and aluminum are evaporated in a vacuum chamber and make the coating layer with 500 nm thickness on the glass surface. These donors are made in the Coatings Laboratory of Optics and Atomic Physics Institute at the Technical University of Berlin. Fig.4.3 shows the copper coated layer on the glass with 0.49 μm thickness.

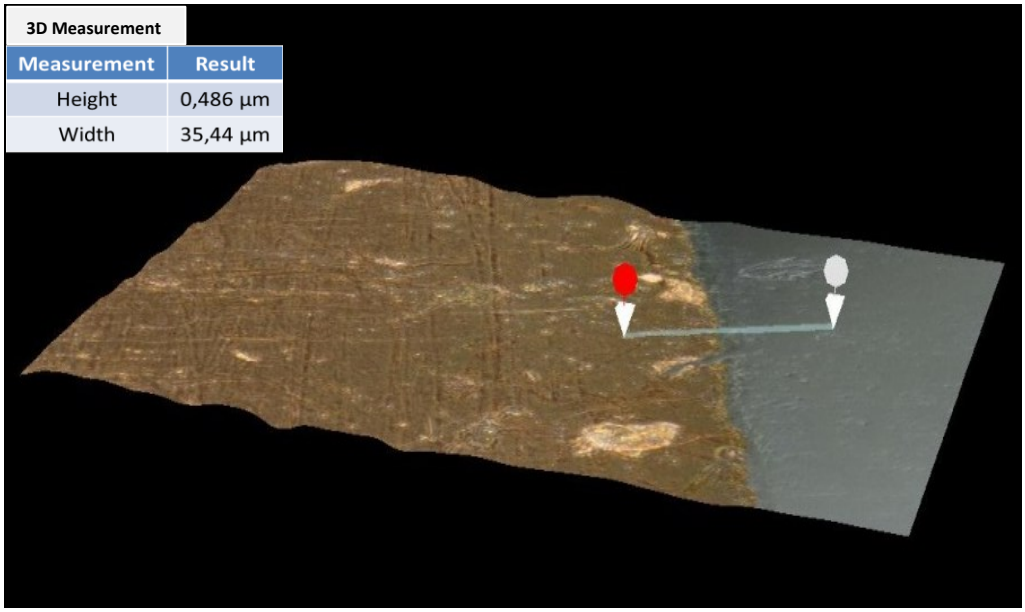

Fig.4.3 Measurement of copper coated thickness on the donor glass

The focus diameter corresponds to the lateral resolution. Tighter focusing is possible with shorter wavelengths, which can be generated by frequency conversion of the Infra-red laser to the green one. The beam diameter of the IR laser is measured as 60μm and 30μm for the laser with 515 nm wavelength.

Laser energy has shown little effect on the particle size. To have a large material removal rate while preserving the applicable features of the ultra-short pulse laser, low pulse energy in combination with a high repetition rate should be applied.

For ultra-short pulse lasers, the effect of heat propagation is minimal. This heat distribution implies that the energy is deposited over a length comparable to the optical penetration depth, 1/α, which is the order of 10 nm for many metals.

Nano particles can be fabricated safety and cost effective by immersing the target material in a liquid and then removing material from the surface by

irradiating with a laser beam. Pulsed laser ablation enables the preparation of pure nano particles without unwanted chemical residues which are currently a common problem for a chemical combination of nano particles. In order to check the mechanical reliability of interconnects, the entire samples were immersed in a glass chamber of isopropyl alcohol (IPA) where is placed in an ultrasonic cleaning tank.

A feature of significance in all usages for electroless nickel is the potency to procreate deposits with a high level of thickness consistency. This process is plated on aluminum and copper particles which are transferred by LIFT method for increasing the thickness of the film (2-3 μm) on the silicon wafer substrate. After nickel plating, electroless gold is plated on the nickel (500 nm gold thickness) for soldering the UBM and making the shear test to check how well the solder balls adhered on the pads.

4.2. Activating setup for Electroless nickel plating

The chemical processing is categorized into four primary stages, including Al cleaner for Al and Cu cleaning process for copper; Zincate pre-treatment (for Al) and copper activation (for Cu); electroless nickel deposition and optionally immersion gold bath.

Aluminum reacts immediately with oxygen and builds a thin oxide layer due to its high reactivity. The aluminum cleaning is applied to remove this oxide layer and provide the surface for the following processing step (zincating). The cleaner reacts with an oxide layer to prepare an Al surface with an appropriate roughness to give a suitable place for Zn deposition. Alkaline (PH >9) or acid (PH <4) solutions can dissolve Al oxide. Al is etched by the consequent reaction in an alkaline medium which is implemented in the process.

The cleaning solution should homogeneously remove Al without producing pits. It is necessary to have a successful cleaning for a dense and homogeneous Zn deposition and resulting bump adhesion. After cleaning, a rinsing step is needed. The rinsing ends the cleansing reaction, and no critical amount of cleaner gets into the solution after the process.

The content of the next bath is zincate ions ($Zn(OH)_4^{2-}$) in an alkaline solution. After cleaning and rinsing, Al is passivated again by a thin oxide layer. During zincating, this oxide has to be removed, and a Zn layer will protect the exposed Al against further oxidation.

The Zn layer has to be thin, and delicate grained to produce the best adhesion results. The EN reaction can take place only on catalytic surfaces as well. When the zincated Al surface is immersed in the EN bath, a thin Ni layer is plated by an exchange reaction. In order to avoid Ni oxidation and keep solderability of the bumps for the further shear test, a thin Au layer is applied on the Ni bumps. The deposition reaction ceases when the Ni is completely covered.

The following procedures are utilized in experimental operations to render copper and copper alloys catalytic.

1. Contacting the parts with active metals in the Electroless nickel tank.
2. Treating the surface with an active reducer, including Dimethylamino Borane.
3. Catalyzing the surface by means of immersion in dilute palladium chloride solutions.

The important achievement for copper relies upon the activation system. Copper alloys won't catalytically initiate plating inside the nickel-phosphorus systems without an additional activation process after ordinary preparation. The nickel particles will be plated on the copper lines and make a coalescence, and soft layer with approximately 2-3 μm height. By increasing the time in the nickel bath higher plated thickness could be achieved (from 1-5 μm).

Fig.4.4 shows the aluminum zincating and nickel deposition process. The bath temperature of aluminum cleaning and also nickel plating is written in the picture. The time for each step is optimized. The double zincate treatment, which repeats the conversion treatment twice, demonstrated a remarkable increase in adhesive strength. The main application of EN in this study is electroless nickel immersion gold (ENIG) for surface finishing, which was implemented by the production of UBM for soldering the pad and doing the shear test afterward. It is particularly important for PCB's solderability and corrosion resistance to have the thickness and phosphorous content of the electroless nickel alloy [94, 95]. Regarding the real application of the electroless

film as an anticorrosion layer, the substrate pre-treatment, and the actual plating attests a proper adhesion and constancy of the coating. [96-98].

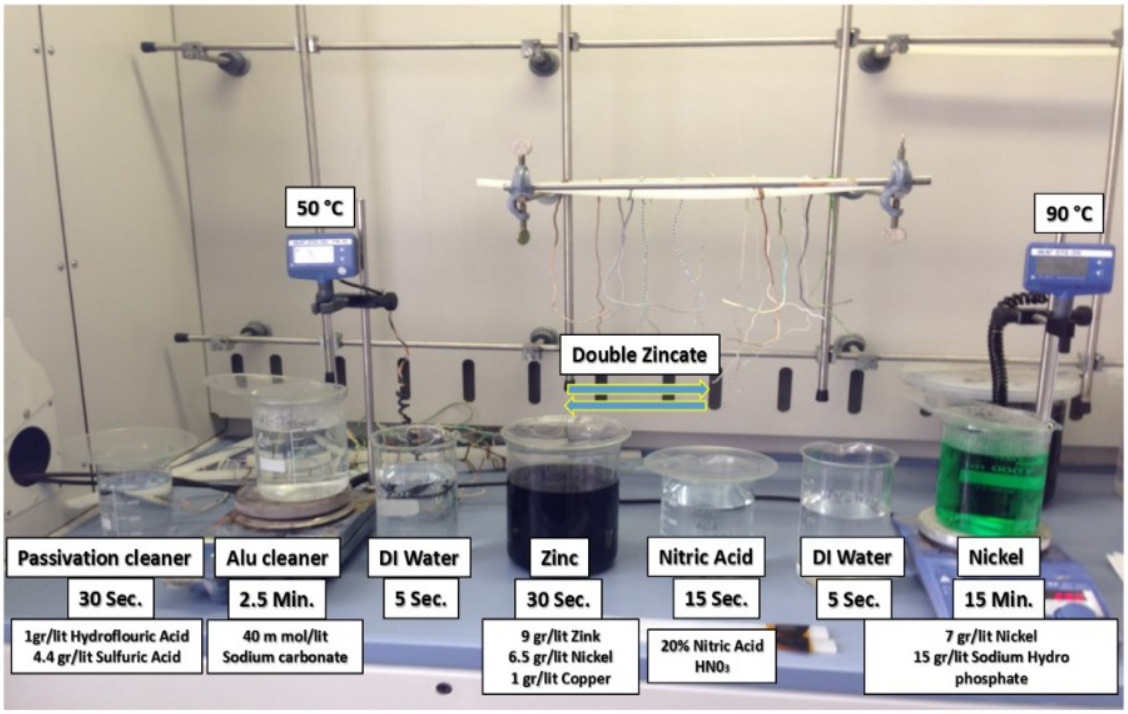

Fig.4.4 Electroless nickel plating process for Aluminum particles

Fig.4.5 shows the Silicon wafer substrate (in black) with Silicon Nitride passivation. The copper or aluminum particles are transferred by Laser direct writing method. The nickel is plated on the printed particles, and finally, 500nm gold is deposited by Electroless plating on the nickel layer.

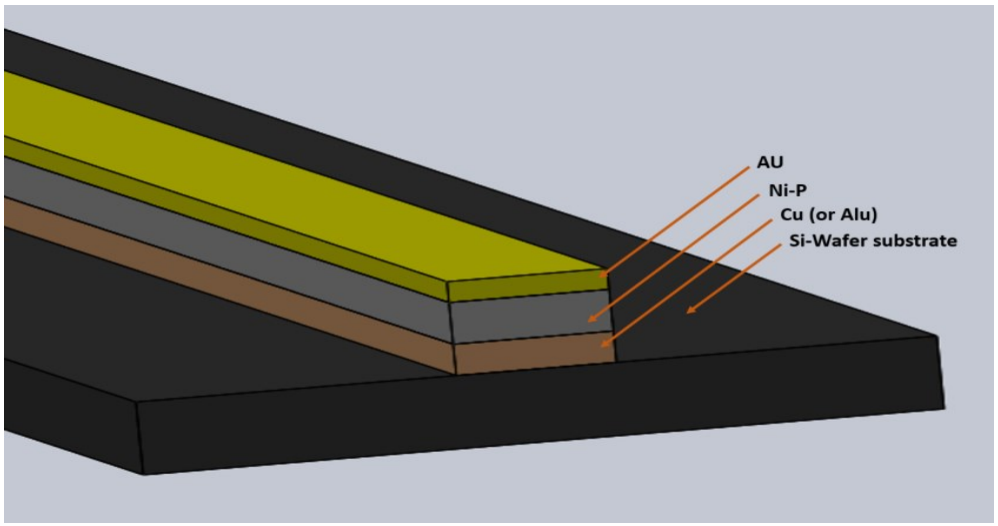

Fig 4.5 Silicon wafer with thin film of Al (or Cu), Nickel and gold deposition

This strength was only a little enhanced after the 1st zincate treatment, however, after the 2nd zincate treatment; the adhesive strength was mainly increased. The nickel particles are plated on the aluminum seeds and make a smooth nickel layer of 2 μm.

Electroless nickel plating (EN) is known as autocatalytic or chemical nickel deposition process which has been used in many microelectronic manufacturing industries such as interconnections, micro electro mechanical systems (MEMS) and PCBs [87-90].

EN is a procedure for placing a nickel compound from aqueous solutions onto a substrate with no utilization of electric current. In the reaction phase, the deposited nickel is provided by some nickel salt. The aqueous solution dissolved the salt and produced ionic nickel. Electrons reduce the nickel ions which are not provided by an external current source; however, they are produced by the reduction of the factor which is dissolved into the solution [91-93]. This process has two significant advantages; its hardness is very high, and the thickness distribution is entirely constant. An increase in the thickening of particles takes place in the activity of the nickel bath by making a deposition with bigger clusters and rising the bath temperature.

5. Measurements and adhesion results

Some different methods have been implemented for micro fabrication techniques in thin film production and thickening the pads for various applications in microelectronic devices [99-101]. The deposition of micro/nano metal particles by laser direct write method from one side coated glass is regarded in the present study. This technique is substantially different from other techniques such as photolithography and micro contact printing, which are utilized as one of the most important technologies for large-scale manufacturing [102-105]. In this chapter, laser direct writing techniques were used as they are more appropriate for prototyping as well as fast fabrication of small features.

5.1. Deposition Test Explanation

As it has been explained in chapter 2, laser direct writing of aluminum and copper particles are done in different test conditions. An Infrared and frequency doubled Nd:YAG laser was used along with eight picosecond pulse duration, beam propagation factor (M^2) 1.15 and two mrad divergence.

Fig.5.1 is illustrative of laser pulse energy and average output power in different repetition rates for the ps Lumera laser which has been used for the tests and measurements.

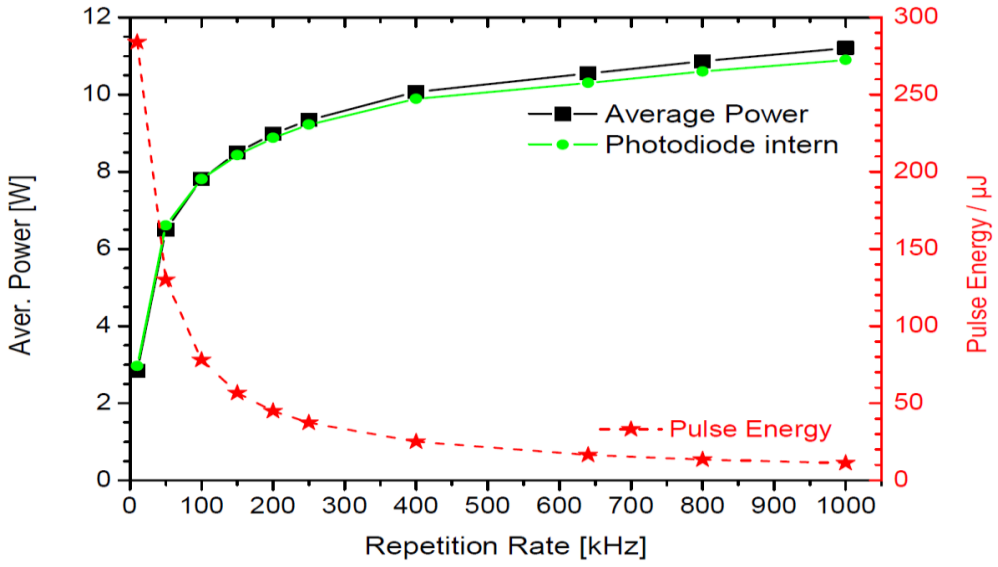

Fig.5.1 Rep.rate versus Average power and Pulse energy- Lumera ps laser

By having a closer look at the diagram, it can be perceived that by increasing the repetition rates, the laser pulse energy decreases drastically. This phenomenon has an essential role to have a smooth deposited layer of particles which has been explained in the following tests. The maximum average output power is approximately 12W, and the highest laser pulse energy is roughly 280 µJ. Based on the detailed explained introduction of the LIFT process in chapter 2, two different lines of aluminum and copper particles are deposited on the silicon wafer substrate. As it can be seen in Fig.5.2, these two sample lines are going to be used for different test conditions and adhesion measurements. Copper and aluminum were transferred, and they are perfectly deposited to the substrate with 8W average power of nanosecond laser which can be used in the application of electrical wire interconnections such as Molded Interconnect Device (MID) in the automotive industry and wire bonding application.

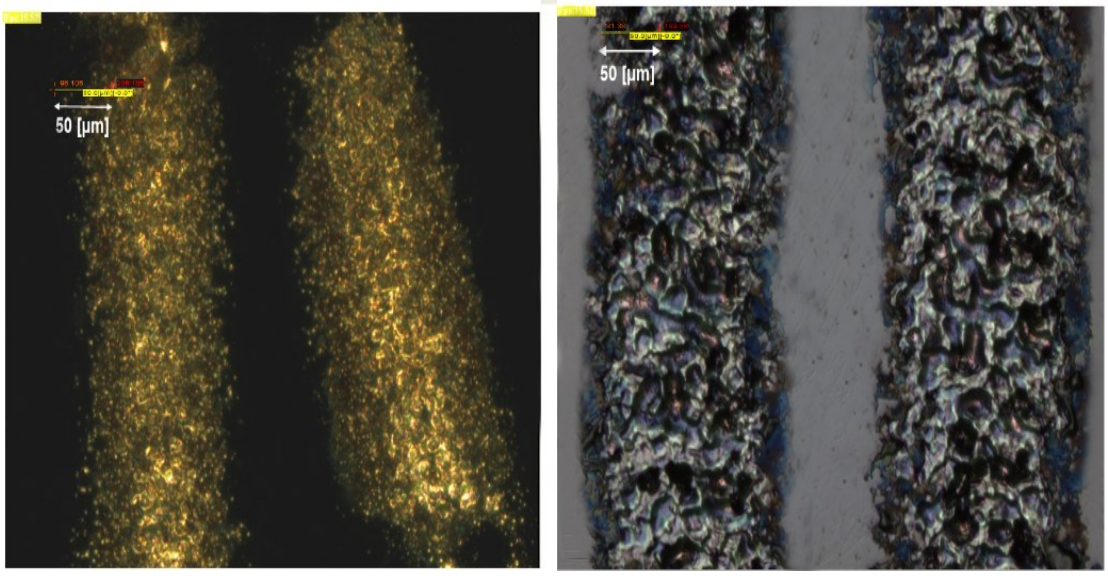

Fig.5.2 Laser deposition of Cu and Al on Si-wafer (Nd:YAG ns laser)

The additional high-density organic layer is used to control the process in adsorption and absorption in deposition level to decrease the exchange of particles in the substrate and preventing the diffusion and desorption stages in thin film production. For this purpose, the silicon wafer is passivated by silicon nitride passivation (Si_3N_4) to involve a composite barrier laminate [6]. The Silicon wafer substrate and the aluminum deposited particles are shown in Figure 5.3. The three right pictures represent the LIFT process after nickel

plating. As it can be seen, different repetition rates (100 kHz, 10 kHz, and 1 kHz) are done for transferring on the substrate with picosecond laser. Lower repetition rates have higher pulse energy, and it causes rough film structure of the Silicon wafer substrate. A change in the magnification of the objective lens and the size of laser spot can flexibly control the line width of the micro patterns. The height of printed particles depends on the reflection and absorption rate of copper and aluminum in different wavelengths. The nickel plating procedure is optimized to have 2-3µm for both copper and aluminum in further tests.

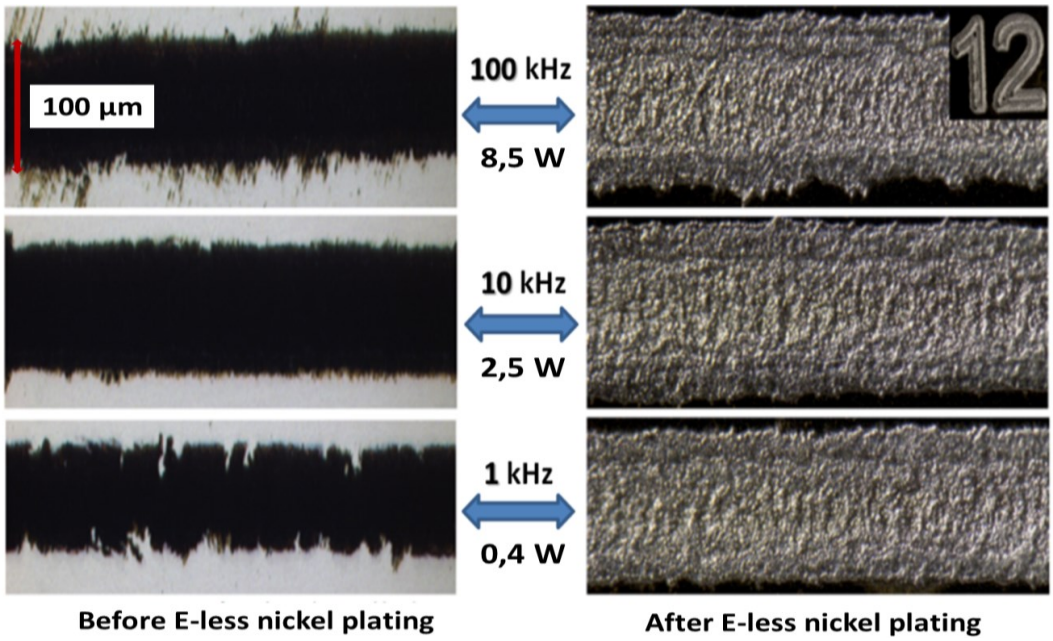

Fig.5.3 Aluminum deposition on Si-Wafer Surface (8 ps Laser)

Fig.5.4 shows a sample of electroless nickel plating on aluminum deposited particles during the LIFT process by ps laser. The EDX analysis illustrates the nickel elements which means that nickel is completely covered the aluminum seeds. Nd:YAG Picosecond laser with an average output power of 7.3W has used for this test. Pulse energy is measured as 0.07mJ, the intensity of 19 $KWcm^{-2}$ and laser Fluence of 0.19 J cm^{-2}. The repetition rate was 100 kHz by considering 80% pulse overlapping. The best result with less heat affected zone has been achieved by a 300µm distance between the substrate and the donor glass. The gap is increased till 1mm, and the particles have been transferred and can be seen on the silicon wafer, but apparently, it is not as much as less distance. Fig.5.4 shows the nickel plating on the Al deposited particles.

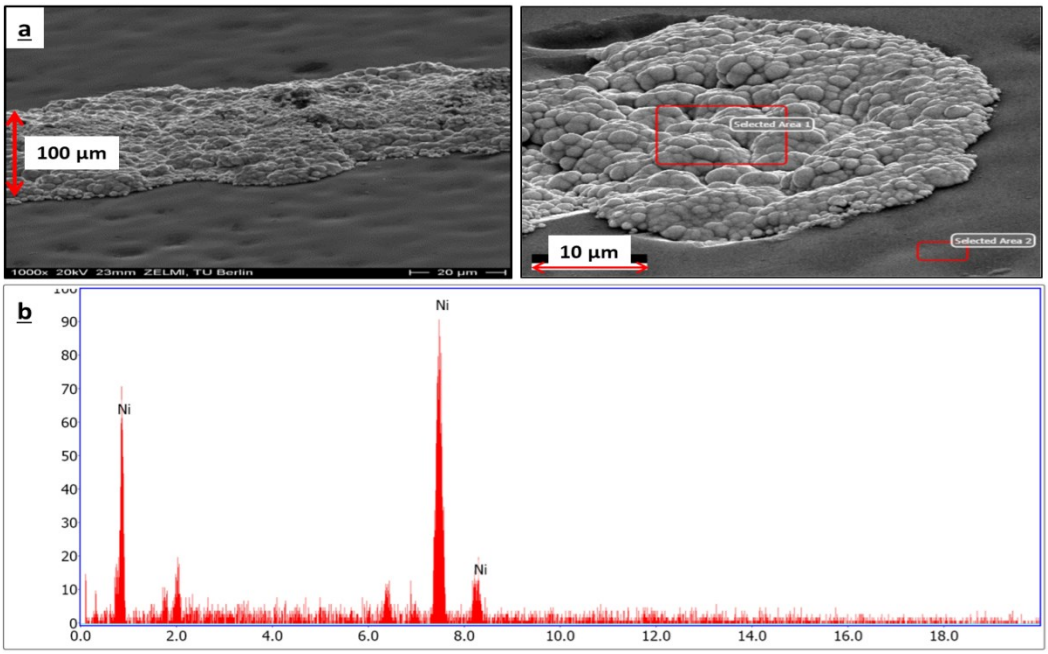

Fig.5.4 Electroless nickel deposition – (a) SEM Electron microscopy of Nickel plated in 45° (b) EDX analysis raising up to 18ev

Fig.5.5 shows the different height between Si-wafer with Si_3N_4 passivation and donor with aluminum coated glass from 0 (the glass is attached to the receiving substrate) to 400 µm. This gap optimization test is also done for the copper coated glass, and roughly the same results occurred. For all the further tests the gap is fixed with 300 µm spacing. The Average power is approximately 8W.

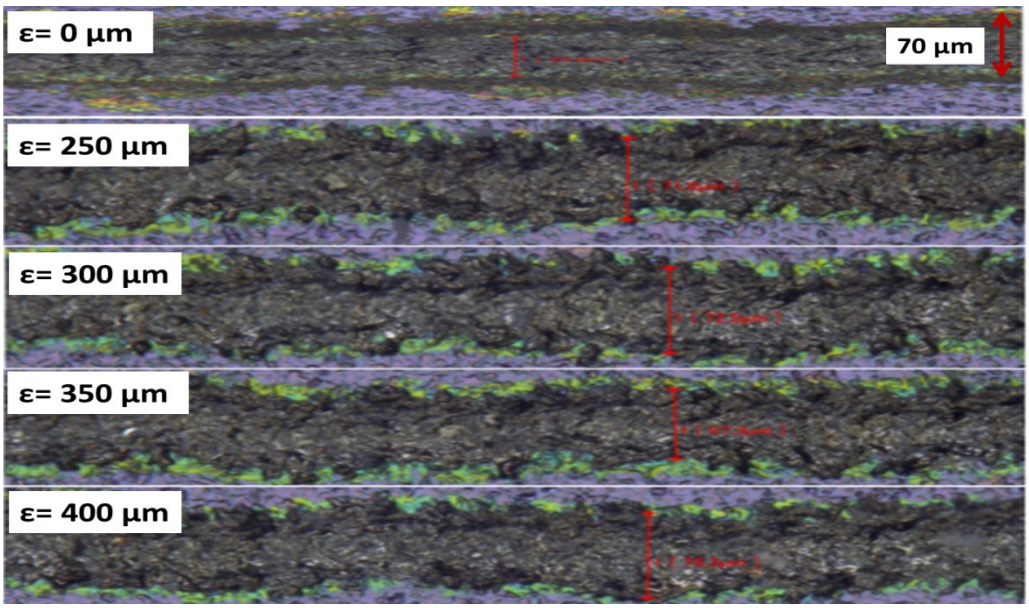

Fig.5.5 Different gap (ε) between Al donor film and Si-wafer substrate

5.2. Adhesion tape test on deposited particles

The tape peel test is a ready variant of the standard peel test. As it has been entirely explained in chapter 3, this test is a pressure sensitive test to determine the quality of the materials that used in conjunction with printed boards.

The tape test provides a precise and quick evaluation of adhesion at the level of 95% confidence, giving users enough certainty to assess the acceptability of the results, although the tape test is qualitative which can provide just a yes-no decision. The adhesion level is divided into six levels, ranked from 0B (more than 65% removal area) to 5B (0% of removal area). The results indicated that in distinct pulses for each position in both samples, better adhesion was obtained from silicon wafer substrate without Silicon Nitride passivation. In other words, much more aluminum was transferred to the passivation side of the Si-wafer than the Si-wafer without passivation by consideration of the existing differences in the reflectivity of the two sides of the Si-wafer. Further, an increase in the repetition rate led to a decrease in the pulse energy, and the smoother surface was also obtained on the substrate.

The tape peel test is considered as a useful and practical method of measurement in some particular applications in spite of the difficulties raised in achieving quantitative results. Further, the test is fast and can be implemented at press side. As it was already mentioned, the tape peel test can evaluate a coating adhesion semi-quantitatively. In order to guarantee a reasonable level of replication, calibration methods and reference samples are required. The precision criteria should be used for distinguishing the acceptability of results at the 95% confidence level. Repeatability is explained when the obtained results by the operator should not differ by more than 1 rating unit for two measurements based on the table in Fig.5.6. As it has been illustrated in the figure, six different classifications are defined and categorized for the investigation.

5B- The edges of the cuts are completely smooth; none of the squares of the lattice are detached.

4B- Small flakes of the coating are separated at intersections; less than 5 % of the area is affected.

3B- Small flakes of the surface are detached along edges and at intersections of cuts. The area affected is 5 to 15 % of the lattice.

2B- The coating has flaked along the sides and on parts of the squares. The area affected is 15 to 35 % of the layer.

1B- The coating has flaked along the edges of cuts in large ribbons, and whole squares have detached. The area affected is 35 to 65 % of the film.

0B- Flaking and detachment is more than 65%.

Classification of Adhesion Test Results

Classification	Percent Area Removed	Surface of Cross-cut Area From Which Flaking has occured for six parallel cuts and Adhesion range by percent.
5B	0% None	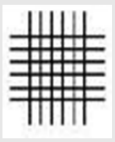
4B	Less than 5%	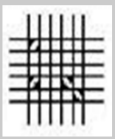
3B	5-15 %	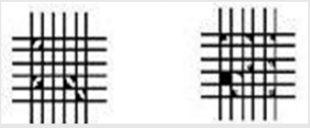
2B	15-35%	
1B	35-65%	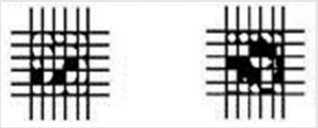
0B	Greater than 65%	

Fig.5.6 Classification chart of tape test and adhesion results [85]

The tape peel test especially appropriates in some situations in which a straightforward, quick test is necessary such as go/no-go evaluation. In some circumstances, this test is recognized to be the most available appropriate test.

No simple theory has been reported for adhesion. Therefore, some variables such as adsorption, electrostatic absorption and diffusion should be integrated into any comprehensive system.

Lumera infrared laser with eight ps pulse duration was used for laser direct writing on a Si-wafer substrate with and without silicon nitride passivation. Aluminum micro/nano particles were forward transferred to the substrate by the implementation of the laser included an 80% shot overlapping and 1-14 pulses per each position. The length of the lines was 150 mm, while it was about 100 μm for the width. As it can be seen in Figure 5.7, the picture is divided into primary rows. The upper row indicates on the test by using the substrate without any passivation and the second row illustrates the Si-wafer with passivation.

The figure includes 5 principal columns for each main row. The first column shows 14 lines which are representative of the number of pulses from 1 in the first line and 14 in the last line. The second central column displays the first column with its specifications after electroless nickel plating. The tape test is performed on the samples which are shown in the third column. The particles are attached to the tape in some different lines. In the passivized silicon wafer the retained particles are much more than the substrate without passivation. The removed lines are a combination of the passivation layer and also the aluminum particles. These lines are shown in the fourth column after adhesion test on the tape. The last column shows the lines which are derived from the donor glass. The quality of the deposited particles was considered after electroless nickel plating to expand the aluminum nucleation by less than 5 μm height.

The adhesion tape test is done based on the defined standard in Fig.5.6. In both samples, the spots, including 1–10 pulses had adhesion in removing areas of more than 65% (0B), resulting in the substrate with silicon nitride passivation. Regarding the laser shots with 10–14 pulses or even more, the adhesion was in the range of 4-5B for both samples, with a peeled zone of less than 5%. The test can estimate quantitative coating adhesion. The size and status of the grains are separately specified by the nucleation rate and the growth, which are directed by the diffusivity and adatom mobility in the system. [106-108].

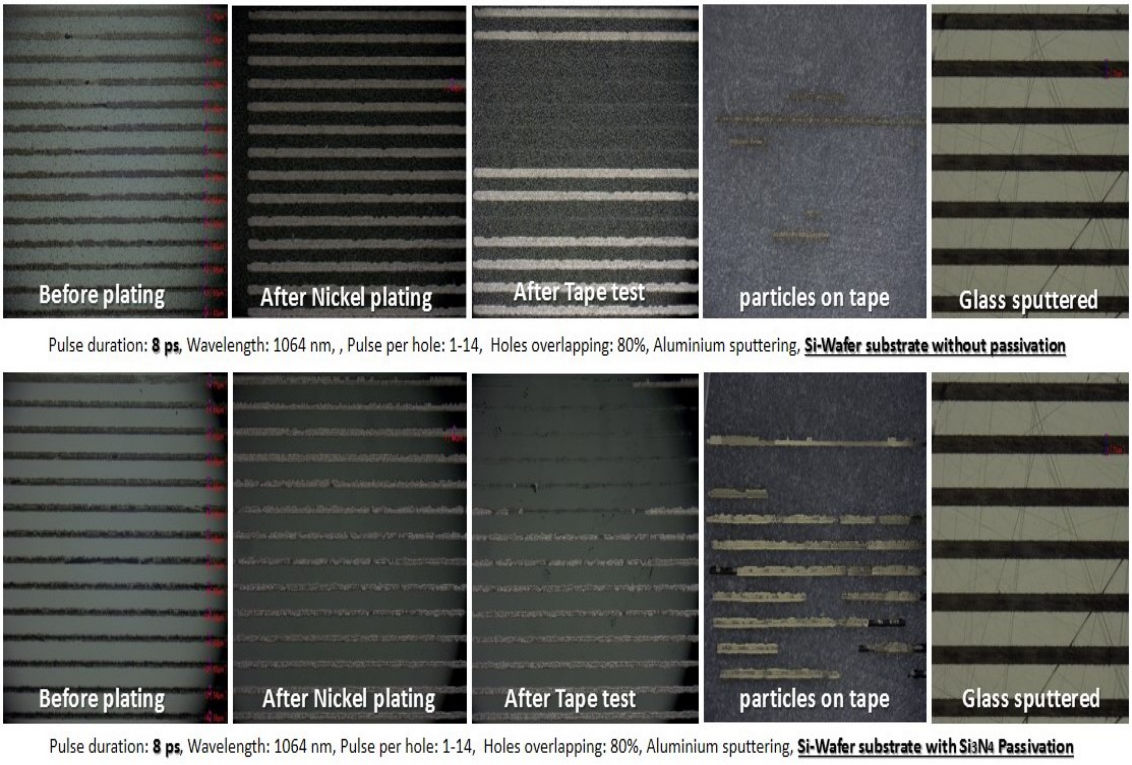

Fig.5.7 Adhesion tape test on Al transferred particles from Si-Wafer

5.3. Adhesion shear test

This test instruction describes the performance of shear test which is measured by force to remove the solder bump mechanically. For that, some different lines are produced by the LIFT process. Copper and aluminum particles are transferred from the coated donor side to the receiving substrate. Electroless nickel deposition plates the lines, and then nano gold particles covered the nickel seed to make a thin film on the silicon wafer substrate. The samples are transferred to the soldering device to be bumped. The SB^2-Jet machine from PacTech GMBH is utilized for the test. The samples are fixed on the table, and 80µm SAC-305 alloy (Sn 96.5%, Ag 3%, Cu 0.5%) is jetted on the lines. The bumped lines on the substrates will be sent to the shear testing machine in the clean room. Each sample is located with tweezers in the vacuum chuck of the test table. The test is carried out with the calibrated device. The shearing tool is fixed in 9µm height from the pad. In order to achieve good statistic results, a series of measurements require 30 shear tests.

Regarding the data collected from the test, the results indicated that a lower ram height and faster shear speed could lead to higher strength of the ball shear.

As it is evident from Fig.5.8 and Fig.5.9, four shear tests having different parameters were performed on the lines for aluminum and copper respectively. The repetition rate was 100 kHz, and 80% of the shots were overlapped to make a smooth line by utilizing a Gaussian beam shape. The left side of the pictures illustrates the lines with bumped solder balls, and the right side shows the film after solder removal. The average required force for each test is written on the pictures. The shear removal speed is performed as its standard mode at 50μm/s. The average pressure which is essential to reach at least 30 solder removals included 45.75, 51.55, 47.75 and 40.44 MPa for the 1, 5, 10 and 20 pulses for each laser shot, respectively. The results of the shear test indicated that the best performance was recorded for five pulses per position; however, this sample could not be able to pass the tape test, and the film peeled the substrate. Ten pulses per laser shot were regarded as the second best result, which necessitated more force to remove the solder balls and it is adhered well to the substrate after performing the tape test. The samples placed in a reflow oven for 30 minutes at 200 °C for thermal curing.

The same test with the upper condition is done for copper as well. As it can be perceived from Fig.5.9, in higher pulses per each laser shot (20), the bump is lifted from the pad, and it means the solder balls are not attached well to the film.

The minimum required pressure based on the standard shear equation is calculated as 40 Mpa.

The minimum required pressure could be passed when the pulses per each position are 1, 5 and 10 and the average removal pressures are 51.78, 64.95 and 56.81 Mpa respectively. The bump height is shown in the middle column of the picture before removal. This height can be changed by variation of laser parameters, gaseous pressure, jet and standard modes in the SB2 -Jet machine. By comparing the shearing results from the aluminum-based pad and Copper-based pad in Figures 5.8 and 5.9, it could be concluded that the

adhesion for the copper-base is much better than the aluminum one. Having a closer look at Fig.5.9, the minimum required pressure for solder removal adhesion test belongs to the first test by having just 1 pulse per each position. The shear test results can be seen in the last row of the figure. This pressure (51.78 Mpa) which is the least value for the copper-base is higher than the maximum value for the aluminum-base (51.55 MPa). It could be concluded that production of the thin film by LIFT technique can make an appropriate pad line on the Si-wafer substrate which could pass the adhesion shearing test successfully comparing to the standard shear test for UBMs and soldering pads. This emphasizes the fact that, laser direct writing technique is a comparable alternative for the other methods of pad production in UBM applications. The mean standard deviation and specific force limitation of each shear test have been shown on Fig.5.8. The solder removal after shear test has two times more magnification than the left side pictures in the figure.

Fig.5.8 Al-based pad, ps laser, 80% laser shots overlapping, Rep.rate: 100 kHz, Wavelength: 1064 nm, Si-wafer with Si_3N_4 Passivation

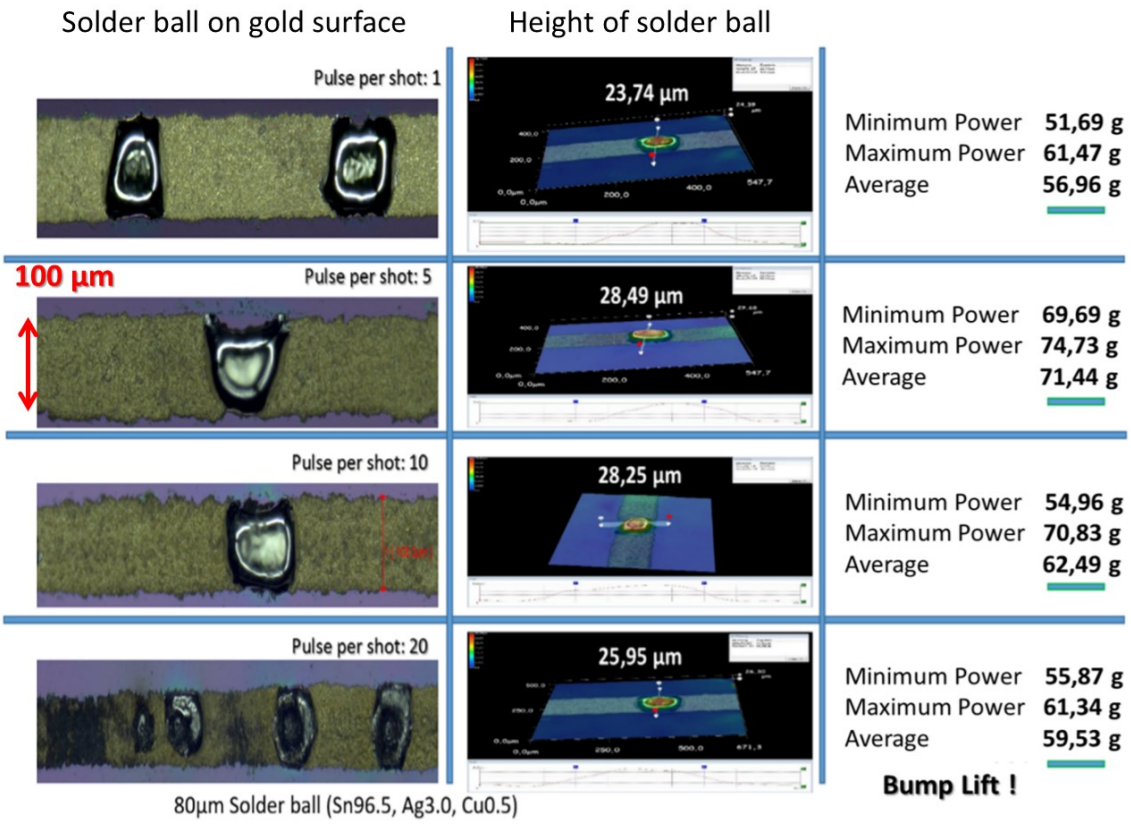

Fig.5.9 Cu-based pad, ps laser, 80% laser shots overlapping, Rep.rate: 100 kHz, Wavelength: 1064 nm, Si-wafer with Si_3N_4 Passivation

5.4. Step-By-Step optimization process

In the optimization process, three parameters including repetition rate, number of pulses per position, and laser pulse overlapping are exposed to modification. There is a change in one parameter in each step while the other parameters remained inflexible. In order to get more information on the effect of changes in the parameter, some lines were made with 100µm width. The diameter of the laser beam was calculated as around 60 µm by using 163mm focal lens with the following equation:

$$d = \frac{4.M^2.f.\lambda}{\pi.D} \quad (5.1)$$

Where, d: beam diameter in focus; M^2: beam quality; f: focal lens diameter; λ: wavelength; D: collimated beam diameter.

When the lines were made, E-less nickel was plated and accordingly gold-plated by ensuring passivation for growth and consolidation of the particles. The ps Lumera laser was used during the optimization process. The optimization of the laser pulse energy will be described in 5.4.1.

5.4.1 Determination of optimum pulse energy

In these tests, the repetition rate is changed from 45-120 kHz, and the laser pulse energy is measured for each segment. The aluminum and copper printed particles on a Si-wafer substrate is illustrated in Figures 5.10 and 5.11 respectively. Upper row with red color indicates the repetition rates in kHz and the second row represents the average output power, measured by the external power meter. This power is measured while the laser is pulsed (Q-switch). Two downer rows are regarded laser pulse intensity (blue) and laser energy (green). The repetition rate in the following tests is noted. It is measured by observing the output pulse on an oscilloscope and determining the pulse numbers per second. Energy per pulse is defined by dividing the average power by the repetition rate. Laser parameters can be calculated based on the following equations:

$$\mathrm{E(Energy\ in\ Joules)} = \frac{\mathrm{P\ (Average\ power\ in\ Watts)}}{\mathrm{R.rate\ (Repetition\ rate\ in\ pulse\ per\ second)}} \tag{5.2}$$

The peak power of an optical pulse is the most extreme happening optical power. Because of the laser short pulse durations (ns, ps, fs), peak powers can become very high even for energetic pulses.

$$Peak\ Power[W] = \frac{Laser\ Pulse\ Energy\ [j]}{Pulse\ duration\ [s]} \tag{5.3}$$

The laser intensity is the result of photon energy and photon flux. The intensity of a laser beam is the optical power per unit area, which is transmitted through the target surface to the spread direction. The units of the optical intensity (*or* light intensity*)* are W/m^2 or more commonly W/cm^2.

$$Intensity\ \left[\frac{Watts}{cm^2}\right] = \frac{Laser\ peak\ Power[W]}{Effective\ focal\ spot\ area\ [cm^2]} \tag{5.4}$$

In the measurements, the Intensity has been calculated by considering the Average output power. Laser fluence defined as the energy which is delivered

per region or active area. Within the group of laser researchers and experts, it is widespread to characterize fluence in units of J/cm^2.

$$Fluence[\frac{jouls}{cm^2}] = \frac{Laser\ Pulse\ Energy\ [j]}{Effective\ focal\ spot\ area\ [cm^2]} \quad (5.5)$$

As it can be seen in Fig.5.10, the printed lines are melted when the repetition rate is below 75 kHz, due to the high pulse energy. The black line in the middle of these films is because of the Gaussian beam profile based on the distribution of special beams and the properties of transformation. The highest energy producing a smooth and appropriate deposition of particles is related to 87 μJ and 230 KW/cm² Intensity which is shown in the picture. The nickel and also gold particles are plated in the seeds on the lines and it shows the line's quality better. Wherever the aluminum particles are deposited perfectly and there is no melted area, the nickel and gold covered the aluminum and makes the pad area bumping applications. Actually the 87μJ is the threshold for this deposition test and by increasing the repetition rate; the laser pulse energy will be reduced and it causes smooth deposition on the Si-wafer. The same experimental setup and test condition with identical laser parameters are done in copper which is shown in Fig.5.11. 500nm coated copper is used as a donor to be transferred on a Si-wafer substrate. The results indicated that optimal parameter in the LIFT process could be achieved for a repetition rate above 80 kHz (6.61W of Average Power and Energy of 82.6μJ).

While using ultrashort laser pulses, the physical processes such as photochemical action play an essential role in the thermal proceeding. Copper has better stability in forward printing on the heated Si-Wafer substrate than aluminum because of notable difference in melting point of them and also heat conductivity. Aluminium particles flowed in the reflow oven chamber due to the weak adhesion. The laser intensity is performed as the boundary situation in the irradiated target area when the heat is distributed on the surface.

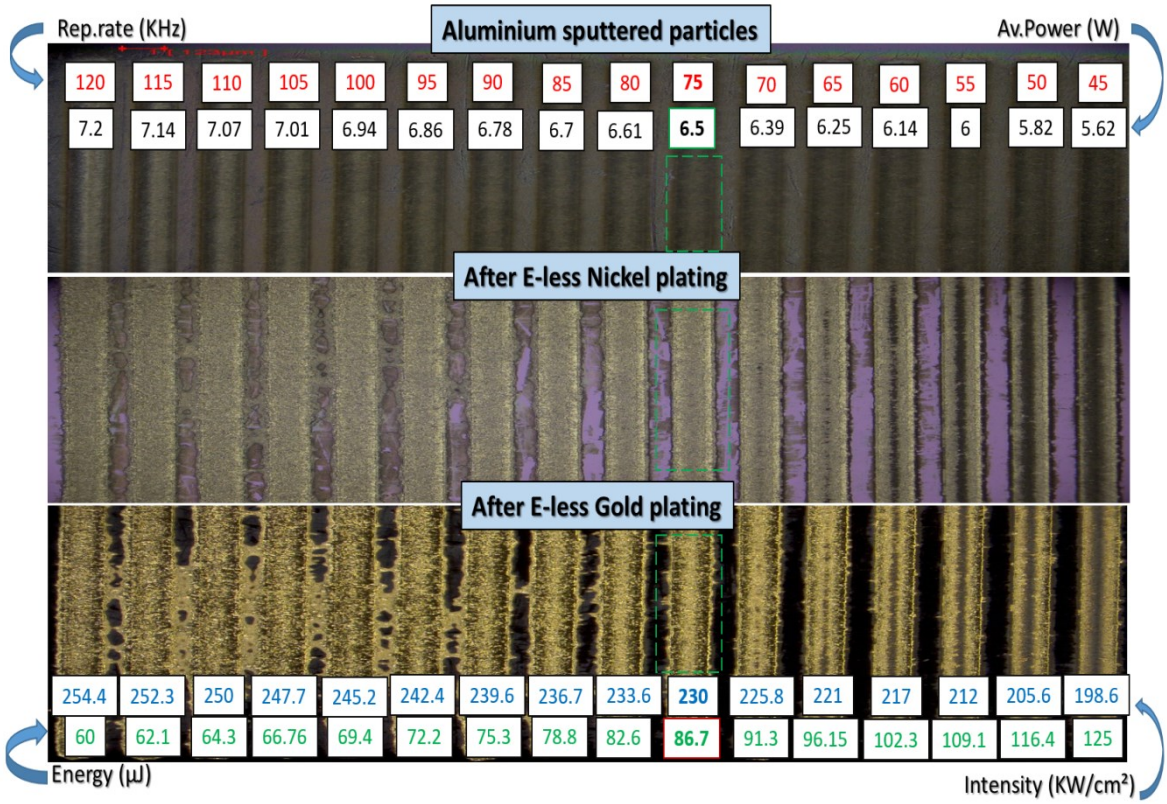

Fig. 5.10 Optimization of Repetition rates and Pulse energy- Aluminum

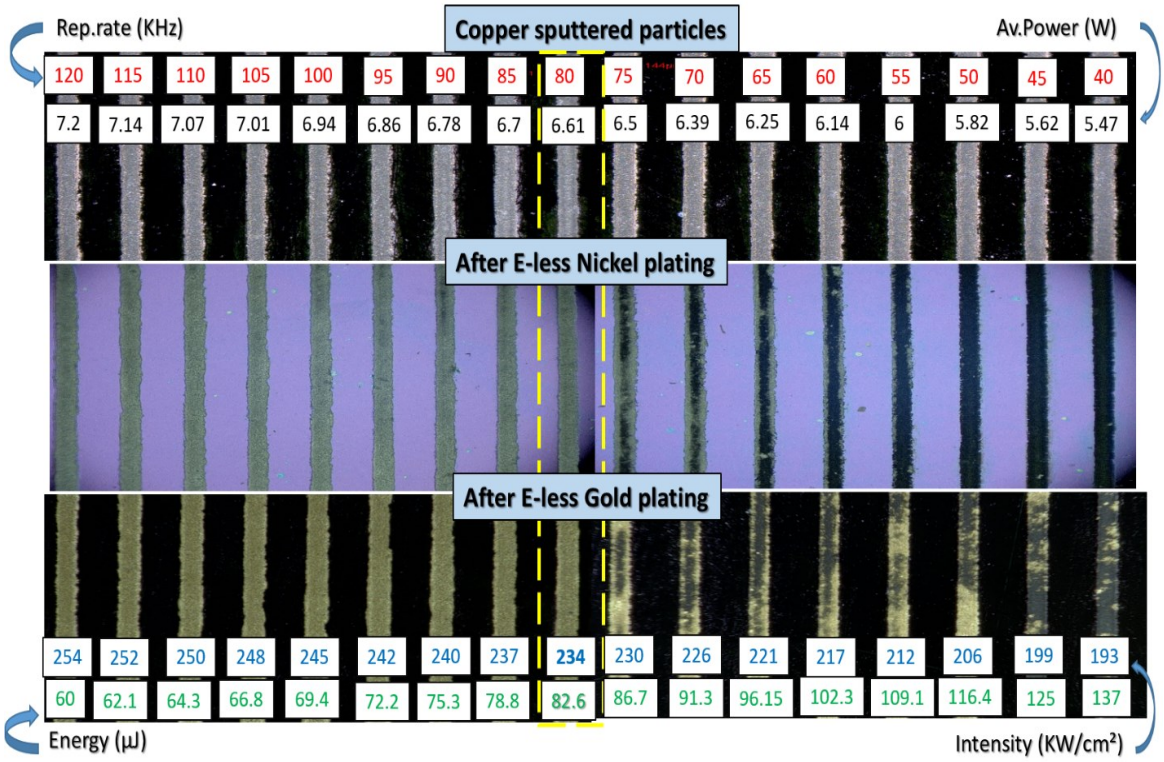

Fig.5.11 Optimization of Repetition rates and Pulse energy- Copper

The yellow line in the picture shows the threshold in the procedure. Having the repetition less than 80 kHz causes the melting area in the center of the lines. By increasing the repetition rate, the film quality will be steady. It is worth mentioning that, higher laser intensity affords smoother lines on the receiving substrate. Figure 5.12 illustrates two repetition rates; 50 kHz (above pictures) and 120 kHz (down pictures) based on distinct pulse energy and intensity. The laser parameters have been written in the figure. The laser energies are 116 µJ and 60 µJ for the repetition rates of 50 kHz and 120 kHz respectively. In the second row of the picture, there was a surplus in the Intensity in comparison with the upper row, and it is the reason that the melting area in the middle of the line cannot be seen. After analyzing through EDX, the whole area was wholly plated with nickel, and no molten area has remained. By having a closer look at the picture, it can be perceived that higher laser energy causes deformation of the thin film. By increasing the repetition rate, the energy will be better and smoother shape appears. The film in Fig.5.12 has thickness of 2 µm nickel and 500 nm gold which have been plated on the Aluminum particles.

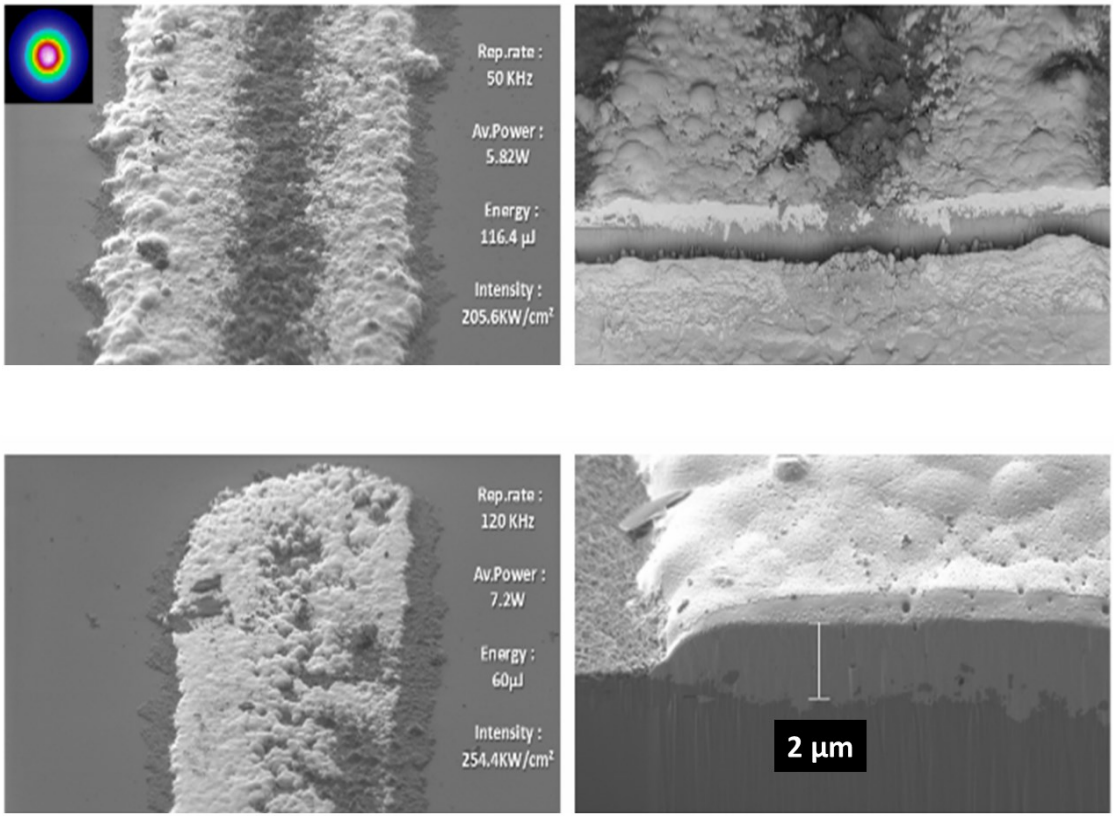

Fig.5.12 Focused Ion beam cross section of Aluminum particles

5.4.2 Optimizing pulses per shot

In this procedure, pulses per laser shot are exposed to be optimized. First, it was observed that good results were obtained for a repetition rate of more than 80 kHz. Therefore, a repetition rate of 100 kHz was utilized in the optimization steps. As the optimization of the overlapping has not done yet, 80% is considered for the first step. A change from 1 to 40 took place for the deposition of Al on silicon wafer based on silicon nitride passivation for the pulses per position. Al includes a relatively high and fixed reflectance in the observable and an infrared range of wavelength. The results for pulses per shot in the range of 7- 13 can be illustrated in Figure 5.13. Having 8-10 pulses per each position causes soft deposition as it can be seen in the picture. The higher number of pulses more than 15 affords surface deformation, and the transferred aluminum particles will make the diffusion layer with the substrates, and no nickel will be plated on the grains.

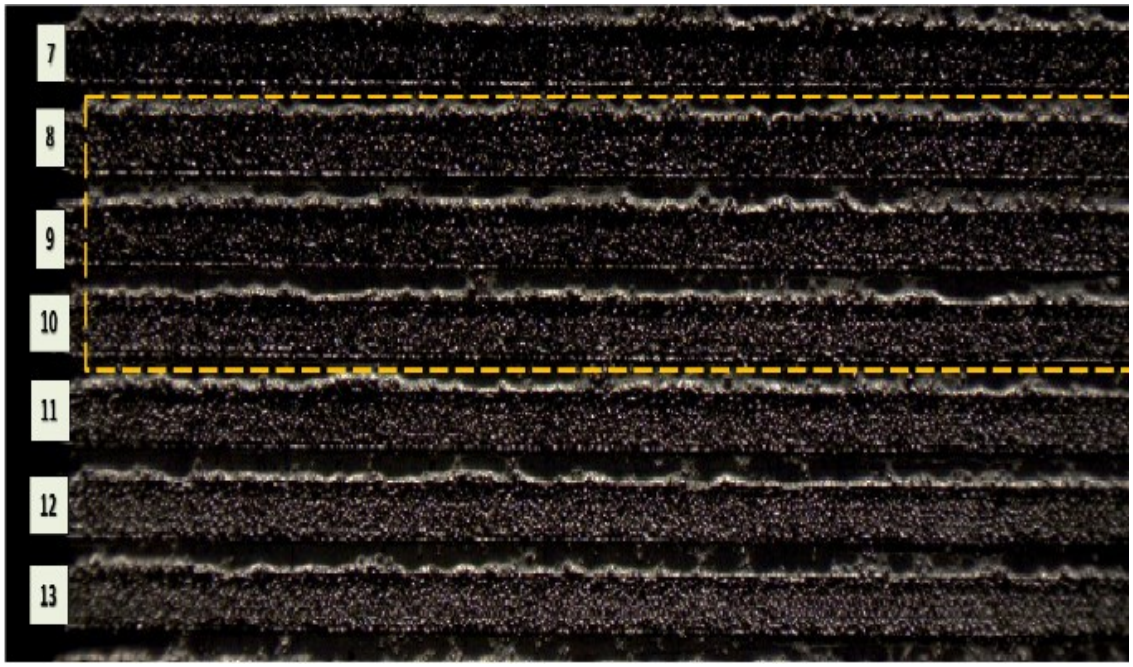

Fig.5.13 Optimization of pulses per laser shot in Aluminum

Based on the results, the particles were not deposited well on the substrate for less than eight pulses per position which caused the samples to fail the

adhesion tape test. A suitable deposition result was observed at 8-10 pulses for aluminum and 8-9 pulses for copper which has been illustrated in Fig.5.14.
The high energy paves the way for an impaired layer on the substrate when the number of pulses increased to more than 15 like the same for aluminum. The best parameter as to pulse per shot optimization for both aluminum and copper, which could have simultaneously smooth deposition and could also pass the scratch tape test is 9. The Head affected Zone (HAZ) will cause unsmooth surface around the lines when the pulse numbers are too high. Line numbers 11-13 in the Fig.5.14 indicates this fact.

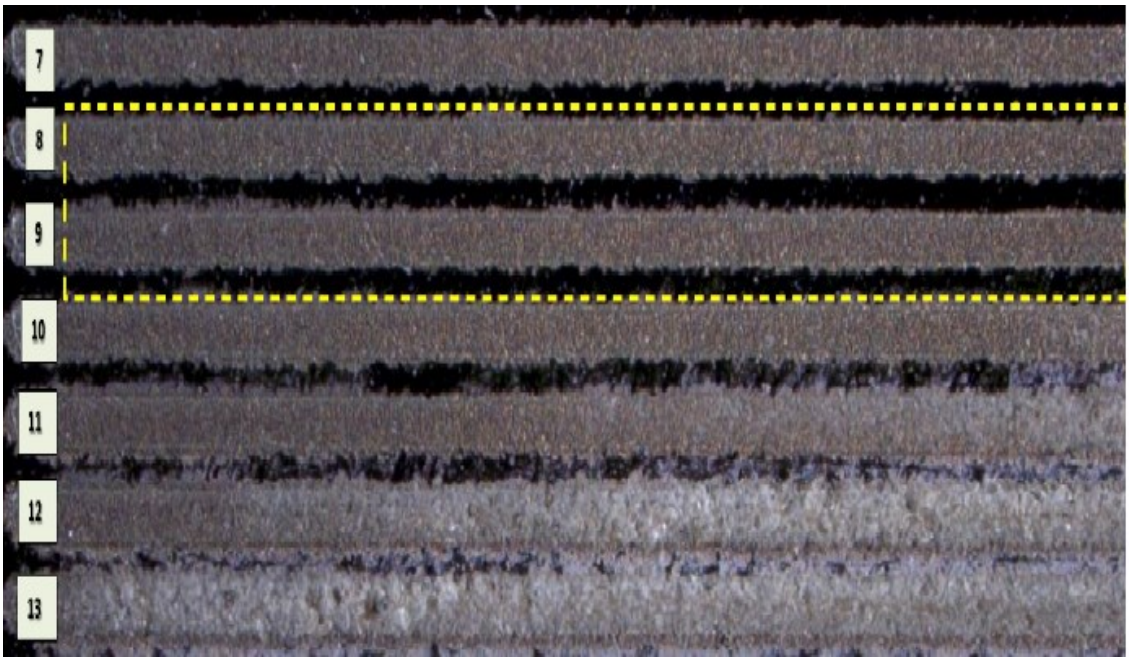

Fig.5.14 Optimization of pulses per laser shot in Copper

5.4.3 Optimizing shot-to-shot overlap

Finally, the overlapping was exposed to optimization. Based on the previous step in which nine pulses per shot could obtain excellent results for aluminum and copper both. There was a change in the range of 1-40 µm center to center for the distances among the laser shots. As it is clear from Figure 5.15, the laser pulses by having 5-13 µm distance is shown in 9 lines. The distance of 10µm and 11µm was able to generate perfect lines with smooth layers. If the gaps between each laser shot are more than 20µm, the distortion can be clearly

observed on the edges. The picture displays the test after nickel plating as well. The film shapes show the melted lines in 5-7µm distances within the first three lines.

The same setup and test parameters are done for copper particles which have been illustrated in Figure 5.16. The optimal distance between laser shots for copper was identified as 10-11 µm. The copper lines are plated with nickel as well as for the aluminum which represented in Fig.5.15. It is concluded that 80% overlapping could ensure the production of perfect lines for both aluminum and copper. With less than 10µm distances between each laser shot, the lines have more overlap which can be seen in the pictures after nickel plating. The diffusion layer occurs when the intervals between each laser pulses are too less. In a specific position and a small gap between each laser shot, the printed particles will be implemented in the substrates, and the silicon dioxide will cover the transferring grains in the upper side of the Si-Wafer. Therefore, the four right lines in the picture (lines 10-13) have adsorption stage based on figure 2.5 in Chapter 2.

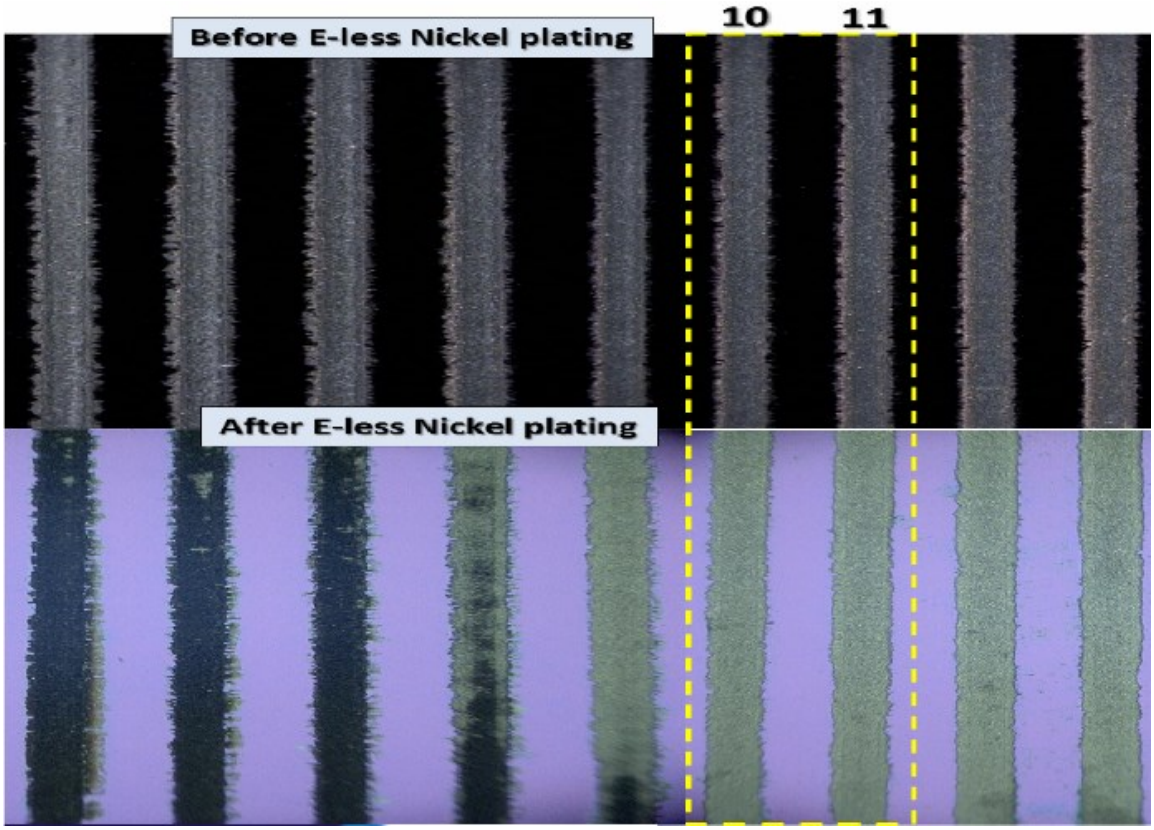

Fig.5.15 overlapping optimization of shots in deposition process; Aluminum

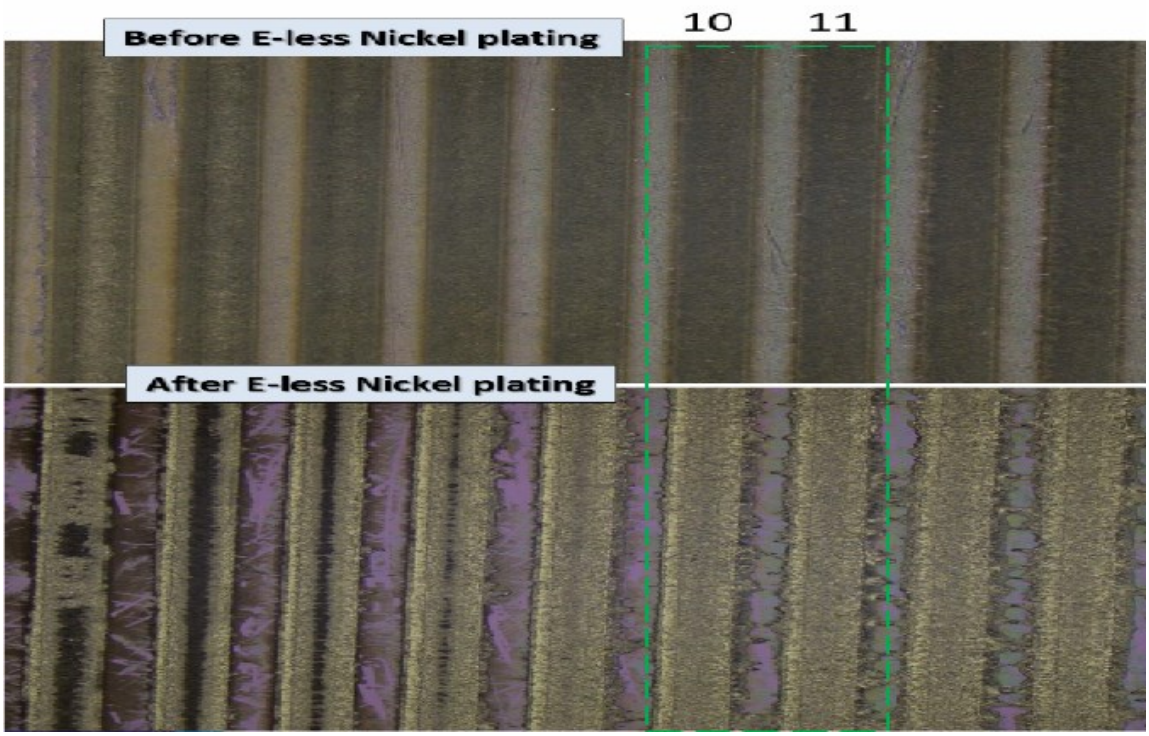

Fig.5.16 overlapping optimization of shots in deposition process; Copper

5.5. Focused Ion Beam (FIB) analysis

A focused ion beam (FIB) system is a novel technology that has a high level of analogy with a focused electron beam system, for instance, scanning electron microscope (SEM) or a transmission electron microscope (TEM). In these systems, the electron beam is coordinated towards the specimen, and it generates signals that are utilized to make high magnification pictures of the sample. The Gallium (Ga+) ion beam hit the layer of the sample, and very small amount of material in nano ranges will be sputtered. The signal from the ions which are sputtered makes the image. FIB would be used in microscopic defects or cracks and also artificial microstructures in the surfaces.

Based on the optimal parameter set specified in the mentioned steps in 5.4.1, 5.4.2 and 5.4.3, lines including 100µm width were deposited on silicon substrate. When Al and Cu are forward transferred, an ordered intermetallic alloy will be generated. As explained before, first, electroless nickel was plated with 3-4µm height, and then 500 nm gold was plated for the coalescence of the particles.

As it can be seen in the following figures 5.17 and 5.18 different number of laser pulses is made of aluminum and copper respectively. The left side of these pictures illustrates just one pulse per each position while the right side indicates the 20 pulses. The FIB cross section shows the deposited particle on the substrate. The height of the printed particles after Electroless nickel plating are measured as approximately 4-5 µm for aluminum and 1.7- 4 µm for copper. Al involves high reflection index for different ranges of laser wavelengths. Also, aluminum can react spontaneously with air to establish aluminum oxide because of highly reactive properties [125, 126]. For both following figures, the same test parameters as before have been used; Lumera laser with eight ps pulse duration, 1064nm wavelength, aluminum and copper coated glass by the evaporating method with 500 nm thickness and the 300µm gap to the Si-wafer with Si_3N_4 Passivation. The laser shots have 80% pulse overlapping and 100 kHz repetition rate. The smooth layer with just one pulse indicates the appropriate energy for the LIFT process; however, the adhesive tape test could not pass these specific test parameters with acceptable results. The green lines in the Fig.5.17 show the melted area.

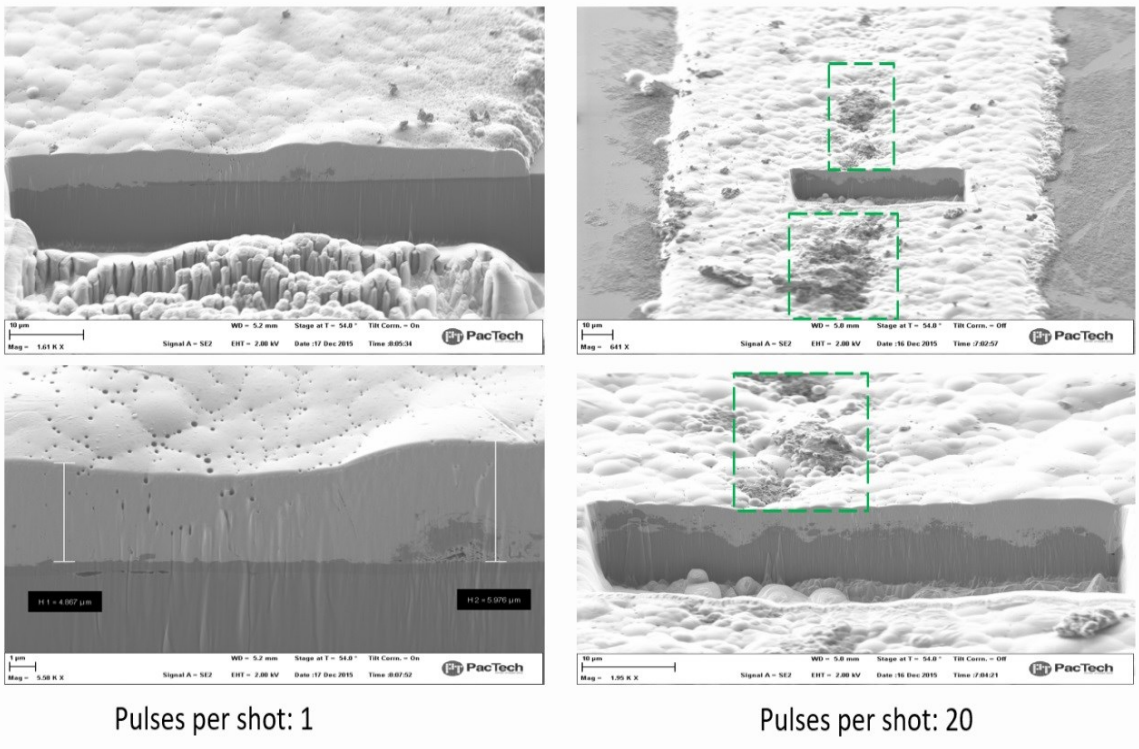

Fig.5.17 Different laser pulses per shot for aluminum material deposition

The pulse numbers per shot are too much, and it causes deformation through the lines. The pictures are taken by scanning electron microscopy (SEM) in the clean room, and the cut in the film is made by Focused Ion Beam at PacTech GmbH.

Fig.5.18 represents the utilization of copper material for deposition. The roughly flat area with nanometer deviations is made by just one pulse while the deformation layer arises with 20 pulses per each shot. The surface is cut horizontally with a focused ion beam under visual inspection. The materials (aluminum and copper) are removed with a small depth of the substrate (Si-wafer). The cutting surface can be positioned with submicrometer accuracy so that even the most minor structures can be represented in the cross-section.

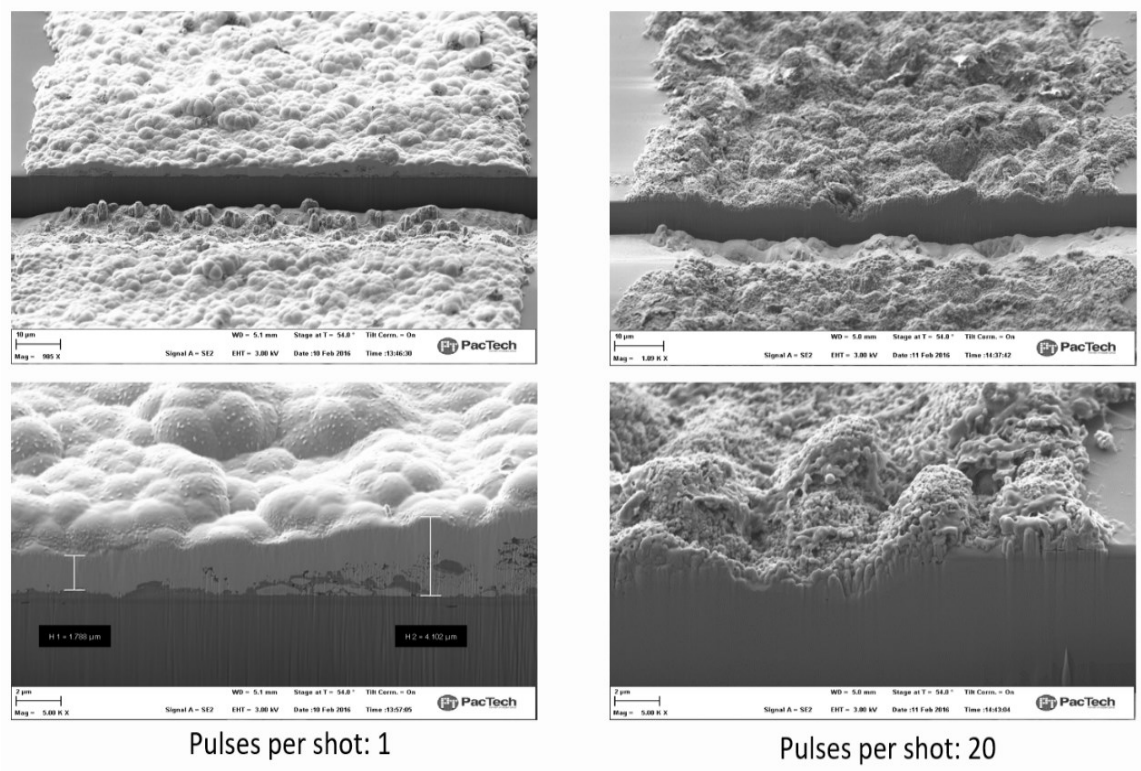

Fig.5.18 Different laser pulses per shot for copper material deposition

In Fig.5.19, four pictures are illustrative of different laser wavelengths (Infrared & green) and two different materials; Al and Cu. The same test condition of the previous tests is used for these investigations, but the pulse per shot is shown as just 1, and the nickel is not plated on the surfaces. The upper left picture is illustrative of copper in a frequency doubled laser, and the picture on its right

side represents the same material in a picosecond infrared laser. Two downer pictures in the following figure show the aluminum particles which are induced forward transfer by green and infrared laser in left and right respectively. The coating thickness of aluminum and copper on the donor glass is 500 nm. It can be perceived that copper particles are deposited successfully and make the seeds from both distinction laser wavelengths.

The result of Energy-dispersive X-ray spectroscopy of each picture is shown in the upper left side of them. The EDX analysis illustrates the roughly equal percentages of copper (80%) on the Silicon wafer substrate for both lasers, but with distinguished higher oxidized layers in infra-red laser effect. The copper has 15% copper oxide (CuO) with the infrared laser, but it has only 5% CuO in the green laser. Copper has surface reflectivity (R) of 95.8% and approximately 58% at 1064 nm and 515 nm wavelength respectively. The copper oxide layer in the infrared laser is because of the less absorption index for copper in this wavelength.

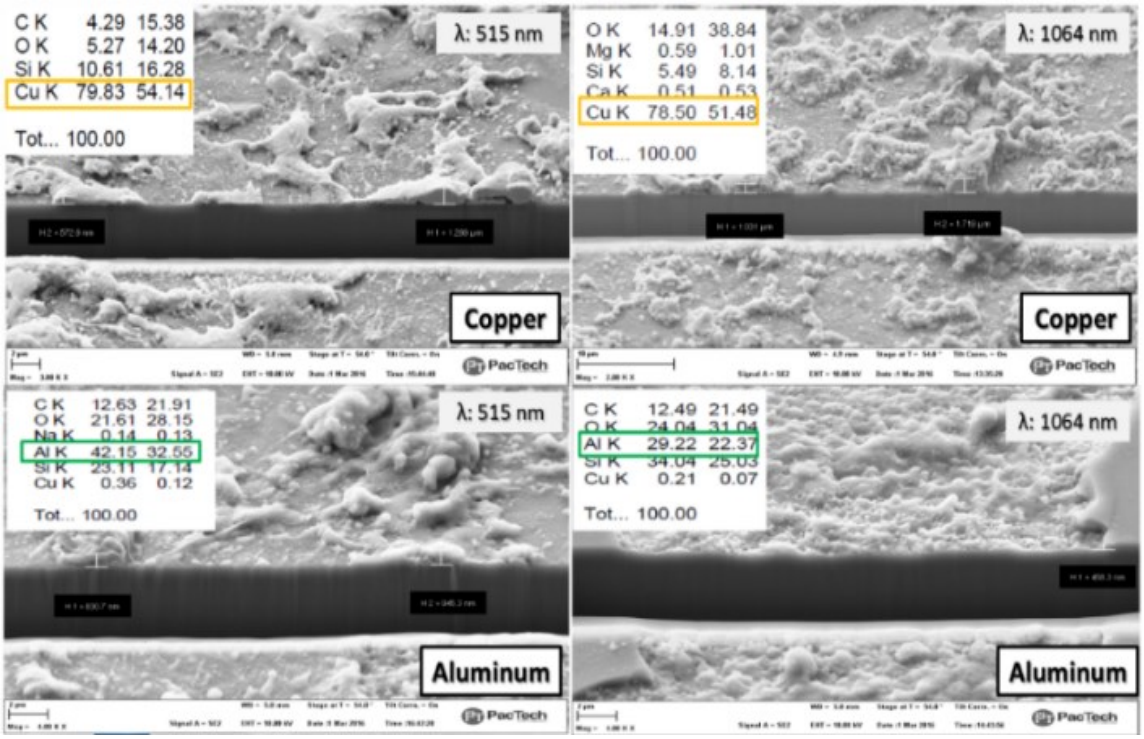

Fig.5.19 LDW of Al and Cu particles by different laser wavelengths and repetition rates; Pulse duration: 8 ps, Substrate: Si-Wafer with Si_3N_4 Passivation, Pulse per each shot: 1, distance between each shot: 10µm, Rep.rate: 100 kHz, distance between donor and substrate: 300µm

Two downer pictures are representative of aluminum utilization. The roughly same aluminum dioxide layer from the EDX analysis is because of the same reflection index of aluminum for both lasers. The FIB cross-sectioning of particles on the substrate indicates the wettability and smooth surface which could be utilized in the production of electronic pads in shape and diameters [12, 13].

Copper and aluminum have both high heat conductivity (Cu: 400 & Al: 250 ($W.m^{-1}.K^{-1}$)) and they are different in specific heat capacity (Cu: 0.4 & Al: 0.9 ((J/g-°C). It means that copper is better at heat transfer than aluminum, but aluminum is able to radiate the heat into the air more than copper because of its lower density (Cu: 8.96 & Al: 2.7 (g/cm^3)). It could be summarized that specific physical property of aluminum and copper cause occurring different specification of deposited particles in shapes, orientation, size, HAZ, and roughness on Si-Wafer during the LIFT process. The form of deposits produced by the LIFT procedure depends on the removal process of the aluminum and copper in the target as well as on the interaction of the incoming molten material with the substrate. The removal process exposes itself to the distribution of the material on the substrate. The optimum operating parameters have been achieved for aluminum and copper; e.g., laser pulse energy, donor film thickness, quality of the laser beam, and pulse width for efficient transfer of the features in the LIFT process. It was also found that the micro aluminum and copper particles with a smooth surface morphology are obtained at a fluence level just over the printing origin for the sample. This deposition threshold is conditioned on the sample thickness, duration of the laser pulse, etc. The laser power, the donor thickness, and the paste substrate gap are identified as critical variables in the process.

5.6. Roughness measurement test

Laser direct writing is used for deposition of aluminum and copper particles on the Si-wafer substrate based on 1064 nm (Infrared) and 515nm (green) as two kinds of different picosecond laser wavelengths. The line width of each material is elastically controlled by changing the magnification of the lens. The material

line widths are around 70μm and 35μm for infrared and green laser, respectively. Both of these lasers were optimized for approximately 70 μJ pulse energy in 100 kHz repetition rate. In order to get more information on the particles transferred to the substrate, different adhesion tests have been implemented for the selected samples. Various factors play a role in adhesion, such as interface contamination, structure, chemical dependency and interface broadness with modification of ion energy and ion species, although the properties of the thin film may not be considered [114, 115].

For preparing the samples, ethanol and deionized water were used to wash Si-wafers and then they were dried at 100°C in the oven. Furthermore, the implanted substrates immersed in the ethanol beaker in the ultrasonic cleaner tank with 80°C were used to investigate the mechanical stability of thin films on Si-wafers. No significant difference was reported for ultrasonic cleaning on the samples with high-frequency vibration before and after 30 minutes.

Surface roughness regarded as the quality of having a heterogeneous or irregular layer. This index plays a significant role as it is used to determine the way of interaction between the transferred particles with the silicon wafer substrate. The surface is rough when the deviation of the real surface from its ideal form is enormous. A profilometer instrument is utilized to measure the quality of the surface profile. Among the most common parameters of roughness, Ra, Rz, and Rsk are going to be mentioned. Ra represents an average of the roughness of the deposited aluminum and copper particles by implementing laser-induced forward transfer. The roughness considered as the area existing between the roughness profile and its average line. Ra cannot be regarded as a complete index to represent the line shapes although it is the most common parameter used for measuring the surface profile. Some profiles may have different deep peak and valleys in their shape even if they involve the same Ra. Rz (ISO) is described as the mean of roughness depth, which represents the mean distance between the five highest peaks and the five lowest valleys in each length of the sampling. Skewness (Rsk) is regarded as another important parameter used to measure the printed micro/nano particles, which is in charge of describing the profile shape [116-118]. Rsk represents the

symmetry of the variation of a profile about its mean line. More random surfaces include a skew near zero. Rsk has different distributions as follows:

Rsk = 0: Symmetrical about the average line (normal distribution)

Rsk > 0: Skewed downward relative to the average line

Rsk < 0: Skewed upward relative to the average line

As it is observed from Figure 5.20, the reflection rate varies about some factors such as the wavelength of laser light, material types and surface state. The horizontal axis illustrates the laser wavelength while the vertical one indicates the percentage of reflectivity percentage 20 intervals.

In the material having a high coefficient of absorption, the laser beam can change to heat energy, leading to an increase in the temperature the surface. Thin coated layer on the glass is ablated and removed by the power of the focused laser while implanting the material on the adsorption layer of silicon wafer substrate [122, 123]; however, high laser power involving short pulses leads to the very little thermal impact on the substrate.

By looking at the diagram in fig.5.20, more carefully, it is concluded that ultraviolet laser has a higher rate of absorption and Infrared light has a higher rate of reflection based on copper, silver and gold alloy. As far as aluminum is concerned, the amount is nearly fixed or unchanged. When a Green or IR laser is used, less than 5% difference is reported for the reflection.

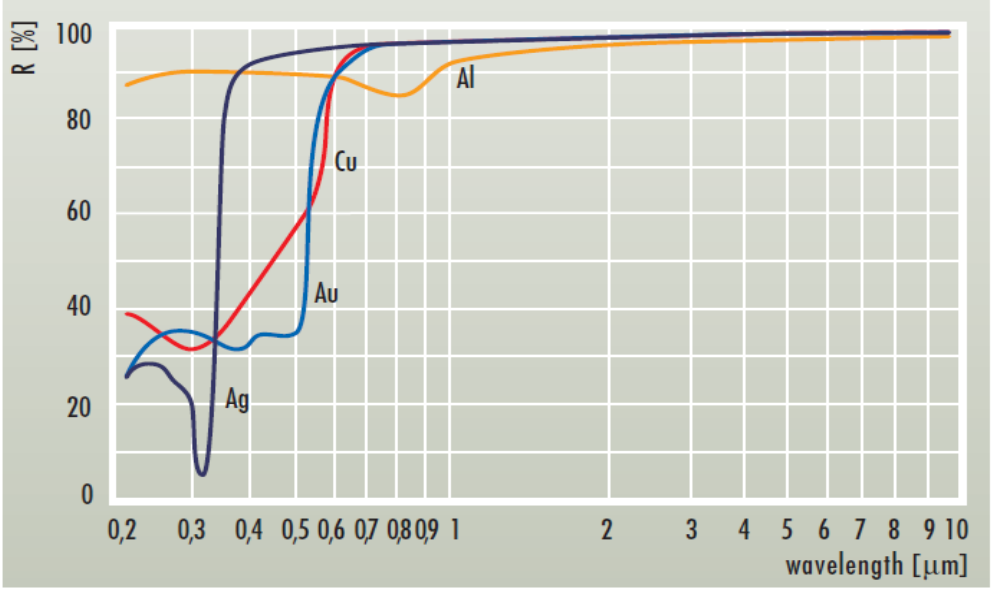

Fig.5.20 Reflectance diagram vs. wavelength for different materials [121]

Copper includes a very high reflectivity (98%-99%) during the infrared, but there is a limited reflectivity (60%) regarding the green spectral regions.
A decrease in the reflectivity and an increase in the transmission of the surface are possible when the thickness and density of metal coatings are controlled.
The roughness measuring test is done by using Infrared Lumera picosecond laser and green Trumpf laser with the same pulse duration. The repetition rate is fixed at 100 kHz for both lasers and the number of pulses per shot considered as 9 for both copper and aluminum. 80% overlapping is carried out for both tests. The main roughness parameters for copper and aluminum for the mentioned different wavelength is summarized in table 5.1.
As it is evident from the table, the mean roughness depth is around 1 μm based on infrared laser and aluminum while the Rz drastically increased to 2.34 μm for the same wavelength with copper, which can represent the smoother surface of the particles of the aluminum donor, compared to copper coated glass.
As it has been explained, the reflectivity of aluminum remains approximately fixed in two different wavelengths; however, the results are different regarding the laser with 515 nm wavelength. The green laser with copper material by 1.33 μm height difference is placed the second smoothest area. By looking again at the reflectance diagram, 58% reflection belongs to copper, based on the frequency doubled laser. Rz represents the softest level of copper particles on the substrate, although the average of roughness is slightly high (0.2μm).

Table.5.1 Different picosecond laser wavelengths on aluminum and copper

	Rsk (μm)	Ra (μm)	Rz (μm)
Green Laser Aluminum	1.55	0.177	2.15
IR Laser Aluminum	0.394	0.108	✓ 1.03
Green Laser Copper	1.05	0.2	✓ 1.33
IR Laser Copper	0.825	0.234	2.34

The skewness of the lines is shown in the first column of the table. When the value of Rsk is greater than 1.5 in magnitude (positive or negative), the surface fails to have a smooth form and a simple parameter such as average roughness is apparently not adequate to characterize the surface quality. Furthermore, Rsk near zero can represent the homogeneous line made of aluminum involving 1064 nm wavelength. Different curves from the roughness measurements (Rz) from Table.5.1 are shown in Fig.5.21 which illustrates the maximum deviation of peaks and valleys.

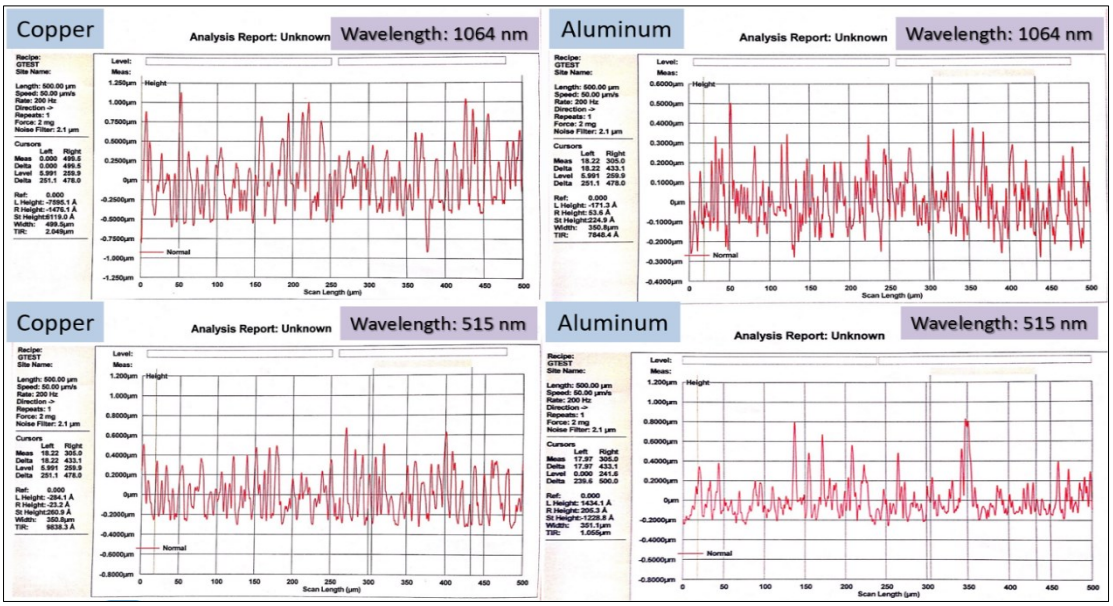

Fig.5.21 Cu and Al roughness diagrams for different laser wavelengths

Laser wavelength and the materials are written on all sides of the Fig.5.21. The existence of the difference in the skewness of copper and aluminum lines is represented according to their absorption and reflection index. The radiation of the laser beam on the processing surface includes a high density of energy. Laser beams are reflected on the surface of materials through the material reflection or attracted by the density of light. The rate of reflection on coated glass plays a significant role in utilizing the laser for special processing.

The ablation threshold of metal particles is correlated to the mean of the dissociation energy of a coated glass and the ability to reflect or attracting ultra-short laser pulse radiation [119]. A shorter wavelength leads to a rise in reflection while there is an increase in absorption when expansion takes place

in photon energy [120]. Laser radiation on the silicon wafer causes aluminum and copper particles to be transferred, which leads to the creation of some lines. As it can be seen in Fig.5.22 and Fig.5.23, four lines are made by laser direct writing method. The distance between each laser shot was optimized by 10μm, 9 pulses per each position and the 100 kHz repetition rate, which is shown in Fig.5.22 and 40 kHz in Fig.5.23.

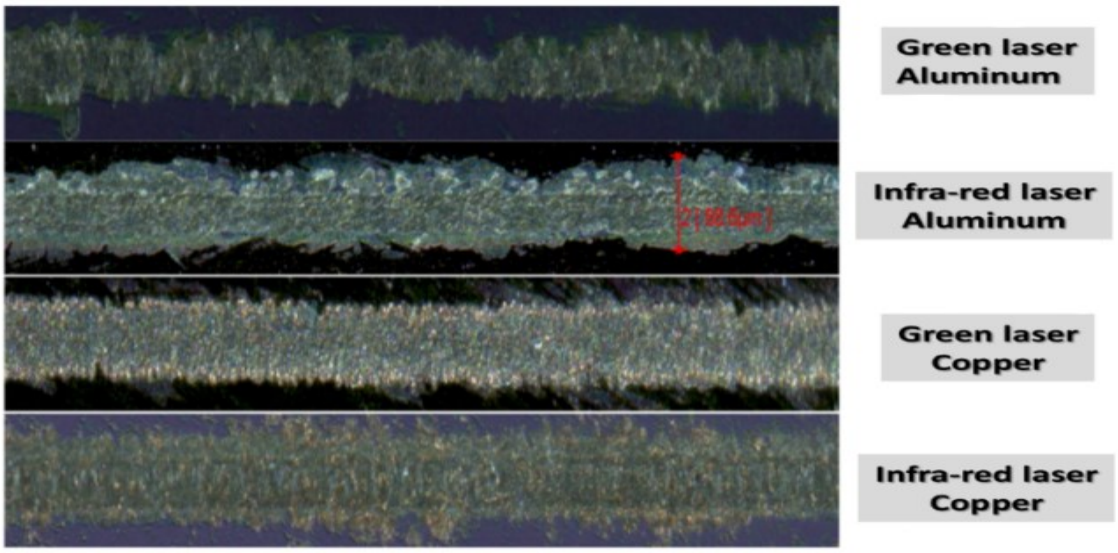

Fig.5.22 100 kHz repetition rate versus different laser wavelengths for aluminum and copper particles

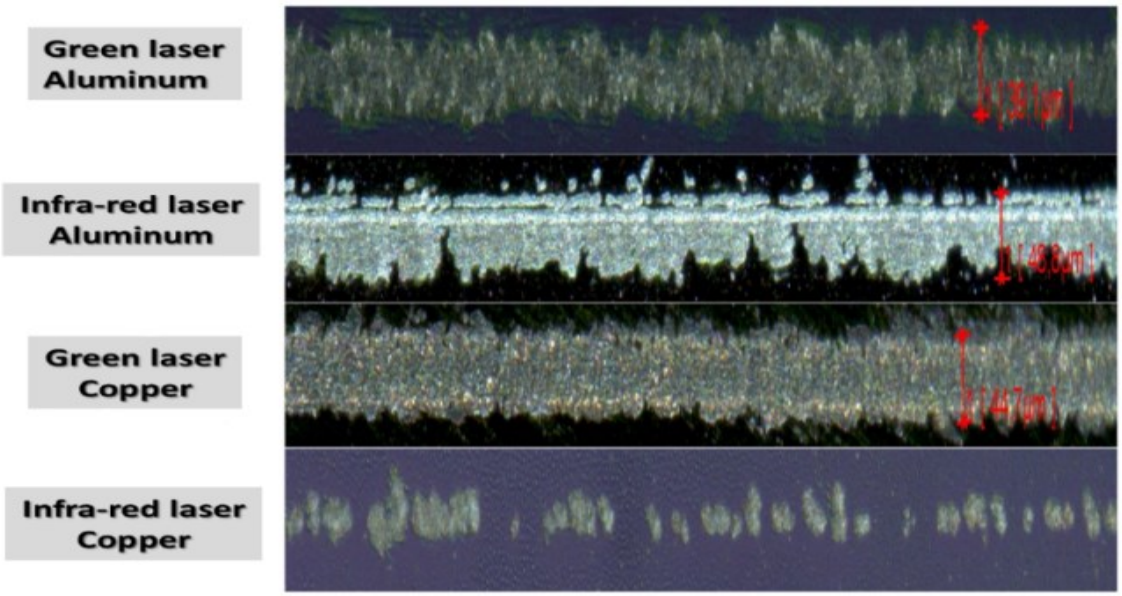

Fig.5.23 40 kHz repetition rate versus different laser wavelengths for aluminum and copper particles

Pulse energy equals to 137 μJ for both lasers (infrared and green) with a 40 kHz repetition rate. The first line in figures 5.22 and 5.23, indicated aluminum particles as the donor based on the frequency doubled laser (λ=515nm), which are deposited on the substrate. The infrared laser (λ=1064) is used for aluminum particles as it is evident in the second line. By looking at the third and fourth lines, copper is applied for positioning particles with green and IR laser, respectively. The pulse energy of the IR laser for aluminum and copper equaled to 69.5 μJ, based on 100 kHz repetition rate and 7 W output power. As for aluminum and copper, the laser intensity with 1.064 μm wavelength was 245 KW/cm². Therefore, it can be concluded that the copper has an appropriate wettability for both different laser wavelengths. However, considerable high pulse energy at 40 kHz leads to the implantation of the uneven surface. It is clear that the quality of lines with lower intensity is not the same as higher density. In other words, the higher laser intensity leads to more transfer of particles in the solid membrane and creates a desorption structure for the layer. The silicon nitride layer (Si_3N_4) leads to the passivation of the silicon wafer to reduce the permeation of particles in Si-wafer substrates, accordingly hinders diffusion phenomenon [124]. The coating thickness of aluminum and copper was 500 nm on a standard glass based on the diameter of 250mm and the thickness of 1.1mm.

Figure 5.24 illustrates the LIFT tests on copper particles in 3 phases; copper transferred on a Si-wafer substrate, nickel plated on copper particles and finally, electroless gold is plated on nickel grains. The tests are executed by infrared ps Lumera laser with 100 kHz optimized repetition rate and the 9μm distance between each laser shot. The first row in the picture is illustrative of 1 pulse per each position while the second row shows just five pulses. Row 3 and 4 represent 10 and 20 pulses per each position respectively. Each line has around 100 μm width and 15 mm length. It is evident by increasing the pulse numbers from 5 to 10 and 10 to 20, the film is not going to be transferred in the Si-wafer, and it creates molten and rough areas on the substrate which nickel and gold could not be adequately plated on the particles. Having fewer pulses

per shot bring smooth and flat pad lines, but the adhesion should be considered in these test conditions.

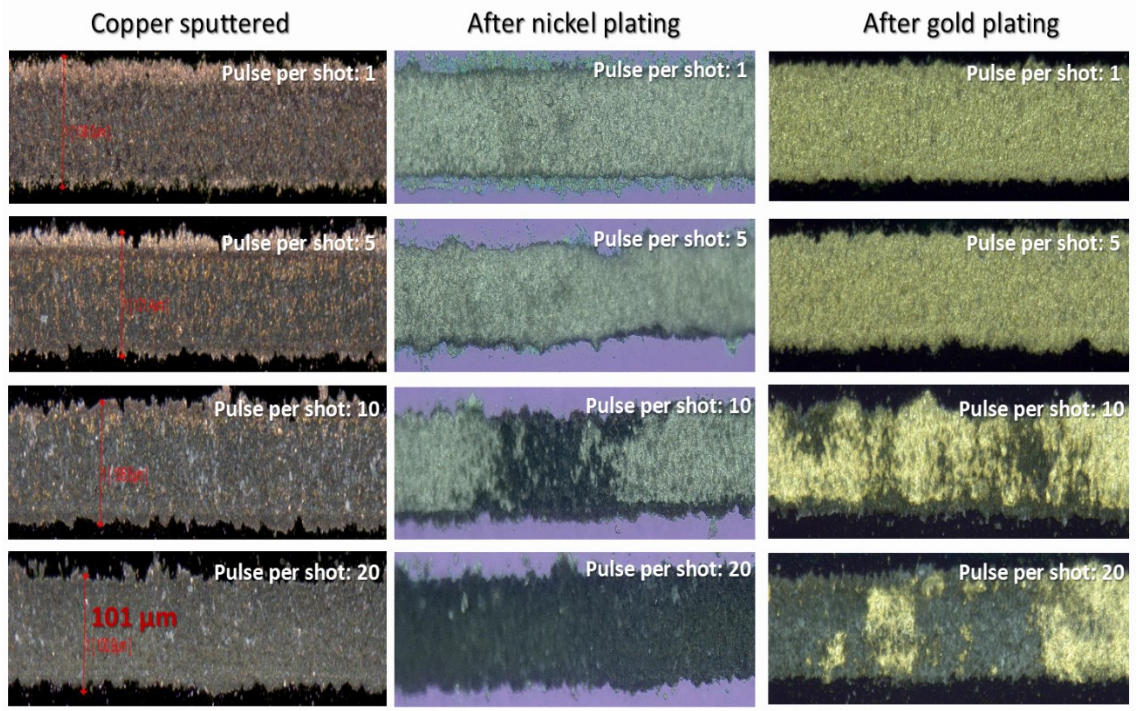

Fig.5.24 Copper deposition particles by LIFT technique by considering different pulses per laser shot in 3 stages; copper transferred particles, after nickel plating and after gold plating process

The following diagram in Fig.5.25 provides information regarding roughness measurements in different test conditions. While the vertical axis represents mean roughness depth (Rz) with an interval of 1, the horizontal one depicts the different test numbers based on table.A.1 in the Appendix. The infra-red ps laser with different deposition parameter is performed for the surface profile measuring. By having a closer look at the diagram, it can be perceived that copper makes a smoother film on the silicon wafer in comparison with aluminum. The maximum Rz for copper belongs to test number 49 with 50 kHz repetition rate, 15 pulses per shot, the 5µm distance between each laser shot and 116µJ energy. The second higher Rz is for test number 33 with 116 µJ pulse energy and 50 kHz repetition rate. The least average roughness (Ra) for copper is with highest repetition rate and lower pulse energy by considering the least pulse overlapping (Test 48). Besides, the best group of roughly a flat area

for copper is for tests 13-16 which the pulse number is just 1 and with 20μm pulse intervals. For aluminum, the measured roughness is worse than copper. When the number of the pulses increases, it causes a drastic rise in the average roughness. The worst results belong to the tests with the highest pulse overlapping (tests 113-116) and especially for test number 97. The smoothest measurement is for test number 96 by paying attention to its test parameters; highest repetition rate, least pulse energy, five pulses per each shot and maximum distance between each laser shot.

As it can be seen in fig.5.26, skewness has been measured in different test conditions. When Rsk is bigger than 1.5, the surface does not have a smooth form, and the best results for skewness should be close to zero to provide the homogeneous film on a silicon wafer. By having a closer look at the table A.1 in the appendix and diagram in fig.5.26, it is evident that copper has better results in skewness than aluminum. The quantity of bigger Rsk than 1.5 for aluminum is much more than copper. The worst outcome for aluminum belongs to the test number 87 with 200 kHz repetition rate, five pulses per each position and 10μm distances between each laser shot. The laser pulse energy is calculated as 40 μJ. For copper, the worst results belong to test numbers 36 and 42 which both have ten pulses per each position and pulse energy of 25μJ and 69μJ respectively. The error deviation has been calculated for each test parameters, and it is shown in the figures as well. By calculating the standard deviation of Rsk for aluminum and copper with Minitab Software, it can be concluded that copper has better profile shape than aluminum in the printed lines. The standard deviation of measured skewness of aluminum and copper is 1.51 and 0.82 respectively. This variation is calculated for Rz as well. Aluminum had 2.81 aberrations while copper possesses just 1.33. It means that copper has a smoother surface in comparison with aluminum. The reason is that of the difference in physical specification of copper and aluminum. The specific mass (ρ) of copper is roughly three times more than aluminum (Al: 2.71; Cu: 8.96 (Kg m^{-3})). In addition, copper has a much higher melting point than aluminum. It means appropriate laser energy could transfer copper particles and make a soft layer while it causes uneven surface of aluminum.

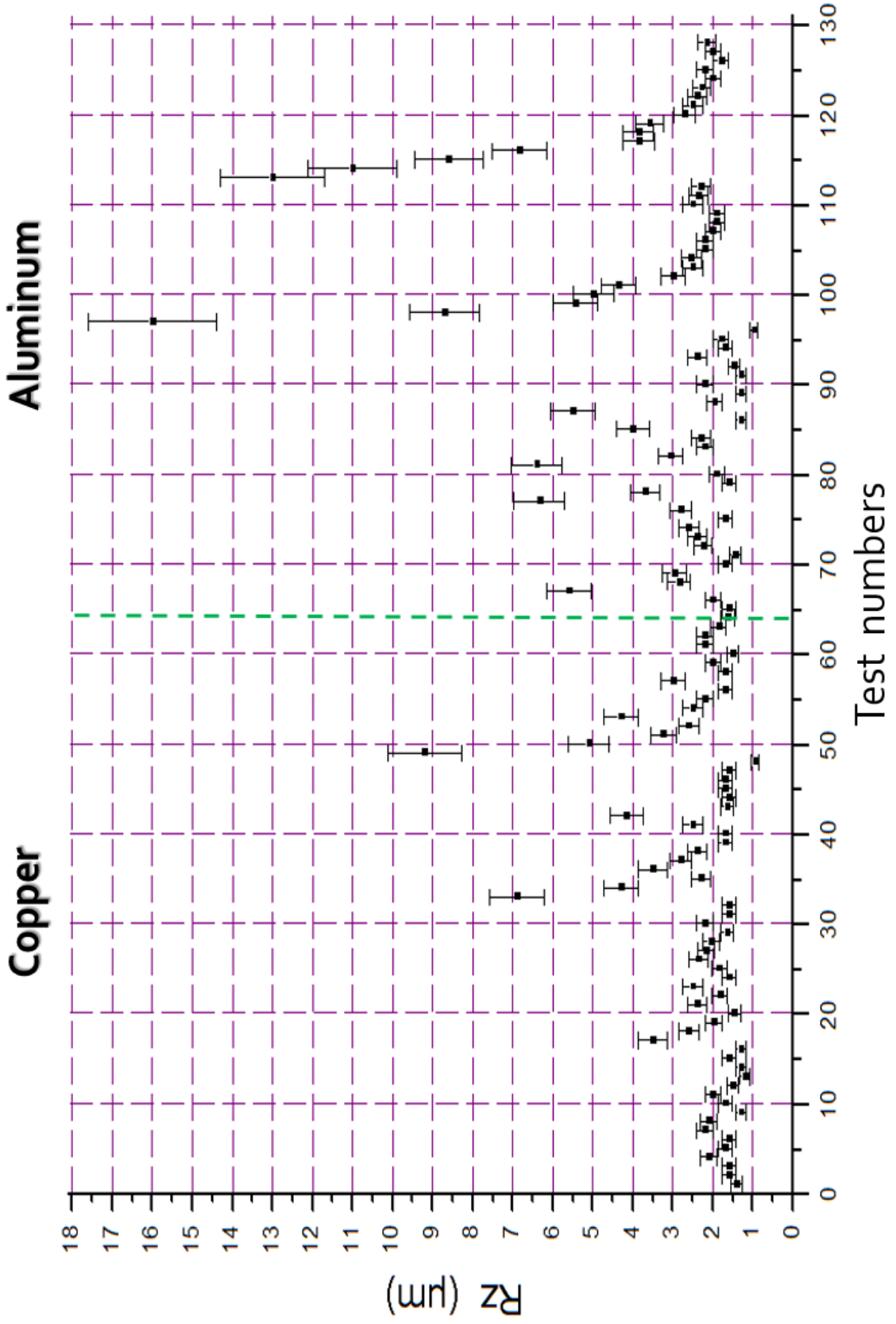

Fig.5.25 Aluminum and Copper average roughness diagram

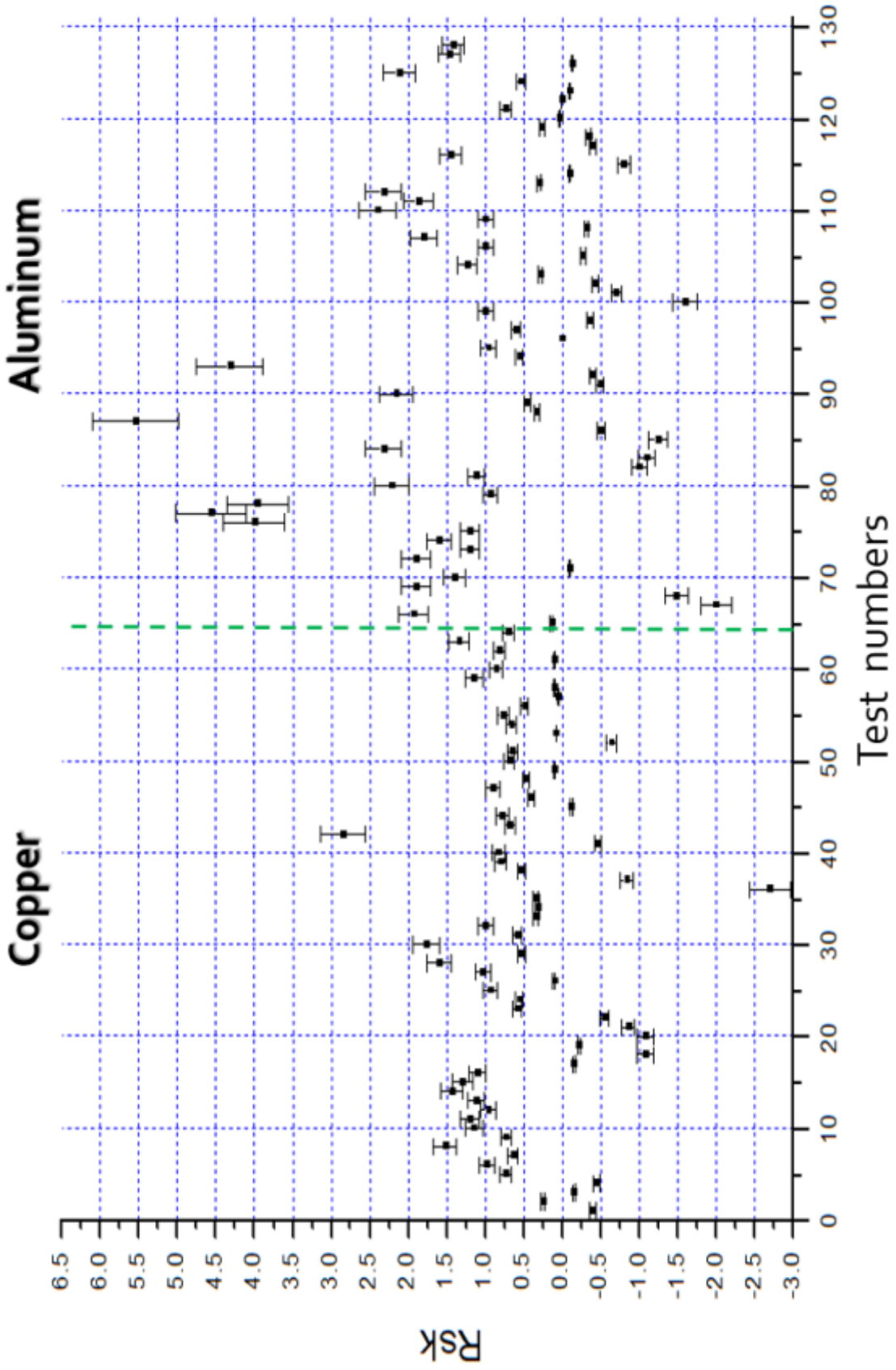

Fig.5.26 Aluminum and Copper skewness measurements

Multilayer thin films play a significant role in microelectronic applications, MEMS and nano electromechanical systems [127-130].

This chapter aimed to demonstrate how parameters can be optimized for nano particles transferring. First, the threshold of repetition rate was measured to transfer the aluminum and copper. Then, pulse energy and Cu onto the Si-wafer substrate were measured accordingly. Furthermore, the pulse-overlapping and also the number of laser pulses per each position were optimized. After Al and Cu nano particle were deposited, Ni was plated on Al seeds to reach an approximately 4-5 μm of the extra Ni layer. Longer plating times resulted in thicker coatings, although a reduction of the plating rate happened over time. The higher surface coverage is regarded as the result of depositing smaller particles directly onto the silicon, which led to a higher homogeneity and better adhesion. The growth of thickness was largely controlled by temperature and time.

The scientific progress of this study goes on the advantages of the LIFT process, especially in metal grids in solar cell applications (CIGS) which can be generalized in production lines. LIFT is an adequate substitute for traditional metal gridding techniques like Photolithography and Evaporation method. The main advantages of the LIFT comparing to the Photolithography are the higher transferring speed (up to 30 m/s), maskless process and no etching requisition which has chemical pollution during the process.

In evaporation technique, the mask is going to be covered with vaporized material, and it should be cleaned after several usages, which increases the process steps and also raise the costs and the process cycle time. Equal line widths and heights could be achieved in the Laser direct writing procedure. In spite of the evaporating technique, LIFT has a very fast transferring process, and it is applicable even in very large substrates (1-4 m^2) with different materials (glass, epoxy, silicon wafers and etc.)

6. Conclusion and Outlook

In the present study, the goal was the implementation of a new technique to produce thin films of a material into a surface. The laser-induced forward transfer has been characterized of aluminum and copper by using ps laser pulses with different wavelengths from a coated donor glass. The optimum operating parameters for aluminum and Copper are evaluated, For instance; laser fluence, focus quality, pulse duration, repetition rate, pulse per each laser shot and shot overlapping for efficient transfer of the particles in the LIFT process.

Laser pulse energy and the thickness of the coated glass layer were regarded as the parameters included in this process. The printed lines are smoother and more homogeneous at lower pulse energies, which are regarded as the result of high repetition rate with modifications in the optical features of the glass.

Laser parameters play a significant role in the profile of the deposited particles on the target substrate. By establishing all the deposition parameters, the optimized pulses per each shot starts from 9 and 10 based on the laser power, which could pass both tape and shear adhesion tests successfully. It determines the achievement of the uniform thickness across the wafer for both aluminum and Copper. By decreasing the laser pulse numbers from 10 to 1, the laser pulse energy is not sufficient to transfer aluminum and copper particles perfectly. Besides, by increasing them from 10 to 20, the pulse energy is too high, which pave the way for devastating the film layer and causes creating the unsmoothed surface of the absorption layer of silicon wafer substrate.

Copper involves a smoother surface by laser direct transfer, along with the wavelength of 515 nm in comparison with aluminum. The penetration of the particles is much higher in 40 kHz repetition rate, for both copper and aluminum, which is regarded as the main reason for the rough shape on the silicon wafer substrate. Fewer particles were transferred onto the substrate because of high pulse energy at lower repletion rates.

The nickel is plated on the particles to create more coalescence on the target substrate for doing the shear test. The height and thickness of nickel are based

on the amount of aluminum, copper, or other materials which are deposited onto the target surface.

In order to transmit the particles from the coated side of the glass to the target, pulsed laser energy should be placed higher than the threshold energy. This deposition threshold is dependent on the sample thickness, quality of focus, and duration of the laser pulse as well as laser intensity. The minimum required energy to achieve smoothly transferred particles on a Si-wafer substrate by using a donor with 500 nm coated thickness was 83 μJ and 87 μJ for copper and aluminum respectively. By increasing the laser fluence above the deposition threshold, broad areas around the deposited particles are seen because of the heat affected zone (HAZ).

Adhesion is regarded as an applicable method of showing how well two different materials adhered together. The measurement of the adherence indicates the essential force for separating the particles from the surface. The excellent film adhesion can be reached in the LIFT technique after passing the tape and shear test successfully. The size, shape, and the phase state of the transferred particles can be controlled by the laser fluence and by the thickness of the donor film.

In the LIFT process, there is no need for a clean room, chemical compounds, and vacuum chambers despite the Photolithography, sputtering, evaporation technique and LCVD process. Most of the LIFT processes are carried out under ambient atmospheric conditions. Also, LIFT has high flexibility to make the lines, shapes, structures in different substrates (glass, Si-wafer, Epoxy material, etc.).

By optimizing the laser parameters and also the coating specification on the donor glass, feature sizes could be achieved success on the order of 1-2 μm in the LIFT process. This simple, fast, one-step technique has great application potential in research on micro- and nano-device fabrication. Wire bonding and interconnection of microelectronic devices in micro scales, as well as soldering in less than 30 μm, are regarded as some applications of implementing the proposed method in the near future. The non-contact 3-dimensional laser direct-write technique has the ability of adaptation and outperforms the 3D interconnect processes and TSVs (Through Silicon Via). In other words, the

implementation of this technique for deposition accurately and assembling the building blocks of different shapes and sizes may result in utilizing electronic and MEMS devices for a variety of applications by decreasing costs and complexity.

Appendix

Table A.1 shows 128 tests with different laser parameters for aluminum and Copper. As it can be seen, test numbers 1-64 belongs to copper and 65-128 is for aluminum. 3rd column in the table relates to different repetition rates during the test. 50,100,200 and 400 kHz repetition rate is adjusted for each test. A number of the laser pulses vary from 1 to 20 in four subdivisions; 1,5,10 and 15 passes for each position. The fifth column is illustrative of pulse overlapping. The distance of each laser shot has been performed as 5, 10, 15 and 20 µm. The laser pulse energy has been calculated for each test with its specific parameters. Columns 7-17 represent the roughness parameters for each row. In order to explain these parameters, some terminologies are going to be introduced:

Sampling Length (l):

Sampling length or Cut-off Length is the normal wavelength for distinguishing the roughness and waviness.

Evaluation Length (L):

Evaluation length or Assessment Length is the length that the value of surface parameters is measured.

Mean Line (M):

Mean Line is the border line for measuring the profile deviations of the roughness.

Profile Peak:

Profile Peak is the maximum height in the profile that lies above the mean line

Profile valley:

Profile Valley is the maximum depth in the profile that lies below the mean line.

Profile Irregularity:

Profile Irregularity is a profile peak adjoining the profile valley.

By having all, we can define the roughness parameters as follows: R_p and R_v are maximum profile peak height and maximum profile valley depth from the mean line respectively. In the other word, they are the highest and lowest point in the measuring profile. Rz which belongs to the 9th column in the table

provides information regarding the average maximum profile of the five highest peaks-to-valleys in the appraised area. Rz is one of the essential roughnesses measuring parameters which are helpful for surface evaluation texture. Rc (mean height of profile irregularities) is the mean height of profile elements illustrates the average value of the height of the curve element in the test length. Rt is the maximum height of the sampling profile. In the other word, Rt is the vertical distance between the highest and lowest points of the profile in the evaluation length. Ra (Average roughness) is the average of the points of the profile heights over the evaluation length. Ra is usually utilized to explain the roughness of the surface; however, Rz has more precision value, and it has been shown in Fig.5.25. The Rq (Root Mean Square) provides information about the average between the height deviations and the mean line over the evaluation length. Rq or RMS is a functional parameter to show the skew and kurtosis in the profile. Rsk is a measure of the asymmetry of the profile regarding the mean line. Skewness illustrates the characteristics of the process. Negative skew shows the valley dominations and the positive ones indicate the surfaces with peaks. The best parameter for skewness is zero. The 15th column in table demonstrates the Rku which is representative of kurtosis in the profile. Rku is a measure of edges above and below the mean line. A perfect surface has Rku=3. This index is used to control and to measure the stress fractures. Rmr is defined as the fraction of a line and states as a percentage and Rdc is Profile high section difference in μm.

Table A.1 Roughness measurement by considering laser parameters

No.	Material	Rep. (KHz)	#Pulse	shot dis.(µm)	energy (µJ)	Rp (µm)	Rv (µm)	Rz (µm)	Rc (µm)	Rt (µm)	Ra (µm)	Rq (µm)	Rsk	Rku	Rmr (%)	Rdc (µm)
1	Copper	50	1	5	116	0,69	0,72	1,40	0,52	1,4	0,13	0,18	-0,4	4,6	94	0,26
2	Copper	100	1	5	69	0,88	0,72	1,60	0,51	1,6	0,15	0,21	0,25	4,4	76,2	0,29
3	Copper	200	1	5	40	0,74	0,88	1,60	0,49	1,63	0,17	0,23	-0,15	3,7	87	0,33
4	Copper	400	1	5	25	0,98	1,2	2,10	0,61	2,15	0,2	0,28	-0,45	4	58,4	0,4
5	Copper	50	1	10	116	1,08	0,62	1,70	0,5	1,7	0,14	0,2	0,74	6	22	0,24
6	Copper	100	1	10	69	1	0,57	1,60	0,46	1,6	0,14	0,2	0,98	6,6	43	0,27
7	Copper	200	1	10	40	1,2	0,99	2,20	0,53	2,2	0,16	0,23	0,64	5,5	12	0,28
8	Copper	400	1	10	25	1,44	0,63	2,10	0,65	2,1	0,17	0,25	1,52	8,2	5,11	0,3
9	Copper	50	1	15	116	0,86	0,41	1,30	0,39	1,3	0,13	0,18	0,73	4,1	80	0,26
10	Copper	100	1	15	69	1,25	0,46	1,70	0,43	1,7	0,13	0,18	1,15	7,5	7,9	0,26
11	Copper	200	1	15	40	1,32	0,72	2	0,45	2	0,18	0,26	1,2	6,5	10,8	0,3
12	Copper	400	1	15	25	1	0,54	1,50	0,41	1,5	0,16	0,21	0,96	5,1	43,4	0,31
13	Copper	50	1	20	116	0,82	0,38	1,20	0,32	1,2	0,1	0,15	1,12	6,8	91,3	0,18
14	Copper	100	1	20	69	0,95	0,39	1,30	0,33	1,3	0,11	0,16	1,43	7,2	62	0,19
15	Copper	200	1	20	40	1,2	0,44	1,60	0,39	1,6	0,13	0,19	1,3	7,6	13	0,24
16	Copper	400	1	20	25	0,9	0,44	1,30	0,36	1,3	0,15	0,2	1,1	5,5	71	0,29
17	Copper	50	5	5	116	1,9	1,6	3,50	1,5	3,5	0,25	0,45	-0,15	6,3	3	0,28
18	Copper	100	5	5	69	1	1,6	2,60	1	2,6	0,15	0,28	-1,08	7,1	66	0,13
19	Copper	200	5	5	40	1,06	0,92	1,98	0,74	1,98	0,11	0,21	-0,22	6,9	17	0,07
20	Copper	400	5	5	25	0,65	0,8	1,46	0,48	1,46	0,09	0,17	-1,08	7,2	95	0,05
21	Copper	50	5	10	116	1	1,37	2,40	0,66	2,4	0,14	0,23	-0,86	7	33	0,21
22	Copper	100	5	10	69	0,87	0,96	1,83	0,64	1,83	0,14	0,22	-0,55	5,8	79	0,21
23	Copper	200	5	10	40	1,47	1	2,50	0,7	2,5	0,13	0,23	0,59	10	2,5	0,18
24	Copper	400	5	10	25	0,97	0,6	1,60	0,49	1,57	0,13	0,2	0,56	6,8	69,3	0,2
25	Copper	50	5	15	116	1,14	0,7	1,85	0,58	1,85	0,13	0,2	0,93	7,5	12,4	0,15
26	Copper	100	5	15	69	1,32	1	2,35	0,6	2,35	0,19	0,3	0,11	4,8	9,3	0,32
27	Copper	200	5	15	40	1,48	0,7	2,17	0,53	2,17	0,14	0,21	1,03	7,9	3	0,22
28	Copper	400	5	15	25	1,48	0,57	2,05	0,45	2,05	0,14	0,21	1,6	11	2,66	0,2
29	Copper	50	5	20	116	1,04	0,61	1,65	0,44	1,65	0,13	0,18	0,53	6	25	0,19
30	Copper	100	5	20	69	1,66	0,53	2,20	0,5	2,2	0,16	0,24	1,77	11	1,8	0,27
31	Copper	200	5	20	40	0,98	0,6	1,60	0,37	1,6	0,14	0,19	0,59	4,8	37,6	0,26

32	Copper	400	5	20	25	1,14	0,46	1,60	0,42	1,6	0,15	0,2	1	6,3	19,5	0,25
33	Copper	50	10	5	116	3,7	3,24	6,90	2,2	6,9	0,54	0,8	0,34	5,7	0,74	1,1
34	Copper	100	10	5	69	1,83	2,44	4,30	1,2	4,3	0,35	0,53	0,32	5,5	7,6	0,6
35	Copper	200	10	5	40	1,2	1,08	2,30	0,63	2,3	0,18	0,27	0,34	5,8	13,2	0,34
36	Copper	400	10	5	25	0,85	2,7	3,50	0,69	3,5	0,16	0,26	-2,7	22	79	0,29
37	Copper	50	10	10	116	1,3	1,54	2,80	0,88	2,8	0,23	0,36	-0,84	5	13,2	0,44
38	Copper	100	10	10	69	1,07	1,33	2,40	0,73	2,4	0,23	0,33	0,53	4,3	27,3	0,4
39	Copper	200	10	10	40	1,06	0,67	1,70	0,45	1,7	0,17	0,24	0,8	4,7	28	0,33
40	Copper	400	10	10	25	1	0,72	1,70	0,45	1,7	0,14	0,2	0,83	5,7	40	0,26
41	Copper	50	10	15	116	1,3	1,2	2,50	0,91	2,5	0,18	0,3	-0,46	5,8	8,4	0,33
42	Copper	100	10	15	69	3,2	0,96	4,16	1,1	4,16	0,23	0,38	2,85	20	0,54	0,34
43	Copper	200	10	15	40	1,06	0,6	1,65	0,4	1,65	0,16	0,23	0,68	4,8	25,6	0,3
44	Copper	400	10	15	25	0,8	0,79	1,60	0,35	1,6	0,13	0,18	0,78	4,8	90	0,26
45	Copper	50	10	20	116	0,84	0,9	1,70	0,63	1,7	0,18	0,26	-0,12	4	77,7	0,34
46	Copper	100	10	20	69	0,86	0,87	1,70	0,47	1,7	0,17	0,22	0,4	3,8	77,2	0,32
47	Copper	200	10	20	40	1,05	0,53	1,60	0,35	1,6	0,14	0,2	0,9	5,6	27,4	0,27
48	Copper	400	10	20	25	0,58	0,37	0,95	0,3	0,95	0,11	0,14	0,47	3,8	100	0,22
49	Copper	50	15	5	116	5,1	4,1	9,20	3,7	9,2	0,88	1,3	0,1	4,7	0,64	1,6
50	Copper	100	15	5	69	2,78	2,33	5,10	1,5	5,1	0,51	0,7	0,69	4	2,8	1
51	Copper	200	15	5	40	2,2	1	3,24	0,94	3,24	0,25	0,34	0,65	6,3	0,67	0,52
52	Copper	400	15	5	25	1,3	1,4	2,60	0,75	2,6	0,18	0,28	-0,64	6,6	10	0,3
53	Copper	50	15	10	116	2,2	2,15	4,30	1,4	4,3	0,34	0,51	0,08	5	2,5	0,66
54	Copper	100	15	10	69	1,3	1,2	2,50	0,8	2,5	0,32	0,44	0,66	3,6	18,6	0,64
55	Copper	200	15	10	40	1,3	0,87	2,20	0,6	2,2	0,18	0,26	0,77	5,6	7,4	0,35
56	Copper	400	15	10	25	1	0,69	1,70	0,42	1,7	0,13	0,19	0,49	5,5	31	0,23
57	Copper	50	15	15	116	1,7	1,33	3,00	1	3	0,24	0,37	0,05	5,2	4,3	0,42
58	Copper	100	15	15	69	0,87	0,8	1,70	0,45	1,7	0,19	0,27	0,1	4	73	0,32
59	Copper	200	15	15	40	1,5	0,54	2,00	0,43	2	0,16	0,23	1,15	7	3,8	0,26
60	Copper	400	15	15	25	1	0,44	1,50	0,37	1,5	0,14	0,18	0,86	5,5	27,3	0,25
61	Copper	50	15	20	116	1,11	1,08	2,20	0,62	2,2	0,2	0,29	0,1	4,7	22,1	0,36
62	Copper	100	15	20	69	1,34	0,84	2,20	0,5	2,2	0,2	0,28	0,82	4,7	11,4	0,36
63	Copper	200	15	20	40	1,36	0,5	1,86	0,36	1,86	0,14	0,2	1,34	8,8	4,13	0,23
64	Copper	400	15	20	25	1,1	0,53	1,63	0,38	1,63	0,14	0,18	0,7	5,6	24,2	0,28

65	Aluminum	50	1	5	116	1	0,55	1,60	0,56	1,6	0,09	0,15	0,14	9,7	15	0,15
66	Aluminum	100	1	5	69	1,3	0,67	2	0,81	2	0,15	0,27	1,94	9,3	7,5	0,2
67	Aluminum	200	1	5	40	2	3,7	5,60	3	5,6	0,33	0,52	-2	13	2	0,56
68	Aluminum	400	1	5	25	0,75	2,1	2,84	0,77	2,84	0,24	0,34	-1,48	7,3	79,4	0,44
69	Aluminum	50	1	10	116	2,2	0,7	2,97	0,78	2,97	0,27	0,39	1,9	8,3	1,7	0,47
70	Aluminum	100	1	10	69	1,1	0,58	1,70	0,49	1,7	0,15	0,21	1,4	7,5	18,5	0,29
71	Aluminum	200	1	10	40	0,74	0,7	1,45	0,46	1,45	0,18	0,24	-0,1	3,4	84	0,35
72	Aluminum	400	1	10	25	1,7	0,5	2,24	0,35	2,24	0,14	0,23	1,9	13	1,65	0,25
73	Aluminum	50	1	15	116	1,7	0,7	2,40	0,69	2,42	0,2	0,3	1,2	7,1	2,1	0,4
74	Aluminum	100	1	15	69	1,88	0,74	2,60	0,68	2,6	0,21	0,3	1,6	8,1	1,4	0,37
75	Aluminum	200	1	15	40	1,1	0,5	1,70	0,56	1,7	0,14	0,2	1,2	8,4	10,9	0,25
76	Aluminum	400	1	15	25	2,3	0,47	2,80	0,6	2,8	0,13	0,22	4	40	0,5	0,22
77	Aluminum	50	1	20	116	4,99	1,34	6,33	1,2	6,33	0,2	0,33	4,56	51	0,1	0,33
78	Aluminum	100	1	20	69	3,1	0,65	3,70	0,8	3,7	0,3	0,54	3,96	21	2,4	0,39
79	Aluminum	200	1	20	40	1,1	0,47	1,60	0,47	1,6	0,12	0,17	0,94	7,4	14,4	0,23
80	Aluminum	400	1	20	25	1,43	0,48	1,90	0,74	1,9	0,18	0,28	2,22	9,8	6	0,33
81	Aluminum	50	5	5	116	3,7	2,6	6,40	1,5	6,4	0,32	0,55	1,12	16	0,5	0,5
82	Aluminum	100	5	5	69	1,3	1,77	3,05	1	3,05	0,29	0,44	-1	5,3	16,3	0,6
83	Aluminum	200	5	5	40	0,9	1,3	2,20	1	2,2	0,3	0,44	-1,1	3,5	69	0,69
84	Aluminum	400	5	5	25	1,75	0,53	2,30	0,68	2,3	0,21	0,32	2,32	10	3,84	0,37
85	Aluminum	50	5	10	116	1,87	2,11	4	0,74	4	0,23	0,36	-1,24	11	0,83	0,41
86	Aluminum	100	5	10	69	0,6	0,74	1,30	0,45	1,3	0,16	0,21	-0,5	3	96,2	0,34
87	Aluminum	200	5	10	40	4,73	0,77	5,50	1,3	5,5	0,25	0,6	5,55	39	1	0,18
88	Aluminum	400	5	10	25	1,2	0,75	1,96	0,51	1,96	0,17	0,22	0,33	5,4	9,9	0,32
89	Aluminum	50	5	15	116	0,8	0,5	1,30	0,4	1,28	0,17	0,21	0,45	3,5	78,2	0,35
90	Aluminum	100	5	15	69	1,7	0,5	2,20	0,5	2,2	0,15	0,24	2,16	15	1,7	0,28
91	Aluminum	200	5	15	40	0,51	0,78	1,30	0,45	1,3	0,15	0,19	-0,49	3,2	99,2	0,31
92	Aluminum	400	5	15	25	0,6	0,89	1,48	0,42	1,48	0,13	0,174	-0,39	4,4	99	0,26
93	Aluminum	50	5	20	116	1,97	0,43	2,40	0,98	2,4	0,11	0,23	4,32	33	1,17	0,2
94	Aluminum	100	5	20	69	1,07	0,63	1,70	0,5	1,7	0,18	0,23	0,56	4,6	29	0,33
95	Aluminum	200	5	20	40	1,29	0,53	1,80	0,53	1,8	0,17	0,23	0,96	7	6,66	0,35
96	Aluminum	400	5	20	25	0,57	0,4	0,97	0,32	0,97	0,1	0,14	0	3,6	100	0,23
97	Aluminum	50	10	5	116	9,5	6,5	16	5,7	16	1,7	2,2	0,6	4,7	0,6	3,2

98	Aluminum	100	10	5	69	3,5	5,2	8,70	3,2	8,7	1	1,33	-0,36	4	2,4	1,8
99	Aluminum	200	10	5	40	3,2	2,2	5,44	2	5,44	0,53	0,77	1	6,2	2,95	0,83
100	Aluminum	400	10	5	25	2	2,93	4,98	1,33	4,98	0,33	0,48	-1,6	12	1,44	0,6
101	Aluminum	50	10	10	116	1,67	2,7	4,35	1,3	4,35	0,36	0,5	-0,7	5,9	7,6	0,74
102	Aluminum	100	10	10	69	1,5	1,5	3	0,93	3	0,34	0,43	-0,43	3,4	5,17	0,69
103	Aluminum	200	10	10	40	1,4	1,12	2,50	0,86	2,53	0,29	0,34	0,29	3,2	10,2	0,6
104	Aluminum	400	10	10	25	1,67	0,88	2,55	0,6	2,55	0,22	0,3	1,23	8,1	2,63	0,38
105	Aluminum	50	10	15	116	1,15	1,1	2,20	0,77	2,2	0,3	0,36	-0,27	2,8	20	0,51
106	Aluminum	100	10	15	69	1,46	0,74	2,20	0,54	2,2	0,3	0,4	1	4	12,7	0,52
107	Aluminum	200	10	15	40	1,6	0,46	2	0,44	2	0,18	0,25	1,8	11	2,84	0,3
108	Aluminum	400	10	15	25	1,1	0,76	1,90	0,56	1,9	0,24	0,24	-0,31	3,1	21	0,46
109	Aluminum	50	10	20	116	1,44	0,5	1,90	0,6	1,9	0,22	0,28	1	5	6,8	0,36
110	Aluminum	100	10	20	69	1,96	0,53	2,50	0,55	2,5	0,18	0,27	2,4	14	0,89	0,29
111	Aluminum	200	10	20	40	1,87	0,5	2,36	0,83	2,36	0,25	0,34	1,87	8,2	3,3	0,43
112	Aluminum	400	10	20	25	1,75	0,53	2,30	0,68	2,3	0,21	0,32	2,32	10	3,84	0,37
113	Aluminum	50	15	5	116	5,7	7,1	13	4,9	13	1,2	1,74	0,3	4,6	1,35	1,84
114	Aluminum	100	15	5	69	4,65	6,3	11	3,9	11	0,87	1,33	-0,1	5,3	1,4	1,6
115	Aluminum	200	15	5	40	3,44	5,2	8,60	2,6	8,6	0,44	0,76	-0,8	12	0,85	0,66
116	Aluminum	400	15	5	25	3,8	3	6,83	1,96	6,83	0,29	0,57	1,45	17	0,6	0,37
117	Aluminum	50	15	10	116	1,95	1,9	3,85	1,4	3,85	0,38	0,54	-0,4	4,1	2	0,76
118	Aluminum	100	15	10	69	2	1,8	3,86	1,33	3,86	0,4	0,55	-0,34	3,6	1,8	0,87
119	Aluminum	200	15	10	40	1,88	1,7	3,58	1,64	3,58	0,38	0,52	0,26	4,5	4,4	0,75
120	Aluminum	400	15	10	25	1,4	1,3	2,70	0,72	2,7	0,21	0,28	0,04	5,1	5,9	0,44
121	Aluminum	50	15	15	116	1,6	0,9	2,50	0,67	2,5	0,17	0,27	0,74	7,7	2,8	0,28
122	Aluminum	100	15	15	69	1,4	1	2,40	0,6	2,4	0,23	0,32	0,01	4	7	0,5
123	Aluminum	200	15	15	40	1,3	0,99	2,28	0,67	2,28	0,22	0,29	-0,1	4,4	8,5	0,44
124	Aluminum	400	15	15	25	1,12	0,85	2	0,44	2	0,18	0,26	0,54	5,1	20	0,34
125	Aluminum	50	15	20	116	1,6	0,6	2,20	0,6	2,2	0,18	0,29	2,12	8,9	5,4	0,25
126	Aluminum	100	15	20	69	0,99	0,8	1,80	0,6	1,8	0,21	0,28	-0,13	3,6	53	0,43
127	Aluminum	200	15	20	40	1,32	0,68	2	0,6	2	0,2	0,3	1,47	7,1	6,34	0,3
128	Aluminum	400	15	20	25	1,57	0,58	2,15	0,63	2,15	0,25	0,33	1,42	5,1	7,88	0,44

Bibliography

[1] Walter Koechner, ‘’Solid-state laser engineering’’, Springer series in Optical sciences, Springer-verlag, New York Heidelberg, Berlin 1976

[2] Herbert M. Urbassek, ‘’Handbook of Surface Science’’, Volume3, Chapter 17, Sputtering and Laser Ablation, 2008

[3] Zhengwen Li,a Roy G. Gordon,a, ,z Damon B. Farmer,b Youbo Lin,b and Joost Vlassak, ‘’Nucleation and Adhesion of ALD Copper on Cobalt Adhesion Layers and Tungsten Nitride Diffusion Barriers’’, Electrochemical and Solid-State Letters, 2005

[4] A. Klini, P. A. Loukakos, D. Gray, A. Manousaki, and C. Fotakis, ‘’Laser Induced Forward Transfer of metals by temporally shaped femtosecond laser pulses’’, Opt. Express 16, 11300-11309, 2008

[5] M.H.Azhdast, ‘’Arrangement for applying conductive nanoparticles onto a substrate’’, Publication patent number: WO2015117872A1, SmartPac GmBH Technology Services, 2015

[6] M. S. Brown, N. T. Kattamis, and C. B. Arnold, ‘’Time-Resolved Study of Polyimide Film Absorbing Layers for Laser-Induced Forward Transfer’’, Conference on Lasers and Electro-Optics 2010, OSA Technical Digest, Optical Society of America, 2010

[7] M. Woehrmann, Thorsten Fischer, Hans Walter, Michael Toepper, Klaus-Dieter Lang, ‘’Characterization of Thin Polymer Films with the Focus on Lateral Stress and Mechanical Properties and their Relevance to Microelectronics’’, 64th Electronic Components and Technology Conference, 2014

[8] Wang KE, ‘’Development of Lead-free Electroless nickel plating system and metal thin films on silicon and nafion membranes’’, PhD thesis, National University of Singapore, 2008

[9] F. J. Jimenez, ‘’Comprehensive Simulation of Sputter Deposition’’, PhD thesis in Electrical and Computer Engineering Department, Chap.2, University of Alberta, Edmonton, Alberta, 2012

[10] Mgr. Pavel Soucek, ‘’Deposition of functional nanocomposite coatings by PVD and their characterization’’, PhD thesis in Department of Physical Electronics, Chap.2, Masaryk University, Brno, 2013

[11] M d. Julfikar Haider, ‘’Deposition of hard and solid lubricant (TiN+MoSx) coating by Closed-field magnetron sputtering’’, School of Mechanical and Manufacturing Engineering, Dublin City University, Ireland, 2005

[12] M. Alemán, N. Bay, M. Fabritius, S.W. Glunz, ‘’Characterization of Electroless nickel plating on silicon solar cells for the front side mettalization’’, Fraunhofer Institute for Solar Energy Systems, Heidenhofstr.2, D-79110 Freiburg, Germany, 2007

[13] S. Behera and A. Khare, ‘’Characterization of Sapphire (α-Al_2O_4) Thin Film Fabricated By Pulsed Laser Deposition’’, 13th International Conference on Fiber Optics and Photonics, OSA Technical Digest, Optical Society of America, 2016

[14] G.K.Wolf, ‘’Modification of mechanical and chemical properties of thin films by ion bombardment’’, Surface and coatings Technology, 43/44, Physikalisch-Chemisches Institut der Universität, Im Neuenheimer, 1990

[15] Craig B. Arnold, Pere Serra, and Alberto Piqué, ‘’Laser Direct-Write Techniques for Printing of Complex Materials’’, MRS BULLETIN, Vol. 32, 2007

[16] Martynas Beresna, Mindaugas Gecevičius and Peter G.Kazansky, ‘’Ultrafast laser direct writing and nano structuring in transparent materials’’, Adv. Opt. Photon 6, 293-339, 2014

[17] Raymond C. Y. Auyeung, Heungsoo Kim, Scott Mathews, and Alberto Piqué, ‘’Laser forward transfer using structured light’’, Opt. Express 23, 422-430, 2015

[18] Ngoi, B K A, K Venkatakrishnan, P Stanley and L E N Lim, ‘’Femtosecond Pulsed Laser Direct Writing System for Photomask Fabrication’’, Innovation in Manufacturing Systems and Technology (IMST), 2002

[19] Mohammod Aminuzzaman, Akira Watanabe, and Tokuji Miyashita, ‘’Laser Direct Writing of Conductive Silver Micropatterns on Transparent Flexible Double-Decker-Shaped Polysilsesquioxane Film Using Silver Nanoparticle Ink’’, Journal of ELECTRONIC MATERIALS, Vol. 44, 2015

[20] Joseph P. Ulerich, Lara C. Ionescu, Jianbo Chen, Winston O. Soboyejo, Craig B. Arnold, ‘’Modifications of Ti-6Al-4V Surfaces by Direct-Write Laser Machining of Linear Grooves’’, SPIE-The International Society for Optical Engineering Department of Mechanical and Aerospace Engineering, Princeton University, Princeton NJ 08540, USA, 2007

[21] M. H. Azhdast, O. Lux, H. Fritsche, H. J. Eichler, G. Azdasht, H. Lüdeke, V. Glaw, and K. Lang, ‘’Laser Melting of Metal Powders Using Nd:YAG and Compact Diode Laser for Micro Particle Deposition’’, Advanced Solid State Lasers, OSA Technical Digest Optical Society of America, paper AM5A.2, 2015

[22] M. H. Azhdast, G. Azdasht, H. Lüdeke, V. Glaw, and K. Lang, ‘’Nano particle production by laser ablation and metal sputtering on Si-Wafer substrate’’, Advanced Solid State Lasers, OSA Technical Digest Optical Society of America, paper AM5A.3, 2015

[23] Marti Duocastella Sola, ‘’Study of the laser forward transfer for the preparation of miniaturized biosensors’’, PhD thesis, Univ. De Barcelona, 2010

[24] D.k.y. low, h. xie, z. xiong, g.c. lim, ‘’Femtosecond laser direct writing of embedded optical waveguides in aluminosilicate glass’’, Singapore Institute of Manufacturing Technology (SIMTech), 71 Nanyang Drive, Singapore 638075, Appl. Phys. A 81, 1633–1638, 2005

[25] H. Ono and T. Nakano, ‘’Diffusion barrier effects of transition metals for Cu/M/Si multilayers (M=Cr, Ti, Nb, Mo, Ta, W)’’, Applied Physics Letters, 64(12):1511, 1994

[26] P. H. Holloway and C. C. Nelson, ‘’In situ formation of diffusion barriers in thin film metallization systems’’, Thin Solid Films, 35(1):L13–6, 1976

[27] Milton Ohring, ‘’The Materials Science of Thin Films, volume 1, ACADEMIC PRESS LIMITED’’, San Diego, United Kingdom edition, 1992

[28] L. Chouanine, M. Takano, O. Kamiya, and M. Nishida, ‘’Nanomechanical characterization of thin Ti-Pt-Au multilayers deposited on top of $linbo_3$ wafer’’, Composites Science and Technology, 65(9):1414–1420, 2005

[29] Yifang Cao, Seyed Allameh, Derek Nankivil, Steve Sethiaraj, Tom Otiti, and Wole Soboyejo, ‘’Nano indentation measurements of the mechanical properties

of polycrystalline Au and Ag thin films on silicon substrates: Effects of grain size and film thickness'', Mat. Science and Engineering: A, 427(1-2):232–240, 2006

[30] Golnaz Bassiri Jahromi, ''Investigation of the near surface mechanical properties of Au-Ti thin films'', Bachelor of Science in Mechanical Engineering Oklahoma State University Tulsa, 2008

[31] Thierry Cardinal, Bertrand Poumellec, and Kazuyuki Hirao, ''Introduction: Femtosecond Direct Laser Writing and Structuring of Materials (FDLW) feature'', Opt. Mater. Express 1, 996-997, 2011

[32] A. Holmes, K. Sugioka, and B. Gu, ''Industrial Applications of Laser Direct-Write Processing'', Conference on Lasers and Electro-Optics/Quantum Electronics and Laser Science Conference and Photonic Applications Systems Technologies, OSA paper JWB3, 2007

[33] Burks HE, Phamduy TB, Azimi MS, Saksena J, Burow ME, Collins-Burow BM, Chrisey DB, Murfee WL, ''Laser Direct-Write Onto Live Tissues: A Novel Model for Studying Cancer Cell Migration'', J Cell Physiol.231(11):2333-8, 2016

[34] X. Ding, Y. Kawaguchi, H. Niino, A. Yabe, ''Laser-induced high-quality etching of fused silica using a novel aqueous medium'', Applied Physics A 75, 641-645, 2002

[35] V. Tornari, V. Zafiropulos, A. Bonarou, N.A. Vainos, C. Fotakis, J. Opt, ''Modern technology in artwork conservation: a laser-based approach for process control and evaluation'', Lasers in Engineering 34, 309-326, 2000

[36] David J. Hwang and Costas P. Grigoropoulos, ''Efficiency of silicon micromachining by femtosecond laser pulses in ambient air'', Journal of Applied Physics 99, 083101, 2006

[37] Matthias Lenzner, J. Krüger, Wolfgang Kautek, F. Krausz, ''Precision laser ablation of dielectrics in the 10-fs regime'', Appl. Physics A 68(3):369-371, 1999

[38] K. Hirota, K. Nagino, and G. Ohbayashi, ''Local structure of amorphous GeTe and PdGeSbTe alloy for phase change optical recording'', Journal of Applied Physics 82, 65, 1997

[39] David L. Bourell, Harris L. Marcus, Joel W. Barlow, and Joseph J. Beaman, ''Selective laser sintering of metals and ceramics'', Int. Journal of Powder Metallurgy volume 28, p. 369, 1992

[40] Kazuyoshi Itoh, Wataru Watanabe, Stefan Nolte and Chris B. Schaffer, ‘’Ultrafast Processes for Bulk Modification of Transparent Materials’’, Volume 31, Issue 8 Ultrafast Lasers in Materials Research, 2011

[41] E.N.Glezer, M.Milosavljevic, L.Huang, R.J.Finlay, T.-H.Her, J.P.Callan, and E. Mazur, ‘’Three-dimensional optical storage inside transparent materials’’, Opt. Lett. 21, 2023-2025, 1996

[42] P.RHerman, R.SMarjoribanks, AOettl, KChen,Konovalov SNess, ‘’Laser shaping of photonic materials: deep-ultraviolet and ultrafast lasers’’, Applied Surface Science, Volumes 154–155, , Pages 577-586, 2000

[43] Arnaud Zoubir, Martin Richardson, Clara Rivero, Alfons Schulte, Cedric Lopez, Kathleen Richardson, Nicolas Hô, and Réal Vallée, ‘’Direct femtosecond laser writing of waveguides in As_2S_3 thin films’’, Opt. Lett. 29, 748-750, 2004

[44] D. Linden and T.B. Reddy, eds. ‘’Handbook of Batteries’’, 3rd edition, McGraw-Hill, New York, 2001

[45] J.A. Barron, D.B. Krizman, and B.R. Ringeisen, ‘’ Laser Printing of Single Cells: Statistical Analysis, Cell Viability, and Stress’’, Annals of Biomedical Engineering.33 p.121, 2005

[46] Alberto Piqué, Raymond C.Y. Auyeung, Kristin M. Metkus, Heungsoo Kim, Scott Mathews, Thomas Bailey, Xianhai Chen and Lydia J. Young, ‘’Laser Decal Transfer of Electronic Materials with Thin Film Characteristics’’, A Naval Research Laboratory, 4555 Overlook Avenue, SW, Washington, DC, USA 20375, 2008

[47] Sudipta Bera, A. J. Sabbah, J. M. Yarbrough, C. G. Allen, Beau Winters, Charles G. Durfee, and Jeff A, ‘’Optimization study of the femtosecond laser-induced forward-transfer process with thin Aluminum films’’, Squier Department of Physics, Colorado School of Mines, Colorado 80401 USA, 2007

[48] P.L. Liu, R. Yen, N. Bloembergen, ‘’ Picosecond laser-induced melting and resolidification morphology on Si‘’, Applied Physics Letters 34, 864, 1979

[49] Tsing-Hua Her, Richard J Finlay, Claudia Wu, Shrenik Deliwala, Eric Mazur, ‘’ Microstructuring of silicon with femtosecond laser pulses’’, Applied Physics Letters, P.1673-1675, 1998

[50] J. Bonse, S. Baudach, J. Krüger, W. Kautek, M. Lenzner, ‘’Femtosecond laser ablation of silicon–modification thresholds and morphology’’, Springer Verlag, Applied Physics A , Volume 74, Issue 1, pp 19–25, 2002

[51] Britland, Stephen, Peter Clark, Patricia Connolly, and Geoffrey Moores, ‘’ Micropatterned substratum adhesiveness: A model for morphogenetic cues controlling cell behavior‘’, Experimental Cell Research, 198(1): p. 124-129, 1992

[52] X.F. Walboomers, H. J. E. Croes L. A. Ginsel J. A. Jansen, ‘’Contact guidance of rat fibroblasts on various implant materials’’, Journal of Biomedical Materials Research, p. 204-212, 1999

[53] Eugen Zgraggen, Ibrahim Murat Soganci, Folkert Horst, Antonio La Porta, Roger Dangel, Bert Jan Offrein, Steven A. Snow, Jeanette K. Young, Brandon W. Swatowski, Chad M. Amb, Olivier Scholder, Rolf Broennimann, Urs Sennhauser, and Gian-Luca Bona, ‘’Laser Direct Writing of Single-Mode Polysiloxane Optical Waveguides and Devices’’, J. Lightwave Technol. 32, 3036-3042, 2014

[54] A. Piqué, ‘’Laser Transfer Techniques for Digital Microfabrication in Laser Precision Microfabrication’’, edited by K. Sugioka, M. Meunier and A. Piqué, Springer, P.259.Heidelberg, 2010

[55] Alberto Piqué and Heungsoo Kim, ‘’Laser-Induced Forward Transfer of Functional Materials: Advances and Future Directions’’, Materials Science & Technology Division, Naval Research Laboratory, Washington, DC, USA, JLMN-Journal of Laser Micro/Nano engineering Vol. 9, No. 3, 2014

[56] Pere Serra, Juan Marcos Fernandez-Pradas, Mónica Colina, Martí Duocastella, Jorge Dominguez and José Luis Morenza, ‘’Laser-induced forward Transfer: a Direct-writing Technique for Biosensors Preparation’’, Universitat de Barcelona, Departament de Física Aplicada i Òptica, Martí i Franquès 1, E-08028 Barcelona, Spain, 2006

[57] N. T. Kattamis, P. E. Purnick, R. Weiss, C. B. Arnold, ‘’ Thick film laser induced forward transfer for deposition of thermally and mechanically sensitive materials‘’, Applied Physics Letters 91, 171120, 2007

[58] G. Hennig, T. Baldermann, C. Nussbaum, M. Rossier, A. Brockelt, L. Schuler, G. Hochstein, ‘’Lasersonic LIFT process for Large Area Digital Printing’’, Journal of Laser Micro/nanoengineering, VOl.7, No.3, 2012

[59] A. Patrascioiu, J.M. Fernández-Pradas, J.L. Morenza, P. Serra, ‘’Film-free laser printing: Jetting dynamics analyzed through time-resolved imaging’’, Applied Surface Science**,** Volume 302, Pages 303-308, 2014

[60] C Frederik Brasz, Julia H Yang, Craig B Arnold, ‘’tilting of adjacent laser-induced liquid jets’’, Volume 18, Issue 2, Pages: 185-197, Springer berlin Heidelberg, 2015

[61] J.-Y. Zhang, I. W. Boyd, and H. Esrom, ‘’Lamp-induced forward transfer: a new approach for deposition of metal films’’, Journal Material Science. Letter 17, 2037–2040, 1998

[62] Z. Kantor, Z. Toth, and T. Szorenyi, ‘’Metal pattern deposition by laser-induced forward transfer’’, Appl. Surf. Sci. 86, 196– 201, 1995

[63] Vahit Sametoglu, Vincent T. K. Sauer, and Ying Y. Tsu, ‘’Production of 70-nm Cr dots by laser-induced forward transfer’’, Opt. Express 21, 18525-18531, 2013

[64] Nagel D.J., ‘’Technologies for micrometer and nanometer pattern and material transfer’’, Direct-Write Technologies for Rapid Prototyping, pp.557-679, 2002

[65] Bratton D,Yang D., Dai J., Ober C.K., ‘’Recent progress in high resolution lithography’’, Polymers for advanced technologies, Material Science and Engineering, Cornell University, Ithaca, USA, 2006

[66] Alan Douglas Brisbane, ‘’Pattern deposit by laser’’, U.S. patent number: US3560258 A, 1971

[67] Levene M.L., Scott R.D., Siryj B.W., ‘’Material transfer recording’’, Applied Optics IP, vol. 9, Issue 10, p.2260, 1970

[68] Baseman et al., Baseman R.J., Froberg N.M., Andreshak J.C., Schlesinger Z., ‘’Minimum fluence for laser blow-off of thin gold films at 248 and 532 nm’’, Appl. Phys. Lett. 56, 1990

[69] Schultze V. Wagner M., ‘’Laser-induced forward transfer of aluminum’’, Applied Surface Science, Volume 52, Issue 4, Pages 303-309, December 1991

[70] Z. Kántor, Z. Tóth, and T. Szörényi, ‘’Deposition of micrometer-sized tungsten patterns by laser transfer technique’’, Research Group on Laser Physics of the Hungarian Academy of Sciences, Institute for Technical Physics, Budapest, Hungary, Appl. Phys. Lett. 64, 3506, 1994

[71] Sano et al., Sano T., Yamada H., Nakayama T., Miyamoto I., ‘’Experimental investigation of laser induced forward transfer process of metal thin films’’, Appl Surf. Sci. 186, 2002

[72] Chrisey D.B., Pique A., McGill R.A., Horwitz J.S., Ringeisen B.R., Bubb D.M.,Wu P.K., ‘’Laser deposition of polymer and biomaterial films’’, Chem. Rev. 103, 2003

[73] Lianwei Chen, Xiao-Fang Jiang, Ziming Gua, ‘’Tuning Optical Nonlinearity of Laser-Ablation-Synthesized Silicon Nanoparticles via Doping Concentration’’, Journal of Nanomaterial, National University of Singapore, Singapore, 2014

[74] M. H. Azhdast, M. Kossatz, H. J. Eichler, K. Lang, and V. Glaw, ‘’Comparison of nano particle implantation with picosecond lasers by concerning different wavelengths from Aluminum and Copper on Silicon wafer substrate’’, in Conference on Lasers and Electro-Optics, OSA Technical Digest paper ATu4C.2, Optical Society of America, 2017

[75] a.v. simakin, v.v. voronov,n.a. kirichenko, g.a. shafeev, ‘’Nano particles produced by laser ablation of solids in liquid environment’’, General Institute of the Russian Academy of science, Moscow, Russia, 2004

[76] Turkka Salminen, ‘’Production of nanomaterial by pulsed laser ablation’’, Tampere University of technology, Tampere, Finland, 2013

[77] Chi Zhang, Jeanne Hankett, and Zhan Chen, ‘’Molecular Level Understanding of Adhesion Mechanisms at the Epoxy/Polymer Interfaces’’, Department of Chemistry, University of Michigan, Ann Arbor, Michigan 48109, United States, ACS Appl. Mater. Interfaces, 2012, 4 (7), pp 3730–3737, 2012

[78] W.-C. Lee and V. W. Lindberg, ‘’Thin film adhesion measurement using excimer laser ablation and tensile extension tests’’, Materials Science and Engineering Program Rochester Institute of Technology Rochester, New York 14623 P. H. Wojciechowski and F. 1, 14652-3701, 1991

[79] K. L. MITTAL MHV, ‘’Adhesion measurement of thin films System Products Assurance’’, Electrocomponents Science and Technology, Vol. 3, pp. 21-42, IBM Corporation, Poughkeepsie, 1975

[80] M. Arif Butt, Arshad Chughtai, Javaid Ahmad, Rafiq Ahmad, Usman Majeed, I.H. Khan, ‘’Theory of Adhesion and its Practical Implications A Critical Review’’, Journal of Faculty of Engineering & Technology, Pages 21-45, 2008

[81] Kenneth J. Shea, Mingdi Yan, M.Joseph Roberts, ‘’ Molecularly Imprinted Materials- Sensors and other Devices’’, Material Research Society Symposium Proceeding Volume 723, 2002

[82] Thomas S. Williams, Hang Yu and Robert F. Hicks, ‘’Atmospheric Pressure Plasma Activation of Polymers and Composites for Adhesive Bonding: A Critical Review’’, University of California at Los Angeles, Department of Chemical and Biomolecular Engineering, Adhesion Adhesives, Vol. 1, No. 1, 2013

[83] Edgar Alfonso, Jairo Olaya and Gloria, ‘’Thin Film Growth through Sputtering Technique and Its Applications’’, Cubillos Universidad Nacional de Colombia Colombia, DOI: 10.5772/35844, In book: Crystallization - Science and Technology, 2012

[84] M. H. Azhdast, M. Kossatz, H. J. Eichler, K. Lang, and V. Glaw, ‘’Deposition of Al and Cu nanoparticles on Silicon Wafer using a Picosecond Nd:YAG Laser: An Experiment-based Parameter Optimization Guide’’, Conference on Lasers and Electro-Optics, paper JTu5A.12., OSA Technical Digest Optical Society of America, 2017

[85] ASTM Designation: D 3359 – 97 ‘’Standard Test Methods for Measuring Adhesion by Tape Test’’, Copyright ASTM International, PA 19428-2959, West Conshohocken, United States

[86] Robert Lacombe, Taylor and Francis Group, ‘’Adhesion measurement methods, theory and practice’’, CRC Press, FL 33487-2742, 2006

[87] Gawrilov G.G. ‘’Chemical (electroless) Nickel-Plating’’, Portcullis Press Ltd., Redhill, United Kingdom, ISBN: 0861080238, 1979

[88] Mordechay Schlesinger, ‘’Electroless deposition of nickel’’ Modern Electroplating, Fifth Edition, Edited by M. Schlesinger and M. Paunovic, Copyright 2010 John Wiley & Sons, Inc, New York, United States, 2000

[89] Hamano T. and Ikemoto Y. ‘’Electrical characterization of a 500 MHz frequency EBGA package’’, IEEE Transactions on Advanced Packing, 24(4):534541, 2001

[90] Keller C.G. and Howe R.T, ‘’Nickel filled hexsil termally actuated tweezers’’, In Tech. Dig. Papers, Int. Conf. Solid-State Sensors and Actuators, Transducers 95, pages 376379, Stockholm, Sweden, 1995

[91] Guan S., Nelson B.J., and Vollmers K, ‘’Electrochemical codeposition of magnetic particle-ferromagnetic matrix composites for magnetic MEMS actuator applications’’, J. Electrochem, 2004

[92] Coombs C.F. Jr., ‘’Printed Circuit Handbook’’, McGraw-Hill, New York, United States, Sixth edition, 2008

[93] Huang Y.S., Zeng X.T., Hu X.F., and Liu F.M, ‘’Corrosion resistance properties of electroless nickel composite coatings’’ Electrochemica Acta, Volume 49, Issue 25, P.4313-4319, 2004

[94] Kwok R.W.M., Chan K.C.M., and Bayes M.W, ‘’Development of an Electroless nickel immersion gold process for PCB final finishes’’, Circuit World, ISSN: 0305-6120, 1974

[95] Lewis D.B. and Marshall G.W, ‘’Investigation into the structure of electrodeposited nickel-phosphorous alloy deposition’’, Surface and Coating Technology, 78:150156, 1996

[96] Kalle Kantola, ‘’ Modeling, estimation and control of Electroless nickel plating process of printed circuit board manufacturing’’, Helsinki University of Technology Control Engineering Laboratory Department of Automation and Systems Espoo, 2006

[97] The Japan Institute of Light Metals, ‘’Effect of Zincate Treatment on Adhesion of Electroless Ni-P Coating, On to Various Aluminum Alloys’’, Materials Transactions, Vol. 50, No. 9 (2009) pp. 2235 to 2241, 2009

[98] Glenn O.Mallory, Juan B.Hajdu, ‘’Electroless Plating: Fundamentals and Applications’’, published: American Electroplaters and Surface Finishers, 1990

[99] Andrew R. Markelonis, Joanna S. Wang, Bruno Ullrich, Chien M. Wai, Gail J. Brown, ‘’Nanoparticle film deposition using a simple and fast centrifuge sedimentation method’, Applied Nanoscience, Vol.5, Issue 4, pp.457-468, 2015

[100] Kimmo T. Laitinen, Hannu Korhonen, Jari T.T. Leskinen, Arto Koistinen, Reijo Lappalainen, ‘’Improved multilayer coatings by combined use of electrochemical and ultra-short pulsed laser deposition techniques’’ , Surface & Coatings Technology 300, 58–66, 2016

[101] x. li, h. li, y. chen, x. zeng, ‘’Silver conductor fabrication by laser direct writing on Al_2O_3 substrate’’, State key laboratory of laser technology, Huazhong University of Science and Technology (HUST), Wuhan, Hubei, 430074, P.R. China, Appl. Phys. A 79, 1861–1864, 2004

[102] Ryan Wartena a, Aimee E. Curtright a, Craig B. Arnold b, Alberto Piqué b, Karen E. Swider-Lyons , ‘’Li-ion micro batteries generated by a laser direct-write method’’, Nava research Laboratory, Journal of Power Sources 126, P.193–202, 2004

[103] International standard ISO 13565-2:1996, ‘’Geometrical product specifications (GPS)’’ – Surface texture: Profile method; Surfaces having stratified functional properties, International organization for standardization

[104] Min Tang, Zai Chun Chen, Zhi Qiang Huang, Yoo Sang Choo, and Ming Hui Hong, ‘’Maskless multiple-beam laser lithography for large-area nanostructure/microstructure fabrication’’, Appl. Opt. 50, 6536-6542, 2011

[105] Thomas Seuthe, Moritz Grehn, Alexandre Mermillod-Blondin, Jörn Bonse and Markus Eberstein, ‘’Requirements on glasses for femtosecond-laser based micro structuring’’, IMAPS/AcerS 11^{th} international CICMT conference and exhibition, 2015

[106] Sung Chul Joo, ‘’Adhesion mechanism of nano particle silver to electronics packaging materials’’, Georgia Institute of Technology, 2009

[107] K.L.Mittal, ‘’Adhesion measurement of films and coatings, Utrecht, The Netherlands, 1995

[108] S. Louring, ‘’Deposition and characterization of Amorphous, Nanostructured and Nano composite thin films, Department of Physics and Astronomy’’, Aarhus University, Denmark, 2013

[109] Jong-Woong Kim, Seung-Boo Jung, ‘’Re-examination of the solder ball shear test for evaluation of the mechanical joint strength’’, Department of Advanced Materials Engineering, Sungkyunkwan University, South Korea, 2005

[110] Jie Tian, Wei Yan, Yazhao Liu, Jun Luo, Daozhong Zhang, Zhiyuan Li, and Min Qiu, ‘’Optical Quality Improvement of Si Photonic Devices Fabricated by Focused-Ion-Beam Milling’’, J. Lightwave Technol. 27, 4306-4310, 2009

[111] C. A. Volkert, A. M. Minor, ‘’Focused Ion Beam Microscopy and Micromachining’’, MRS Bulletin, 32, pp 389-399. doi:10.1557/mrs2007.62, 2007

[112] Evstatin Krastev, Ian Christopher Mayes, Chan Myat, Armin Struwe [Nordson DAGE], Rene P. Zingg [Zinan GmbH],Ricardo Geelhaar [PacTech GmbH], ‘’Bond tester study of CSP reliability through bump analysis’’, 2015

[113] Xingjia Huang, S.W.Ricky Lee, Chien Chun Yan, and Sam Hui, ‘’Characterization and Analysis on the Solder Ball Shear Testing Conditions’’, Electronic Components and Technology Conference, 2001

[114] Mitutoyo America Corporation, ‘’Surface roughness measurement, practical tips for laboratory and workshop’’, http://www.mitutoyo.com/wp-content/uploads/2012/11/1984_Surf_Roughness_PG.pdf, 3M 1116-04 Printed in USA, 2016

[115] Jeppe Byskov-Nielsen, ‘’Short pulse laser ablation of metals: fundamentals and applications for micro-mechanical interlocking’’, PhD thesis, University of Aarhus, Denmark, 2010

[116] William H.Cubberly, Ramon Bakerjian, ‘’Tool and Manufacturing Engineers Handbook’’, Copyright by Society of Manufacturing Engineers, ISBN No. 0-87263-351-9, 1989

[117] Hisashi Hirabayashi, Tsukasa Matsuo, Hiroaki Ishizawa, Hiroyuki Kanai, Toyonori Nishimatsu, ‘’Surface Roughness Evaluation by Laser Speckle’’, SICE-ICASE International Joint Conference, 2007

[118] P.peng, A.Hu, Y.Zhou, ‘’Laser sintering of silver nanoparticle thin films: microstructure an optical properties’’, Applied Physics and Materials Science & Processing, 2012

[119] M. H. Azhdast, H. J. Eichler, K. D. Lang, and V. Glaw, ‘’Adhesion mechanism between laser sputtered Aluminum nano particles on Si-Wafer by Nd:YAG laser, in Conference on Lasers and Electro-Optics’’, OSA Technical Digest, paper ATh1K.7, Optical Society of America, 2016

[120] Advanced manufacturing laboratory, Columbia University, http://www.aml.engineering.columbia.edu/ntm/level2/ch02/html/l2c02s09.html
[121] Layer tech optical coatings optics, Reflectivity of different metals, Mellingen, Germany, https://www.layertec.de/en/capabilities/coatings/metallic
[122] Khaled Habiba, Vladimir I.Makarov, Brad R.Weiner, and Gerardo Morell, ‘’Fabrication of Nanomaterials by Pulsed Laser Synthesis’’, Manufacturing Nanostructures, UK: one central press, 2014
[123] James M.E, Harper, Jerome J, Cuomo, Richard J, Gambino, ‘’Modification of thin film properties by ion bombardment during deposition’’, Nuclear Instruments and Methods in Physics Research Section B: Beam Interactions with Materials and Atoms, Pages 886-892, 1985
[124] Andreas Hogg, ‘’Development and Characterization of Ultrathin Layer Packaging for Implantable Medical Devices’’, PhD thesis, Bern University, 2014
[125] Hirofumi Hidai, Hitoshi Tokura, ‘’Direct laser writing of Aluminum and copper on glass surfaces from metal powder’’, Applied Surface Science, Volume 174, Issue 2, Pages 118-124, 2001
[126] Shevon Johnson, ‘’Pulsed Laser Deposition of Hydroxyapatite Thin Films’’, Academic Faculty in Partial Fulfillment, Master thesis in Bioengineering, Georgia Institute of Technology, 2005
[127] Ming Lun Tseng, Bo Han Chen, Cheng Hung Chu, Chia Min Chang, Wei Chih Lin, Nien-Nan Chu, Masud Mansuripur, Ai Qun Liu, and Din Ping Tsai, ‘’Fabrication of phase-change chalcogenide, $Ge_2Sb_2Te_5$patterns by laser-induced forward transfer’’, Opt. Express19, 16975-16984, 2011
[128] Matthias Nagel, Romain Fardel, Pascal Feurer, Mark Häberli, Frank A. Nüesch, Thomas Lippert, Alexander Wokaun, Appl, ‘’Aryltriazene photopolymer thin films as sacrificial release layers for laser-assisted forward transfer systems: study of photoablative decomposition and transfer behavior’’, Applied Physics A, Materials Science processing, 2008
[129] P. Serra, ‘’Laser Printing of Functional Materials’’, Conference on Lasers and Electro-Optics, OSA Technical Digest Optical Society of America, paper STh1J.1, 2017

[130] A. Reyes-Contreras, M. Camacho-López, S. Camacho-López, O. Olea-Mejía, A. Esparza-García, J. G. Bañuelos-Muñetón, and M. A. Camacho-López, ‘’Laser-induced periodic surface structures on bismuth thin films with ns laser pulses below ablation threshold’’, Opt. Mater. Express **7**, 1777-1786, 2017

[131] Manoj Kumar Sharma, ‘’Optimization of Laser Induced Forward Transfer by Finite Element Modelling’’, Master thesis, Royal Institute of Technology-KTH, Stockholm, 2013

[132] Romain Fardel, Matthias Nagel, Frank Nüesch, Thomas Lippert, and Alexander Wokaun, ‘’Energy Balance in a Laser-Induced Forward Transfer Process Studied by Shadowgraphy’’, the Journal of Physical Chemistry, 2009

[133] J. H. Bechtel, ‘’Heating of solid targets with laser pulses’’, Journal of Applied Physics, vol. 46, no. 4, pp. 1585–1593, 1975

[134] B. Stuart, M. Feit, S. Herman, A. Rubenchik, B. Shore, and M. Perry, ‘’Nanosecond-to-femtosecond laser-induced breakdown in dielectrics’’, Physical Review B, vol. 53, no. 4, pp. 1749–1761, 1996

[135] S. I. Anisimov, B. L. Kapeliovich, and T. L. Perel`man, ‘’Electron emission from metal surfaces exposed to ultrashort laser pulses’’, Journal of Experimental and Theoretical Physics, vol. 39, no. 2, pp. 375-377, 1974

[136] J. K. Chen, D. Y. Tzou, and J. E. Beraun, ‘’A semi classical two-temperature model for ultrafast laser heating’’, International Journal of Heat and Mass Transfer, vol. 49, no. 1–2, pp. 307–316, 2006

[137] T. Q. Qiu and C. L. Tien, ‘’Short-pulse laser heating on metals’’, International Journal of Heat and Mass Transfer, vol. 35, no. 3, pp. 719–726, 1992

[138] L. Li, D. Zhang, Z. Li, L. Guan, X. Tan, R. Fang, D. Hu, and G. Liu, ‘’The investigation of optical characteristics of metal target in high power laser ablation’’, Physica B: Condensed Matter, vol. 383, no. 2, pp. 194–201, 2006

[139] Y. Ren, J. K. Chen, and Y. Zhang, ‘’Optical properties and thermal response of copper films induced by ultrashort-pulsed lasers’’, Journal of Applied Physics, vol. 110, no. 11, pp. 113102–113102–7, Dec. 2011

[140] P. Nath and K. L. Chopra, ‘’Thermal conductivity of copper films’’, Thin Solid Films, vol. 20, no. 1, pp. 53–62, 1974

[141] J. Bohandy, B. F. Kim, F. J. Adrian, and A. N. Jette, ‘’Metal deposition at 532 nm using a laser transfer technique’’, Journal of Applied Physics, Volume 63, Issue 4, 1158 (1988)

[142] William A. Tolbert, I. Yin Sandy Lee, Mark M. Doxtader, Ernest W. Ellis, Dana D. Dlott, ‘’High-speed color imaging by laser ablation transfer with a dynamic release layer: Fundamental mechanisms’’, Journal of imaging science, volume 37, p.411-421, July 1993

[143] Heungsoo Kim, Joseph S. Melinger, Ani Khachatrian, Nicholas A. Charipar, Raymond C. Y. Auyeung, and Alberto Piqué, ‘’Fabrication of terahertz metamaterials by laser printing’’, Opt. Lett. 35, 4039-4041 (2010)